Chapter 1

INTRODUCTION

Masonry is the oldest building technique. The variety and natural availability of the materials that is needed for masonry combined with the easiness of the construction results in usage of masonry for thousands of years.

The earliest samples of the first stone masonry houses were found near Lake Hullen, Israel (9000-8000BC). Dry stone huts circular and semi-subterranean having diameters of 3 m to 9m were found. Handmade mud bricks were used at Jericho, Palestine where many round and oval houses were found. The mud bricks had indentations on the convex face to give space to the clay mortar (8350-7350BC). One of the earliest recorded burnt brick is referenced in the Bible, Genesis XI, 3-4 that the inhabitants of the Babylonia said one another "Come, let us make bricks and bake them". Then they said "Let us build ourselves a city and tower with its top in heavens". By using the bitumen as mortar, they built the Tower of Babel topped a height of 90m, probably the first skyscraper (Lourenço 1996, p2).

Masonry technique is still widely used that one-third of the world's population lives in earth houses today (Lourenço 1996, p6). As most of the research is done on reinforced concrete and steel structures, the owners of the masonry houses can not get engineering service and the codes on these structures base on empirical knowledge.

A reinforced masonry structure that has the same plan with a reinforced concrete costs approximately 30% less in construction expenses (Orhon 1995, p72). The limited use of reinforced masonry technique seems to be because of general belief that masonry is vulnerable especially due to seismic actions. The undeveloped structural codes and lack of knowledge of the behavior of masonry is the main reason of limited use of reinforced masonry.

The lack of research and underdeveloped codes in masonry results poor applications of masonry technique which cause invaluable loss of lives of people in earthquakes of Guatemala (1976) (Lourenço 1996, p.7), in Erzurum (Demir and Polat 1985), in Çaldiran (Ministry of Public Works and Settlement, Government of Republic of Turkey 1977), in Bem, Iran (Web_1).

Historical structures are the treasures that left behind by the thousands of year's cultural accumulation. They are world's cultural heritage and have to be protected for their survival to the next generations. The deterioration of the materials, seismic actions, differential settlements, alteration of the function, changes in load carrying system, causes structural failures like cracks and collapses. In order to be protected, these structures generally need strengthening. For strengthening, the problems of the structure must be well understood and a comprehensive assessment should be made. An interdisciplinary work has to be carried out in order to diagnose the problem of the structure including architectural restorators, materials scientists and structural engineers. The problem of the structure may consist of material degradation because of moisture and chemical attacks that can be investigated by a materials scientist and because of differential settlement or seismic action that can be assessed by structural engineer. More over, supports may be need from geotechnical engineers for soil survey, geodetics for the measurement survey. With only a harmonious team work could be understood the problems of a historical structure which have been accumulated through passing years.

Structural analysis of historical masonry structures has always been a need for centuries; for the architects and for the strengtheners. Poleni had investigated the cracks on the dome of St Peter by use of chain rule in 18th century (Heyman 1995, p35). The thrust line solution and the funicular polygon have also been used for the analyses of arches, vaults and domes (Heyman 1982).

On the other hand, by the development of powerful computers and the research conducted for numerical simulation of masonry, it is now available to model a historical masonry and test various loading scenarios that challenge the structure.

Strut-tie model was used to analyze the Auguste-Victoria Church (Wenzel et al. 1989, p.475). Generalized matrix formulation was adopted for analysis of masonry structures and comparative analyses with respect to finite element methods have been done and consistent results were obtained (Roca 2001, p291). Hinges were used to model the damage in masonry due to different loads and a step by step analysis of a church was conducted (Stylianidis and Ignatakis 1989, p.131).

The safety of historical masonry structures was determined by use of safety factors which were derived from the axial force-moment interaction diagrams (Ünay 1997).

Finite element method is widely used for modeling masonry. Drucker-Prager's yield criterion was adopted for structural analyses of church steeples (Sofraine et al. 2001, p399) and for analyses of St. Bergius and Bacchus Church (Küçük Ayasofya Cami) (Koçak 1999). Finite element analyses by using discontinue elements and discrete elements were conducted in order to model a masonry test and consistent results were obtained (Giordano et al. 2002, p1057). An interface model for mortar derived from concepts of rock mechanics and tribology was used to model masonry by micro approach in which mortar and units are modeled separately (Giambanco et al. 2001, p6493). An orthotropic damage model was specifically developed for the analysis of masonry under in-plane loading (Berto et al. 2001).

There are two approaches in modeling masonry; micro modeling in which mortar joints and units are modeled separately and macro modeling in which a constitutive relation for overall constituents of masonry is defined.

In micro modeling, by making the assumption that all inelastic response occur in the interface elements, a robust modeling capable of following the complete load path of a structure until total degradation of stiffness was achieved. For the interface elements, a composite interface model which includes a tension cut-off for mode I failure, a Coulomb friction envelope for mode II failure and a cap mode for compressive failure was developed (Lourenço 1996, p43).

Masonry is an orthotropic composite material. In macro modeling of orthotropic behavior, a Hill type yield criterion for compression and a Rankine type yield criterion for tension was proposed (Lourenço 1996, p125).

In this study, finite element analyses of historical masonry structures have been investigated. The study has been conducted on a case study structure, Urla Kamanli Mosque. In order to collect data for finite element analyses, history investigation and measurement survey of the structure were done. Long term observations of moisture, crack opening displacement and wall settlements were done periodically. Nondestructive and destructive material tests on stone, mortar and brick of the structure were applied. A 3D finite element model of the structure was generated on LUSAS, a commercial finite element software. Linear elastic and nonlinear analyses were conducted to determine the vulnerability and the reasons of the structural cracks. The nonlinear analyses were conducted by using appropriate constitutive criterion for masonry.

Chapter 2

THE ASSESSMENTAL APPLICATIONS ON HISTORICAL MASONRIES

The accumulation of material degradations, structural failures like cracks, out of plumbing of walls and many other responses of the historical masonry are due to the environmental effects in the history of the structure. In order to make a reliable and efficient assessment, various procedures can be applied. In this chapter, these procedures will be presented.

2.1. History Investigation

History investigation may enlighten a great amount of data needed to understand the structure. In history investigation, construction technology and time, the strengthenings made on the structure, the hazards like fire, earthquakes and alterations of the structural system are determined. A chronological order of the events that effected the structure should be listed which will help the structural engineer on determining the causes of the damages.

2.2. Visual Investigation and Measurement Survey

Visual investigation is the first procedure that is applied on a historical masonry and seems to be the easiest one but in fact visual investigation may supply most of the information that can be collected totally at the end of the diagnosis step. The material degradations and structural failures like cracks, the tracks of the alterations, the material used in the structure, an overall load carrying mechanism are determined by the visual investigations.

The dimensions of the structure, the failures like cracks and material degradations on the structure, the materials used in different parts are observed in details by making a measurement survey.

2.3. Longterm Observations

Understanding the longterm behaviour of a structure may supply invaluable information about the current situation of the structure. A number of different observations can be carried on.

Crack opening displacements can be observed periodically by mounting studs at opposite sides of a crack and make measurements periodically. Also extensometers and fissurometers that can be used with data loggers may supply real time records and transmit them by use of modems to computers (Croci 1998, p74).

Settlement displacements can be observed by mounting studs on opposite parts of the walls and measure the distance between them periodically.

Periodic moisture observations on the materials can be conducted by moisturemeters, in situ.

Thermal sensors for open air or in materials can be used to observe the variation of temprature. Strain gauges can be used in variation of stresses in materials. Inclinometers can be used for observing the out of plumbness or verticality of the walls. Piezometers can be used to measure the level of water tables in the ground (Croci 1998, p77).

In order to determine the seasonal effects, at least one year period is recommended for the long term observations. The data gathered by longterm observations can enlighten the causes of material degradations, the vulnerability of the structure due to movements, and thermal effects on the structure. Actions can be taken to prevent the structure due to these observations.

2.4. In Situ Tests

In situ tests might give reliable results for assessment but choosing the best locations for the tests and interpreting the data needs expertise on the tests.

2.4.1. Flatjack Test

The distance between two points is measured on the masonry wall and a perpendicular cut to the surface is made. As the cut is made, the distance between points decreases. Flat jack

is inserted in the cut and pressure is given by a hydraulic equipment into the jack. The stress level obtained at the original distance is the stress level of the wall. Flatjack test can be conducted in order to get the current stress level, final strength and the modulus of elasticity of the masonry structure (Croci 1998, p71, Binda et al. 2000 p212).

2.4.2. Dynamic Monitoring

Accelerometers are used in dynamic monitoring which can give us the dynamic characteristics like mode shapes and modal frequencies of the structure. Also the effect of train and auto traffic or other sources of vibrations on the historical structure can be determined by use of dynamic tests. The dynamic test can be done either by use of natural vibrations or forced vibrations. The natural vibrations are traffic, wind, bell ringing for special towers. The forced vibrations can be applied by vibrodyne or local hammering (Binda et al. 2000, p208).

Dynamic tests give data for calibrating finite element (FE) models which can be used in understanding the structural behaviour under different loads (Çakmak et al. 1992).

2.4.3. Pull-out Test

A steel bar is inserted and anchored in a wall, perpendicular to the surface and a tension force is applied by a hydraulic jack until the bar and a portion of the masonry is pulled out of the wall. The tensile and shear resistence of the wall is found by the pull-out test (Croci 1998, p.73).

2.4.4. Thermography Test

The components of masonry have different temperatures. The thermovision detects the infrared radiation emitted by the wall. The results is a thermographic image in a contour scale. The cavities, different materials, presence of water, heating system and moisture are determined by the thermography test (Binda et al. 2000, p.214).

2.4.5. Sonic Tests

A signal is generated by a percussion, electrodynamics or pneumatic device (transmitter) which passes through the wall. The signal is collected through a receiver. The morphology of the wall section, presence of voids, cracks and damage in the wall are determined. Also, the efficiency of injection technique which is applied on the wall for rehabilitation purposes can be tested (Binda et al. 2000, p.215).

2.5. Tests on Constituents of Masonry

Generally testing the constituents of masonry is much more easier than applying some other insitu tests. With a well planned test schedule that requires minimum number of samples and steps to be applied on the samples, a broad information on the chemical, physical and mechanical strength of the constituents of masonry can be determined. These data may enlighten the causes of material degradations, the parameters used in finite element modeling of the structure, the injection type which will be applied on the wall for rehabilitation purposes and much more.

While sampling the bricks, mortars and stones some simple principals can be taken into account;

- Care should be taken in order not to deform the important points like corner stones which are important in future possible measurement surveys;
- The samples can be taken from the previously damaged parts and they may be fallen to ground from the structure;
- Samples from different parts should be taken to represent the whole structure espacially when the material degradations is investigated for different portions;
- The number of samples should be consistent with the tests schedule;
- The stone and brick samples should have the sizes to cut out cores of standart sizes.

2.5.1. Schmidt Hammer Test

This nondestructive test method was developed by Einst Schmidt and is a practical test that can be used insitu or in laboratory (Koçak 1999, p.18). The plunger of the Schmidt hammer is placed on the specimen and depressed. After a hit, the Schmidt hammer gives the surface hardness of the material tested. Ten hits are made for a local area and for every hit, the head of the plunger will be placed at least 1cm away from the other places that were hit before. After collecting 10 hits, the hardness values will be sorted and the lowest 5 are discarded while the average of the highest 5 hardness values gives the hardness value of the specimen. A rock cradle should be used to make the test on cylinder core specimens. By using the tables available on the hammer and in the literature, uniaxial compression strength of the specimens can be determined (Ulusay et al. 2001, p.41).

There are different type of Schmidt hammers which have different impact energies, that can be used on different materials. For concrete, N type Schmidt hammer is used which has an impact energy of 2.2Nm (Proceq 2001). For rocks L type Schmidt hammer is used which has an impact energy of 0.74Nm (Ulusay et al. 2001, p.41). In general, mortar and brick are weaker than stone and a Schmidt hammer that has a lower impact energy, like a PM type of Proceq, can be used for them.

2.5.2. Ultrasonic Pulse Velocity Test

The elastic constants of rock materials like modulus of elasticity and Poisson's ratio are determined by measuring the velocities of compression and shear waves of the specimen. This method can be applied on both isotropic rocks and the rocks that have slight anisotropy (ASTM 1969, D2845).

The elastic constants obtained by this method are generally higher then the values obtained from destructive tests (Ulusay et al 2001, p.137).

The cylinder core samples should have dimensions equal to or greater than AX D=31mm. The length, L and the diameter, D of the sample should be measured. In order to achieve the full contact between the transducers and the sample, grease can be applied on the parallel faces of the sample. The time needed for the compression and shear waves are

measured, T_p and T_s, respectively. The velocity of the compression and shear waves are determined by Eq.2.1 and Eq.2.2.

$$V_p = \frac{L}{T_p} \qquad \text{Eq.2.1}$$

$$V_s = \frac{L}{T_s} \qquad \text{Eq.2.2}$$

where L (m), V_p,V_s (m/sec) are length of the sample and ultra sonic pulse velocities of compression and shear waves, respectively.

The modulus of elasticity can be determined by Eq.2.3.

$$E(Pa) = r \times V_s^{\,2} \times \frac{\left(3 \times V_p^{\,2} - 4 \times V_s^{\,2}\right)}{\left(V_p^{\,2} - V_s^{\,2}\right)} \qquad \text{Eq.2.3}$$

The Poisson's ratio is determined by Eq.2.4.

$$u_{dyn} = \frac{\left(V_p^{\,2} - 2 \times V_s^{\,2}\right)}{2 \times \left(V_p^{\,2} - V_s^{\,2}\right)} \qquad \text{Eq.2.4}$$

The shear modulus is determined by Eq.2.5.

$$G(Pa) = r \times V_s^{\,2} \qquad \text{Eq.2.5}$$

where ? (kg/m^3) is the mass density of the rock (Ulusay et al. 2001, p.140.)

2.5.3. Density-Porosity Test

The measurement of bulk and real densities and porosity of samples can be useful for assessing the extent of some types of stone decay and in determining the extent to which the pore space has been filled by an impregnation treatment.

The samples are dried at 60±5 °C till constant mass. The dry mass, W_{dry}, is measured in grams. The samples are left in vacuum under 2.667Pa, in water for 24 hours. The weight of samples in water, W_{arc}, is measured in water in grams. The samples are wiped with a cloth and the wet weight, W_{wet}, is measured in grams.

The apparent density is determined by Eq.2.6.

$$r_a(kg/m^3) = \frac{W_{dry}}{(W_{wet} - W_{arc})} \times 1000 \qquad \text{Eq.2.6}$$

The real density is determined by Eq.2.7.

$$r_r(kg/m^3) = \frac{W_{dry}}{(W_{dry} - W_{arc})} \times 1000 \qquad \text{Eq.2.7}$$

The porosity is determined by Eq.2.8 (RILEM 1980, p.179).

$$r(\%) = (1 - \frac{r_a}{r_r}) \times 100 \qquad \text{Eq.2.8}$$

2.5.4. Uniaxial Compression Test

This method is used to measure the uniaxial compressive strength of a rock sample in the form of regular geometry and is mainly intended for strength classification and characterization.

Test specimens should be cylinder cores having a height to diameter ratio of 2.5-3 and a diameter preferably of not less than NX (D=54mm). The use of capping materials or end surface treatments other than machining is not permitted. The loading should be applied at

constant rate that the failure will occur within 5-10 min of loading or stress rate will be 0.5-1 MPa/sec (Ulusay et al. 2001, p.77).

The uniaxial compressive strength is determined by Eq.2.9.

$$s_c(Pa) = \frac{F}{A} \qquad \text{Eq.2.9}$$

where F (N) is the load measured at failure, A (m^2) is the cross sectional area of the specimen (Ulusay et al. 2001, p.77).

The modulus of elasticity and Poisson's ratio can be determined by uniaxial compression test by use of strain gauges and linear variable differential transformers. The method is defined at ISRM Part2 in details (Ulusay et al. 2001, p.81).

2.5.5 Indirect Tension (Brazil) Test

This method is used to determine the uniaxial tensile strength of rock samples. This method is far more practical than direct tensile test but gives strength values a little bit higher than the direct tests (Ulusay et. al. 2001, p.69).

The diameter of the rock sample will not be less than NX (D=54mm) and the height will be the same as the diameter of the cylinder core specimen. Loading jaws, as defined are used for loading (Ulusay et. al. 2001, p.70). The load will be applied at a rate for which the failure will occur at 15-30 seconds.

The tensile strength of the rock is determined by Eq.2.10.

$$s_t(MPa) = \frac{0.636 \times F}{D \times t} \qquad \text{Eq.2.10}$$

where F (N), D (mm) and t (mm) are the load at the failure, diameter and thickness of the sample, respectively (Ulusay et al 2001, p.70).

2.5.6. Pointload Test

This method is used to determine the point load strength index which is used to classify the rocks due to their strengths.

A point load device which composes of conical loading heads, a hydraulic manual pump, and a scale giving the pressure in the pump, is used for the test. Cylinder core specimens, block or arbitrary shaped samples can be tested (Ulusay et al. 2001, p47).

Uncorrected point load index is determined by Eq.2.11.

$$I_s = \frac{P}{D^2_e} \qquad \text{Eq.2.11}$$

where P and D_e are the applied load (kN) and equivalent core diameter (m), respectively. Equivalent core diameter (D_e) is determined by Eq.2.12.

$$D_e = \sqrt{\left(\frac{4 \times A}{p}\right)} \qquad \text{Eq.2.12}$$

where A (m^2) is the minimum cross sectional area of the specimen that can be found under the conical heads.

The I_s value has to be corrected according to standart D=50mm core diameter. This correction can be made by using Eq.2.13 and $I_{s(50)}$, the corrected point load index, is determined.

$$I_{s(50)} = F \times I_s \qquad \text{Eq.2.13}$$

where F, size correction factor, can be determined by Eq.2.14 (Ulusay et al. 2001, p51).

$$F = \left(D_e \div 50\right)^{0.45} \qquad \text{Eq. 2.14}$$

The uniaxial compression strength (f_c, MPa) can be determined by Eq. 2.15 (Tunçoku 2001, p.30).

$$f_c = 10.6471 \times I_{s(50)} + 2.4736 \qquad \text{Eq.2.15}$$

2.5.7. X Ray Diffraction, Scanning Electron Microscope and EDX Tests

X-Ray diffraction (XRD) test is used for identifying the crystalline phases present in solid materials and powders and for analyzing structural properties of the crystals. Scanning electron microscope (SEM) is a high-resolution imaging technique providing topographical

and structural information. Especially, the fossils, the impurities and fracture surfaces can be observed by SEM. EDX is used to qualitatively and quantitatively analyze the elements present in a selected area of the SEM image.

2.6. Foundation and Soil Survey

In order to determine the deteriorations and the geometry of the foundations, shafts or core drilling have to be done.

Insitu and laboratory tests on soil can be performed in order to determine the load carrying capacity, the state of stress under loading and for determining the agents that can deteriorate the structure. Also, ground water level can be determined especially if settlement is observed on the structure.

2.7. Basic Techniques of Structural Analyses of Masonry

Understanding the structural behavior of masonry has been an urge for centuries. In 1748, Poleni analysed the reasons of the cracks apparent on the dome of St Peter's, Rome, nearly 200 years after its completion (Heyman 1995, p.35). Figure 2.1 shows the drawing of Poleni of the dome of St Peter's. After performing an extensive literature survey he reached the conclusion "the line of trust should lie anywhere within the masonry".

He observed the meridional cracks on the dome and hypothetically sliced the dome into 50 half spherical lunes (orange slices). He took out a slice and divided each half to 16 sections and calculated the weights of the sections. He loaded a flexible string with 32 unequal weights, each weight in proportion to the corresponding section of the arch. He observed that the shape of the chain lies in the section of the arch as can be seen in Figure 2.2. He concluded that, despite the cracks, the dome was safe (Heyman 1995, p.35).

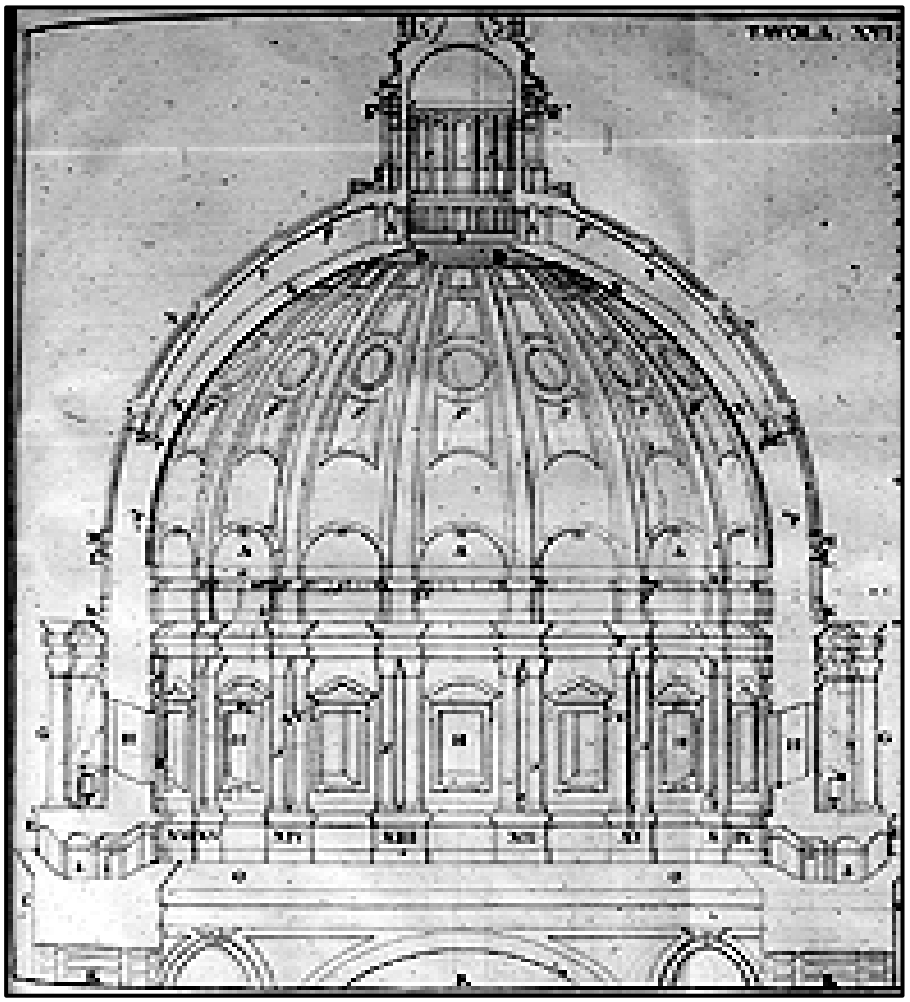

Figure 2.1. Poleni's drawing of the dome of St Peter's (WEB_2).

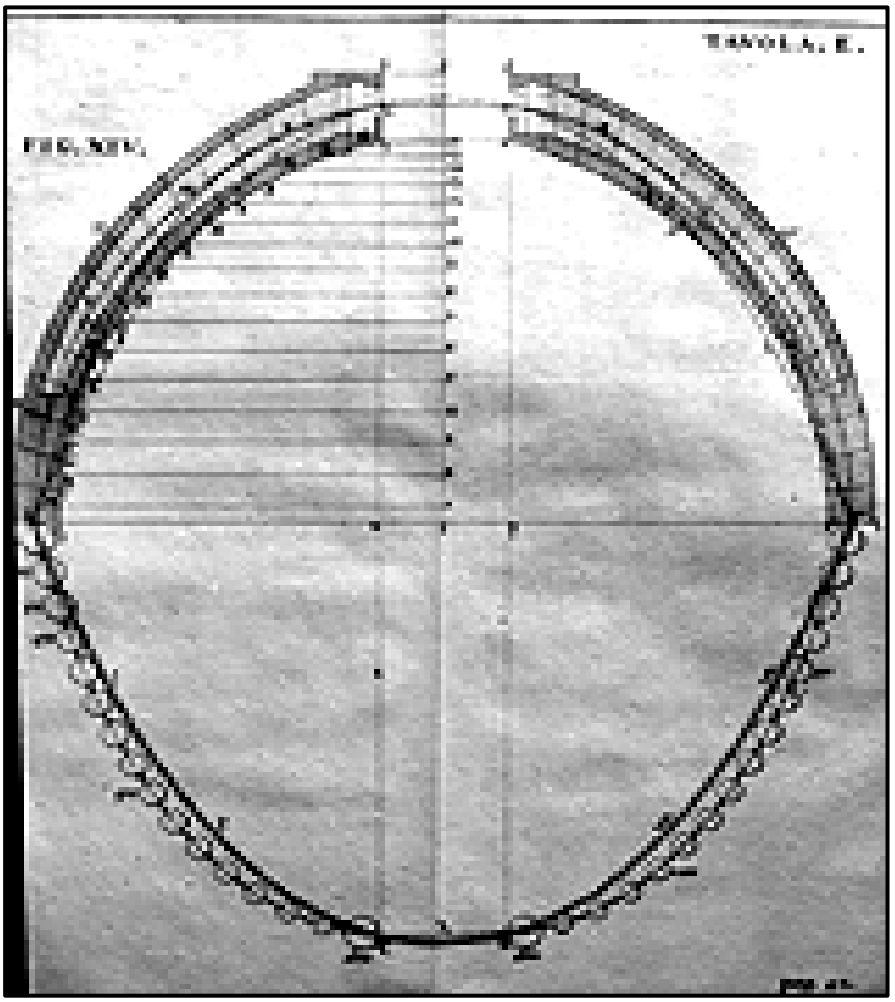

Figure 2.2. Poleni's drawing of his chain for analysis of dome of St Peter's (WEB_2).

The safety theorem of the trust line which states that the structure is safe as long as the trust line stays in the section of the material as shown in Figure 2.3, has been widely used by the strengtheners and the constructers of the masonry structures. For constructing the trust line, namely The Funicular Poligon, for an arch , the forces acting on the arch should be defined as can be seen in Figure 2.4. A random point, O, is selected and by using the W_1, W_2 and W_3 values, Figure.2.5 is drawn. Two points, A and B, is taken on the horizontal plane, and the places of the loads are marked by distances and by drawing paralel lines to the inclined lines from O in Figure.2.5. In order to find the O' which is the actual point of the poligon, a paralel line to AS, in Figure.2.6, is drawn from O and find the X. Drawing a horizontal line from X and intersecting the vertical of O will give O'. The dashed lines in Figure.2.5 should be used and parallels are drawn to them as can be seen in Figure.2.6. AP'Q'R'B is the real trust line of the system (Heyman 1982, p.16).

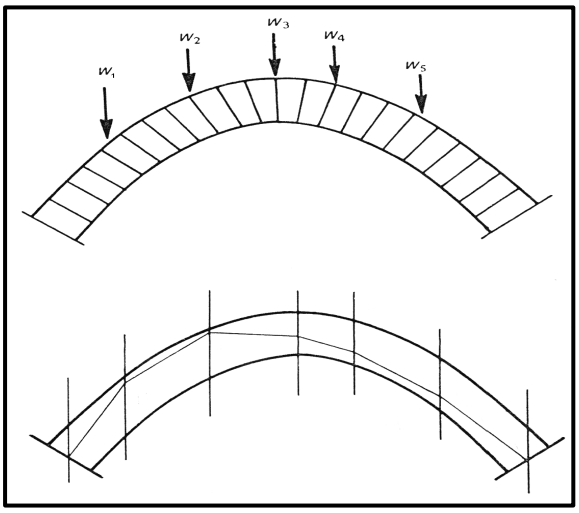

Figure.2.3. Forces and their trust line.

(Heyman 1982, p.21)

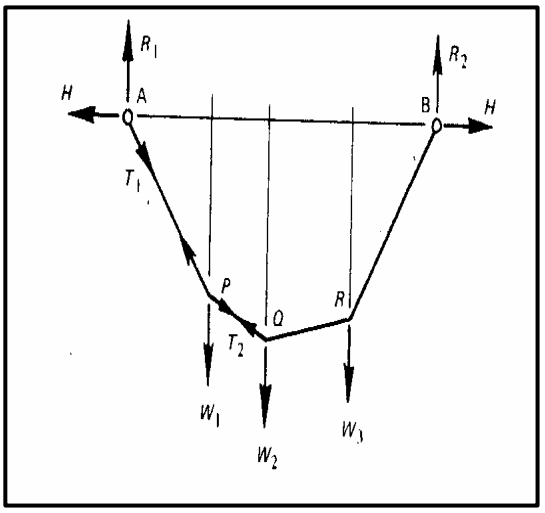

Figure.2.4. Forces acting on an arch.

(Heyman 1982, p.15)

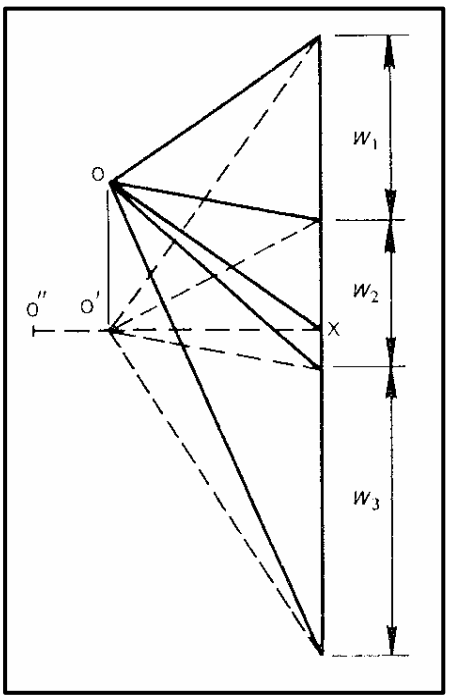

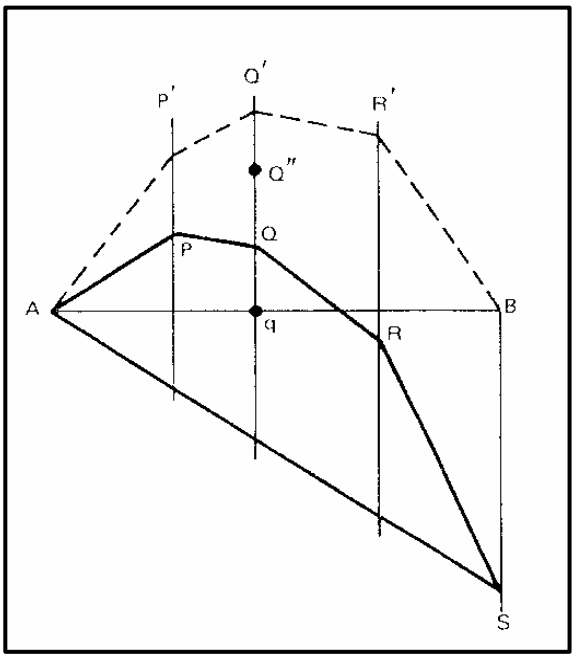

Figure 2.5. The Funicular Poligon (Heyman 1982, p.17). Figure 2.6. The trust line (Heyman 1982, p.17).

Chapter 3

FINITE ELEMENT METHOD AND APPLICATIONS ON MASONRY

Finite element method (FEM) is a powerful tool for numerical solution of wide variety of engineering problems including applications range from deformation and stress analyses of automative, aircraft, building and bridge structures to field analyses of heat flux, fluid flow, magnetic flux, seepage and other flow problems. In Finite Element Method, a complex region defining a continuum is discretized into simple geometric shapes called finite elements. The material properties are assigned to these elements and the governing relationships are considered over these elements and expressed in terms of unknown values at element nodes. An assembly process considering the loading and constraints, results in a set of equations. Solution of these equations gives us the approximate behavior of the system (Chandrupatla and Belegundu 1991, p1).

The reliability of the mathematical model created by FEM is related to the type of element selected, number of elements, the assumptions about the behavior of the elements and the data input for defining the material, geometric properties and the constraints and boundary conditions of the actual phenomena which is modelled.

More infromation on theory and applications of finite element method can be found in various books (Bathe 1996, Chandrupatla and Belegundu 1991, Zienkiewicz and Taylor 1987.a-b). In this chapter, the application of FEM on masonry analysis will be presented.

There are two different methods in finite element analysis of masonry, micro modeling and macro modeling. These approaches are presented in this chapter.

3.1. Micro Modeling

In micro approach the constituents of masonry, stone-brick and mortar, are modeled separately by taking into account their own constitutive relations.

Giambanco et al. modeled masonry with elastic bricks and interface models for the mortar joints. It is thought that all the nonlinear phenomena occur at the mortar joint which is reasonable in case of old masonry structures which have deteriorated mortars because of

environmental agents and weaker then the units (brick or stone). The yield condition for the mortar joints is given in Figure 3.1.

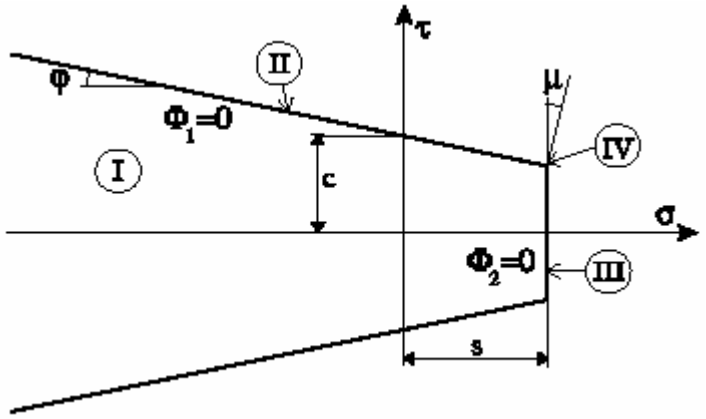

Figure 3.1. Yield condition for the mortar joint (Giambanco et al. 2001, p. 6496).

The regions at the Figure 3.1 denote different limit states and defined at the model. A cohesive frictional joint transition is considered in which during the loss of cohesion process the formation of a rough fracture surface is determined and for pure frictional state a tribological law is used to describe the contact surface. An asperity model is defined for the friction surface shown in Figure 3.2.

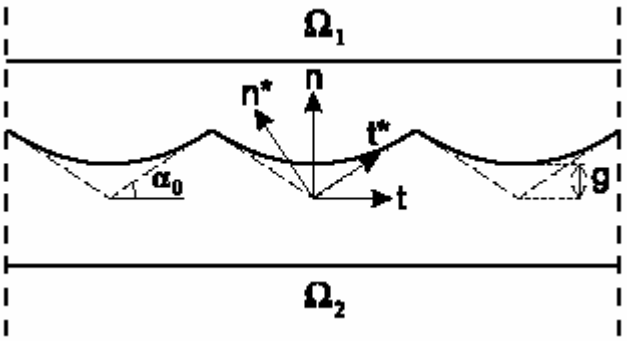

Figure 3.2. Asperity model (Giambanco et al. 2001, p. 6500).

The model was adopted to finite elements and 2 experiments were modelled. The results of experimental and numerical works agree, see Figure 3.3 (Giambanco et al. 2001).

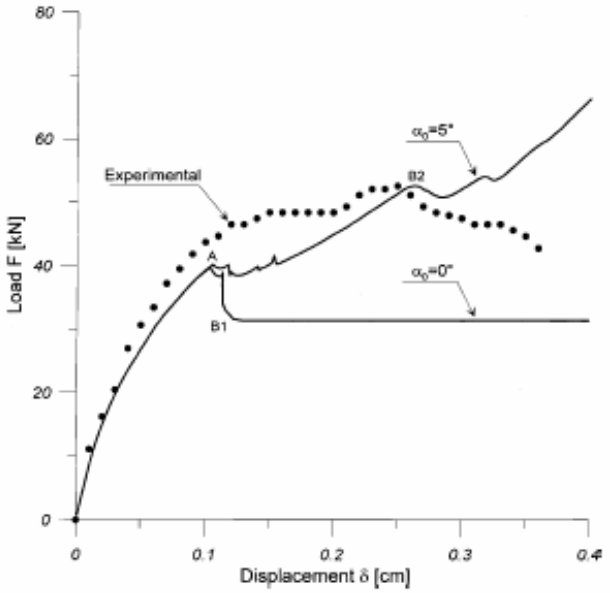

Figure 3.3. Experimental and numerical results (Giambanco et al. 2001, p. 6508).

Giordano et al. modelled masonry by micro approach by use of Finite Element Method with Discontinous Elements (FEMDE) and Discrete Element Method (DEM). For the FEMDE blocks are modelled using conventional continuum elements that may be linear or nonlinear while the mortar joints are modelled with Coulomb friction law with small dilatancy and no cohesion. An experiment was simulated by the model and close results are obtained from numerical simulation, see Figure 3.4 (Giordano et al. 2002, p. 1064). The results of FEMDE are obtained by CASTEM finite element soft ware.

Discrete Element Method (DEM) was also used for modeling masonry. While modeling with DEM, it is assumed that the structure is an assembly of blocks which are rigid or deformable. The blocks interact by unilateral elasto-plastic contact elements which has Coulomb friction criterion. DEM can model large deformations therefore can simulate the failure of a system. During the analysis, new contacts are created due to the motion of the system. UDEC soft ware was used for modeling with DEM. DEM was used for modeling an experiment and the comparison of the experimental and numerical DEM results are given in Figure 3.4. The results of DEM follows the experimental results closely, see Figure 3.4 (Giordano et al. 2002, p. 1058).

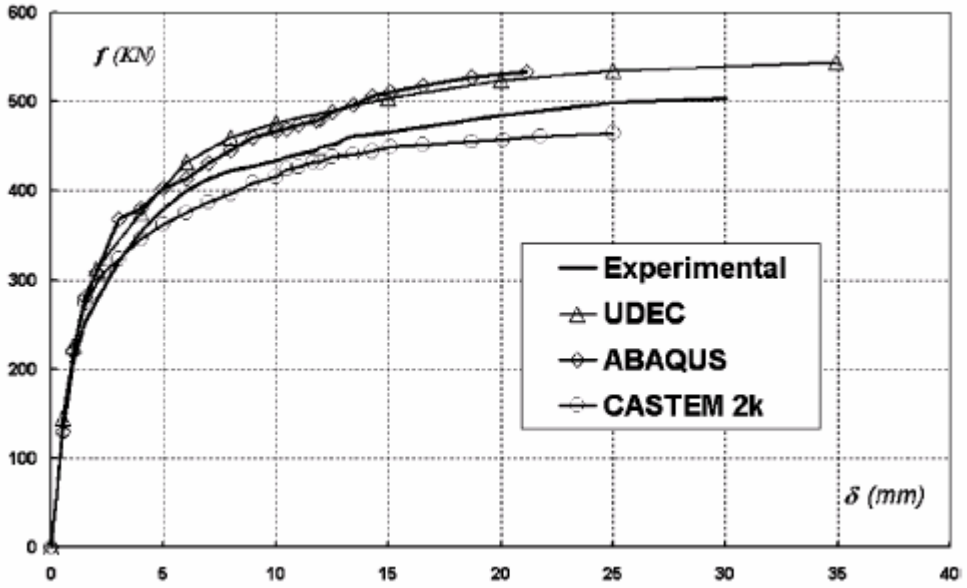

Figure 3.4. Experimental versus numerical results (Giordano et al. 2002, p. 1068).

A detailed micro modeling was presented by Lourenco (Lourenco 1996) therefore it is wise to give the works of Lourenco for micro modeling under a separate part.

3.1.1. Micro Modeling of Lourenco

Determining the failure mechanisms for masonry is one of the most important aspects of modeling masonry. Lourenco determined the failure mechanism of masonry as follows;

1. Cracking of the joints
2. At low values of normal stress, sliding along the bed or head joints
3. Cracking of the units in direct tension
4. Under normal stress enough to develop friction at joints, diagonal tensile cracking of the units
5. Under high normal stress because of mortar dilatancy, splitting of units under tension (Lourenco 1996, p. 43).

The failure modes listed above are presented at Figure 3.5.

The damage is concentrated in the weak joints and in potential pure tensile cracks in the units, placed vertically in the middle of each unit, see Figure 3.6. The interface elements, joints, are modeled as potential crack, slip or crushing planes. Also, the interface elements are

used to model potential cracks in the units. It is assumed that all the inelastic phenomena occur in the interface elements.

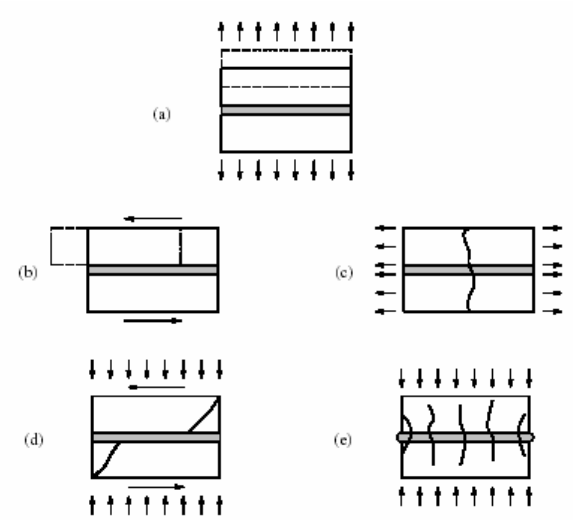

Figure 3.5. Masonry failure mechanisms: (a) joint tensile cracking; (b) joint slipping; (c) unit direct tensile cracking; (d) unit diagonal tensile cracking; (e) masonry crushing (Lourenco 1996, p.44).

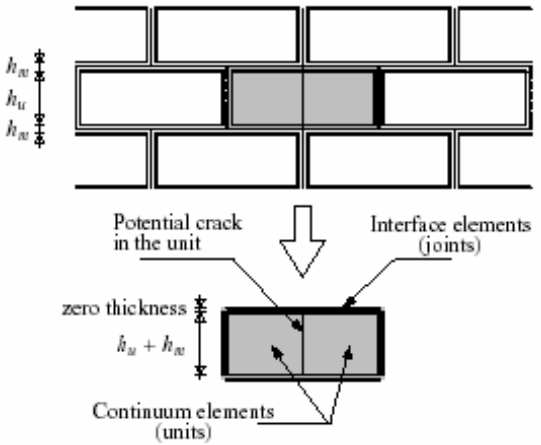

Figure 3.6. Modeling strategy. Units (*u*), which are expanded in both directions by the mortar thickness, are modeled with continuum elements. Mortar joints (*m*) and potential cracks in the units are modeled with zero-thickness interface elements (Lourenco 1996, p.45).

A composite yield criterion which defines a tension cut-off for mode I failure, a Coulomb friction envelope for mode II failure and a cap mode for compressive failure is developed for modeling the interface elements, is given in Figure 3.7.

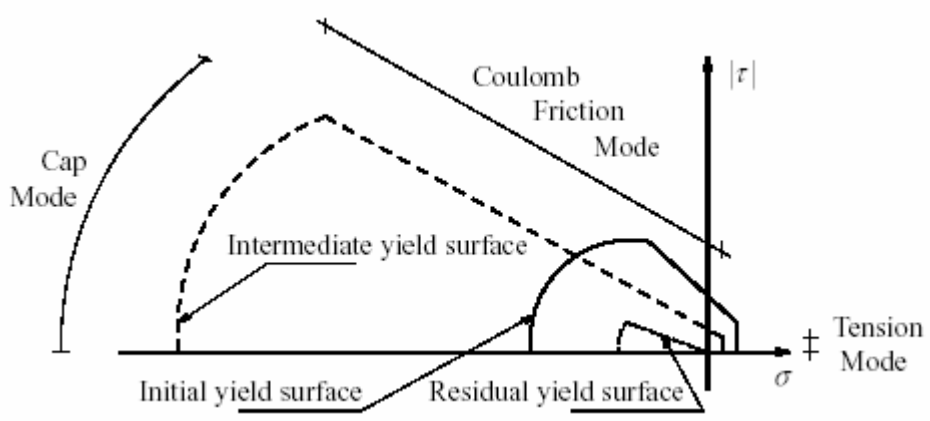

Figure 3.7. Composite yield criterion for interfaces (Lourenco 1996, p.49).

Isotropic softening is assumed which means that the percentages of the cohesion and tensile strength softening are equal throughout the entire degradation process. The formulation of the composite yield criterion for FEM analysis is given by Lourenco (Lourenco 1996).

For the validation of micro model, a number of tests were modeled which can be found in details at (Lourenco 1996, p.60). The experimental and numerical results are close to each other, see Figure 3.8. The “p” values at Figure 3.8 represent the different confining stresses applied at the test.

Detailed information about the theory, formulation and validation of micro modeling can be found at (Lourenco 1996).

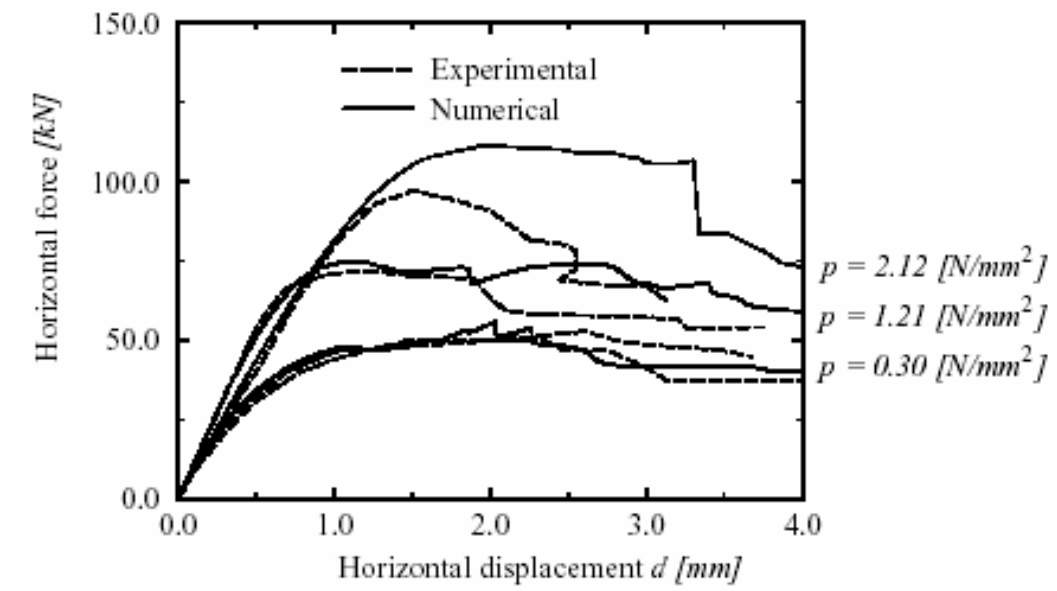

Figure 3.8. Load - displacement diagrams (Lourenco 1996, p.63).

The micro model is an effective approach for modeling tests of masonry panels with a limited number of constituents. Also, a part of a structure, i.e. a facade of a masonry structure with legible masonry weave to get the dimensions of the constituents of masonry, can be modeled by micro approach. On the other hand, modeling a whole structure with 3D by micro approach seems to be impossible not only because of computational hardship as there will be a vast number of elements created, but also because of the lack of data about all constituents geometry and dimensions.

Micro model can be effectively used for calibrating a macro model which will be presented in this chapter. Generally, the parameters of the constituents of the masonry can be determined by sampling and mechanical tests but the parameters of masonry for macro model can not be determined readily without complex structural tests. By using the micro model as a part of a structure as benchmark, the parameters of the macro model can be calibrated due to the comparison of the results. This will lead to reliable parameter estimation for macro model.

3.2. Macro Modeling

A whole masonry structure can not be modelled by micro model due to large number of constituents. Macro modeling in which a relation between average stresses and strains in

the composite material established, can be used for modeling a whole masonry structure (Lourenco 1996, p. 123).

There are fundamentally two aproaches for the failure of brittle structures; discrete approach in which cracking modifies the geometry and smeared approach in which geometry is fixed and cracking modifies constitutive law (Giordano et al. 2002, p.1059). Macro approach of masonry modeling is a smeared approach of brittle failure.

A fixed multi-crack model for concrete was used for macro modeling of masonry (Giordano et al. 2002, p.1060). According to Giordano concrete model can predict the masonry behavior very well as long as proper material definition is provided. ABAQUS FE soft ware was used to model two experiments by concrete model. The results of the tests by the numerical results are in close relation, see Figure 3.4.

A constitutive model of triaxial stress state for concrete was used to model masonry arch bridge barrel while Drucker-Prager material law was used for modeling the fill material of the bridge and consistent results were obtained with respect to field investigations (Fanning and Boothby 2001).

Koçak used Drucker-Prager constitutive law for modeling Küçük Ayasofya Mosque (former Sergius and Bacchus Church), (Koçak 1999).

Berto et al. defined an orthotropic damage model for modeling of masonry structures. It is stated that the development of damage may lead to change in symmetry of the material such that an orthotropic material may have changes towards a more general anisotropy. For that reason, scalar damage variables are defined in relation with each of the principal directions of anisotropy. A double pyramid with a rectangular base which has slopes corresponding to internal friction angles of the material, is defined as the limit surface, see Figure 3.9.

A number of comparisons between tests and numerical results were conducted and good agreement was obtained (Berto et al. 2001).

A detailed macro modeling was presented by Lourenco (Lourenco 1996) therefore it is wise to give the works of Lourenco for macro modeling under a separate part.

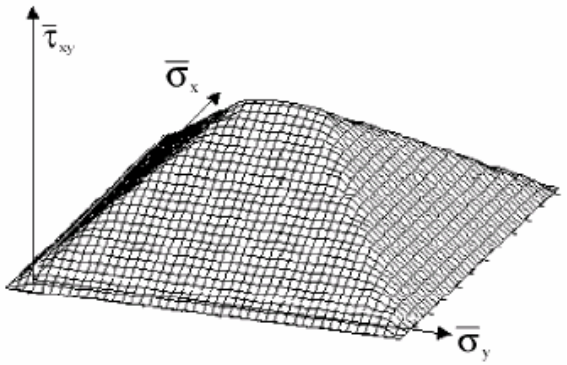

Figure 3.9. Limit surface for the damage model (Berto et al. 2001 p.133).

3.2.1. Macro Modeling of Lourenco

The geometrical arrangements of the units and mortar orthogonally give way to model masonry with anisotropic plasticity models, especially with orthotropic constitutive laws. A composite yield criterion was developed for modeling anisotropic materials under plane stress conditions. Tension failure was associated with a localized fracture process represented by cracking of the material and compressive failure was associated with a more distributed fracture process represented by the crushing of the material. For modeling the orthotropic behavior, a Hill type yield criterion for compression and a Rankine type yield criterion for tension was used, Figure 3.10.

The orthotropic Rankine type yield surface is given in Figure 3.11 while Hill type yield surface is given at Figure 3.12.

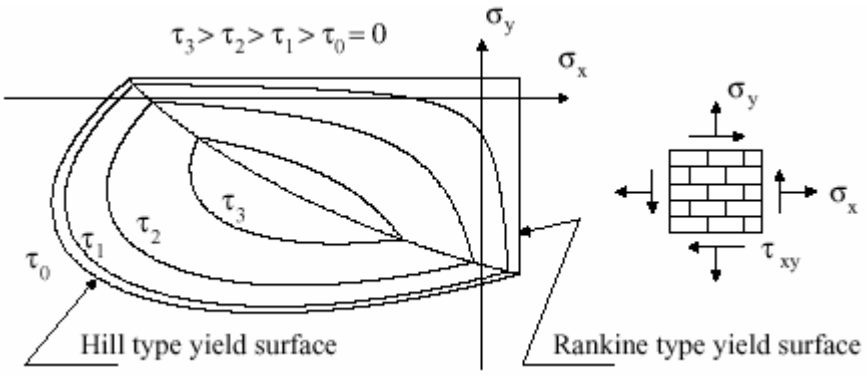

Figure 3.10. A composite otrhotropic yield surface for masonry (Lourenco 1996, p.126).

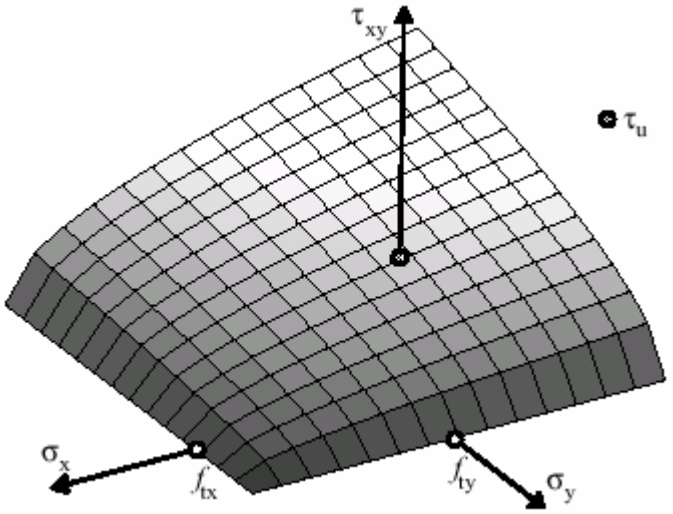

Figure 3.11 Orthotropic Rankine type yield surface (shown for $\tau_{xy}=0$) (Lourenco 1996, p.129).

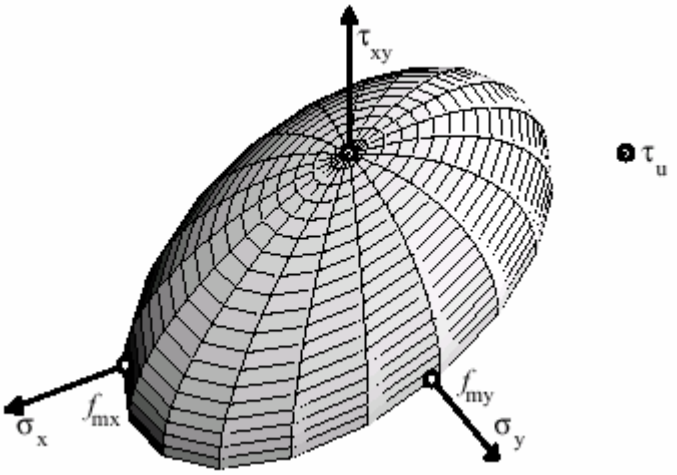

Figure 3.12 The Hill type yield surface (Lourenco 1996, p.133).

The damage of masonry was modelled with a smeared approach in which the damaged material was taken as continuum and the damage was represented by the stiffness degradation.

The material model has seven strength and five inelastic parameters which can be determined by uniaxial and biaxial tests on masonry panels.

The validation of the model was achieved by comparing test results with respect to numerical results and good agreement was found, see Figure 3.13.

Details about the model, formulations and validation can be found at (Lourenco 1996).

Some macro models referred here have too much parameter to determine and especially when modeling a historical masonry, application of the tests on masonry walls for parameter determination can be impossible. Moreover, a sensibility analysis can be time consuming with so much parameter. Development of an easy to use macro model with parameters that can be determined by tests on constituents of masonry is a challenging future work.

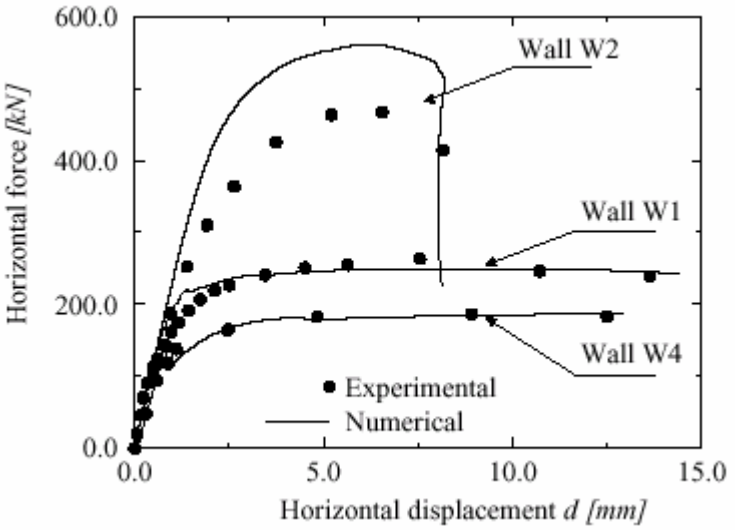

Figure 3.13 Load–displacement curves of experiments and numerical models (Lourenco 1996, p.163).

Chapter 4

CASE STUDY: URLA KAMANLI MOSQUE

The procedures of assessment have been applied on a sample structure, Urla Kamanli Mosque, which is in Urla, Izmir, Turkey. In this chapter, these procedures will be presented.

4.1. Description of the Structure and History Investigation

The structure is on cadastral block of 297, map no of 75, plot no of 1 (from interview with Cadastral Office of Urla). The structure belongs to an ancient fund named "Yahsi Bey Vakfi" which is not active now therefore the owner of the structure is General Directorate of the Funds of Turkey. Urla Kamanli Mosque is a member of a group of structures named "Yahsi Bey Külliyesi", which contains a Turkish Bath, a tomb, two fountain and a primary school. Altough there is not any written document kept about the construction date and constructors, by using comparative methods of architectural elements in light of arthistory it is concluded that the structures date back to an era between early 14^{th} century to mid 15^{th} century (Erim 1995, p. 41).

The structure has a square plan of 10 m×10 m with a wall thickness of 110 cm and the height of the structure is 12.66 m. The walls of the structure are stone masonry with limestones and thick mortar joints. The window arches and the dome are brick masonry with thick mortar joints. The transition from walls to dome on the corners is achieved by use of trompes which are also brick masonry, see Figure 4.1.

The structure has not been used for a long time and open to all environmental effects since the windows and the door of the structure do not exist. Especially, in the first 1 m above the ground level, there is an extensive material degradation because of moisture. The wooden lintels which should surround the walls (along the inner and outer perimeters) at two levels, do not exist, as can be seen in Figure 4.1. Because of that the cross sections of the walls at the wooden lintel levels decrease considerably which challenges the structure.

On the east and west walls, extensive cracks follow the path way of the windows and joins at the key stone of the dome, see Figure 4.1 and Figure 4.2. In this research, the causes of these cracks have been investigated by finite element analyses.

The part of the minerat above the balcony collapsed during a strom, as locals commented, see Figure 4.3. Plant formations on the structure challenges the structure as well; a tree just in front of the minerat has a height of 3 m, which is a clear sign that the structure is not used for a long time. The drum and the west wall of the structure have a more qualified weave than the other walls, see Figure 4.4. According to a conversation with Ferhan Erim who is an arthistorian worked on the structure, because of the primary school on the west side of the mosque, that part is a social zone and so has a more qualified weave than the other walls.

Figure 4.1. East section.

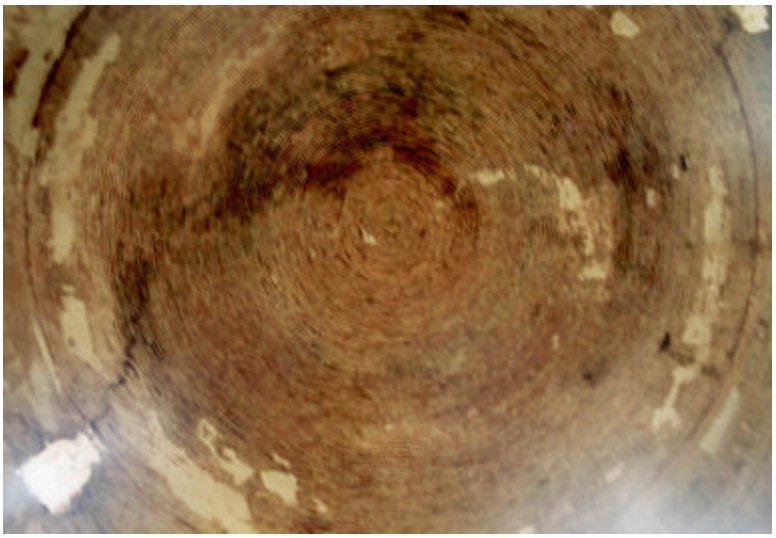

Figure 4.2. Brick masonry dome and the cracks.

Figure 4.3. South Elevation.

Figure 4.4. West Elevation.

4.2. Measurement Survey

The measurement survey was done for purpose of determining the dimensions of the structure, the localizations of the cracks and material degradations for use in 3 dimensional finite element modeling of the structure. The measurement survey was done by classical techniques and during the survey, the structure was investigated in a more detailed way. Measurement survey was achieved by the collaboration of the Architectural Restoration Department at IZTECH. Below are given the plan and the north elevation Autocad drawings of the structure, Figure 4.5, Figure 4.6.

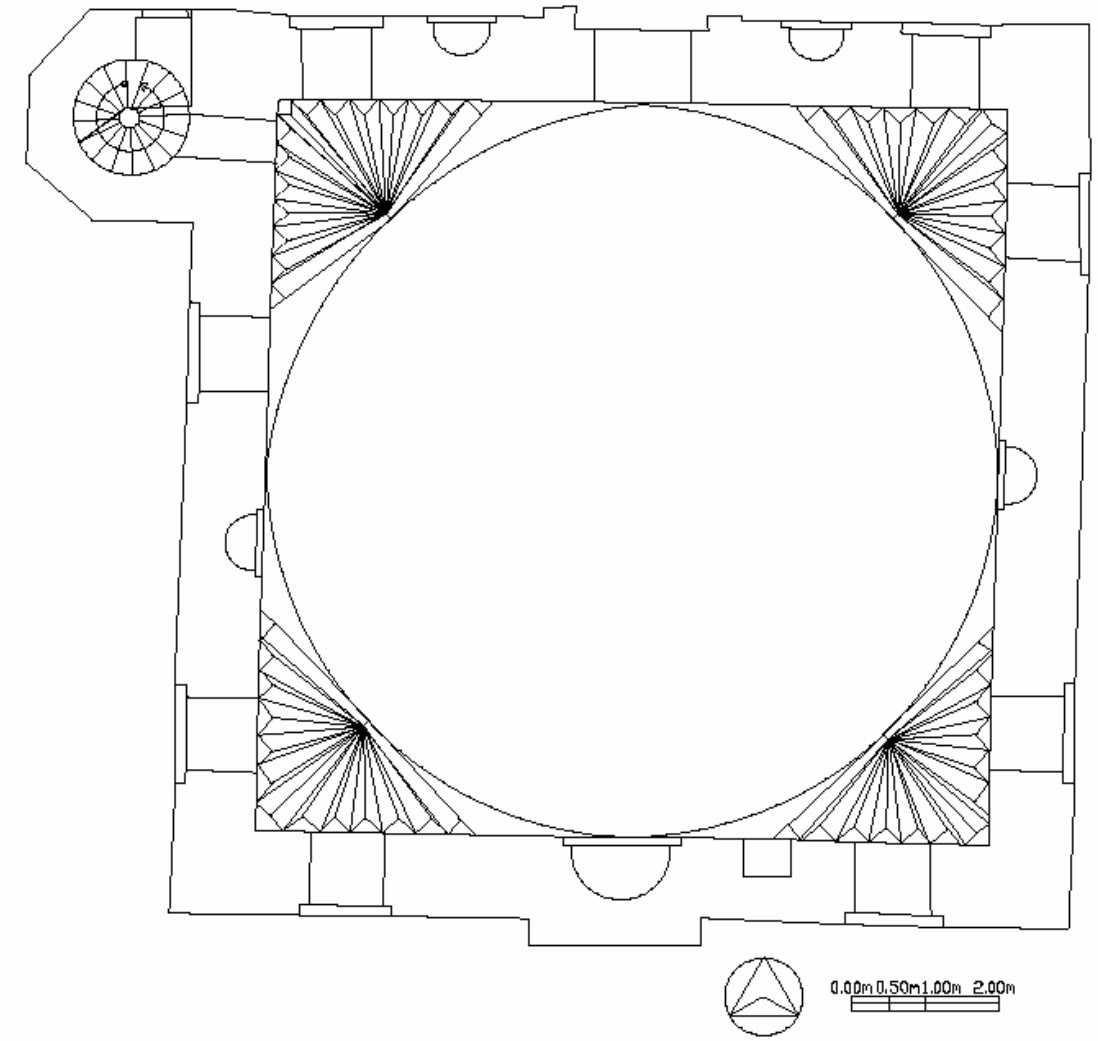

Figure 4.5. Plan (Drawn by Kader Reyhan)

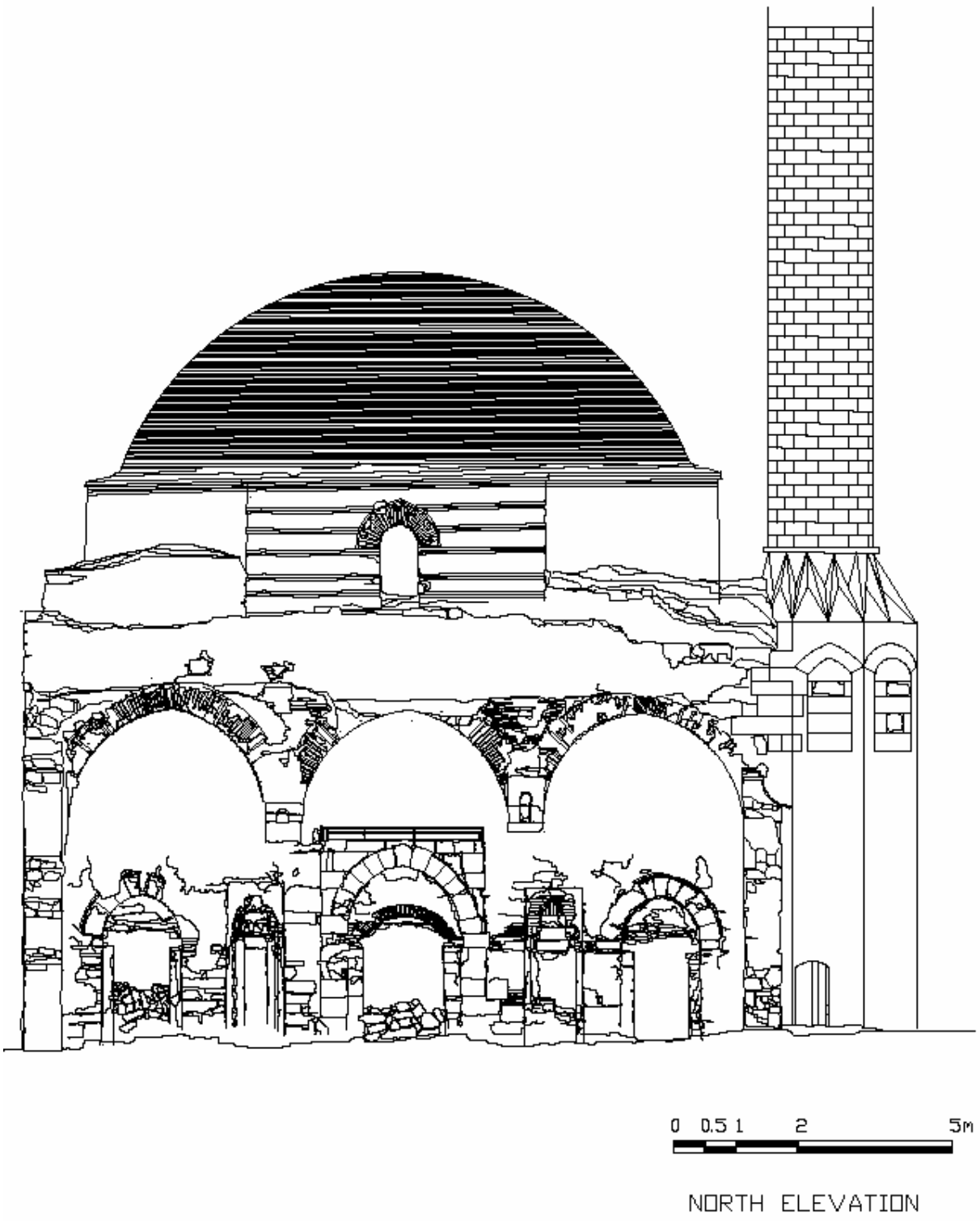

Figure 4.6. North Elevation (Drawn by Kader Reyhan)

4.3. Long Term Observations

In order to understand the behavior of the structure, longterm observations have been carried on insitu for relative mositure**,** crack opening and relative displacements of the walls.

4.3.1. Relative Moisture Observations

There is a vast amount of material degradation which challenges the structure. Especialy, in the first 1 metre from the ground level, in the structure, material deterioration can be observed visually. These regions are thought to be vulnerable in case of a seismic loading where high amount of the shear forces will act on.

It has been observed that, since the structure does not have windows, door and insulations for water, the moisture level in the structure is high. When it rains, the water passes through the dome and rain seep in the structure and since it is a closed space, evaporation rate is low and the moisture level is always higher in the structure than out of the structure.

The material deteriorations are believed to be mostly due to high moisture level in the structure. The relative moisture of the stones and mortars at each section and at bottom and top, totally at 16 locations have been observed by a monthly period. A moisture meter of James Instruments Inc. which uses electromagnetic methods for determining the relative moisture to a depth of 1 inch (25mm) has been used. The instrument is a nondestructive equipment and gives moisture in the Eq. 4.1

$$R(\%) = \frac{W_W}{W_T} \times 100 \qquad \text{Eq.4.1.}$$

where R(%), W_W and W_T are relative moisture, weight of the water in the specimen and total weight of the specimen, respectively. In order to measure the moisture in a material, the circle at the back of the device is touched to the material paying attention not to leave air space between device and the material. The relative moisture of the material is read from the digital screen of the device, see Figure 4.7. The device can be used at three different density levels; HIGH for concrete, brick, stone, granite, sand, soil, rock; MEDIUM and LOW depends processing technique for wood, food, paper, textile materials etc.

Figure 4.7. Moisture meter application.

In general the relative moisture at the bottom stones are higher then the stones at the top measurements, as expected, see Figure 4.8, Figure 4.9, Figure 4.10, Figure 4.11. The relative moisture values at the east section for mortar at the bottom are higher then the values for the mortar at the top, as expected, see Figure 4.11. The relative moisture values of mortar at the west and north sections at the bottom are lower then the values at the top and for the south section they are nearly same which are totaly unexpected observations, see Figure 4.8, Figure 4.9, Figure4.10. These unexpected results occured because the mortar is highly deteriorated and it is almost impossible to obtain a full contact between the device and the mortar surface without having any air between them. As the mortar at the bottom is deteriorated more than the mortar at the top, the surface roughness increases for the mortar at the bottom which leads to improper measurements and low values of moisture measurement. In order to overcome this difficulty, a moisture meter with needle which is penetrated in the sample to observe the level of moisture, may be used but this will destruct the mortar localy and will lead to take the other measurements from different places. The change of moisture values with respect to seasons have been observed. In general, in the winter times the moisture is high where as in the summer the moisture is low, as expected, see Figure 4.11. The observed values are given in Table 4.1.

Table 4.1. Relative Moisture observations R(%).

NO	East Bottom Stone	East Bottom Mortar	East Top Stone	East Top Mortar	West Bottom Stone	West Bottom Mortar	West Top Stone	West Top Mortar	South Bottom Stone	South Bottom Mortar	South Top Stone	South Top Mortar	North Bottom Stone	North Bottom Mortar	North Top Stone	North Top Mortar	Date
1	14	5.1	13	4	7.8	4.2	9.8	8.5	13.5	10.6	10.12	6.06	13.7	3.9	11.9	6.7	24.01.2003
2	13.4	3.38	9.6	1.22	10.9	3.4	8.1	5.5	10.5	6.6	6.5	7.7	11.5	4.1	11.4	6.1	24.02.2003
3	13.6	5.6	7	1.3	12.56	2	7.5	3.5	11.2	5.2	6.2	4	11.2	4.1	12.3	6.8	24.03.2003
4	12.6	6.3	9.6	1.35	7.9	2.5	5	7.77	12.2	7.43	8.27	4.06	10.6	4.3	13	6.8	14.04.2003
5	12.7	4.5	9.3	1.65	9	2.09	8.73	6.72	11.5	5.1	9.96	2.33	11.2	5.6	10.76	6.55	24.04.2003
6	11.3	5	10.3	1.2	6.5	2.3	4.2	6.5	12.6	5.1	9	6	13	4.5	11.8	6	26.05.2003
7	11.04	5.4	6.9	1.2	6.06	1.35	10.1	3.5	11	5.2	7.2	2.1	11.1	3.1	10.5	2.3	01.07.2003
8	12.4	4	7.1	1.55	8.1	3.8	8.9	4.2	8.9	4.3	11.1	5.7	11.6	4.7	8.8	4.8	23.07.2003
9	13.12	5.5	6.88	1.2	12.4	4	9.4	4.35	12.3	6	7.03	6.02	12.2	5.95	11.66	6.7	18.09.2003
10	13.5	6.35	12.13	1.8	6.1	2.8	11.7	4.5	11.5	5.95	11.23	9.32	11.7	5.4	9.52	8.9	05.11.2003
11	14	7	10.75	2	5.6	3.9	11.1	5.1	11.8	5.7	10.3	8.6	11.9	6.1	12.8	9.5	02.12.2003
12	10.1	5.5	10.75	1.28	6.8	4	9.78	5.6	12.5	6.2	10.8	4.7	12.4	6.2	12.1	8.3	27.01.2004
13	14.06	7.4	10.25	1.63	7.73	4	11.34	2.8	11.52	6.6	10.27	10.83	12.33	6.9	12.63	9.54	24.02.2004
14	13.7	6.2	11.5	3.6	6.3	4.2	11.2	3.3	11.4	6.2	10.86	10.8	11	3.8	11.97	7.2	24.03.2004
15	11.2	7.1	11.3	3	5	5.2	10.3	4.3	11.2	8.3	10.3	12.5	11.3	5.7	12.1	7.9	28.04.2004
16	12.8	5.3	10.3	2.1	4.6	4.6	11.2	3	12	7.1	10	12.1	10.7	4.3	11	3.5	01.06.2004

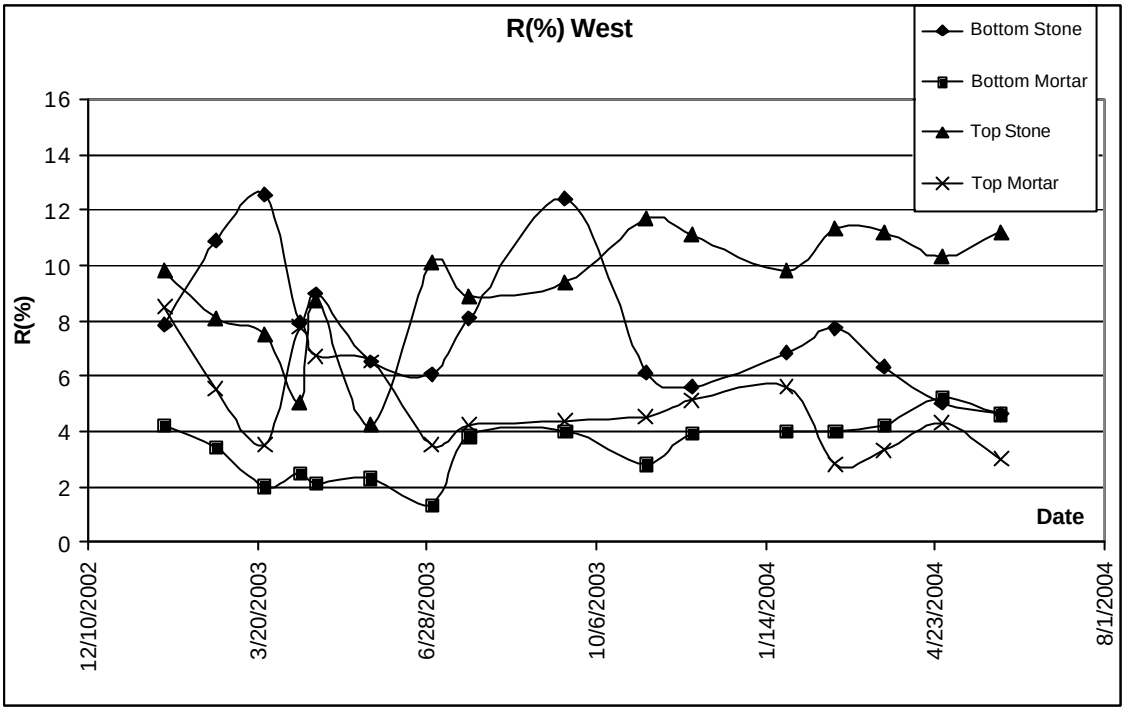

Figure 4.8. Relative moisture at west section

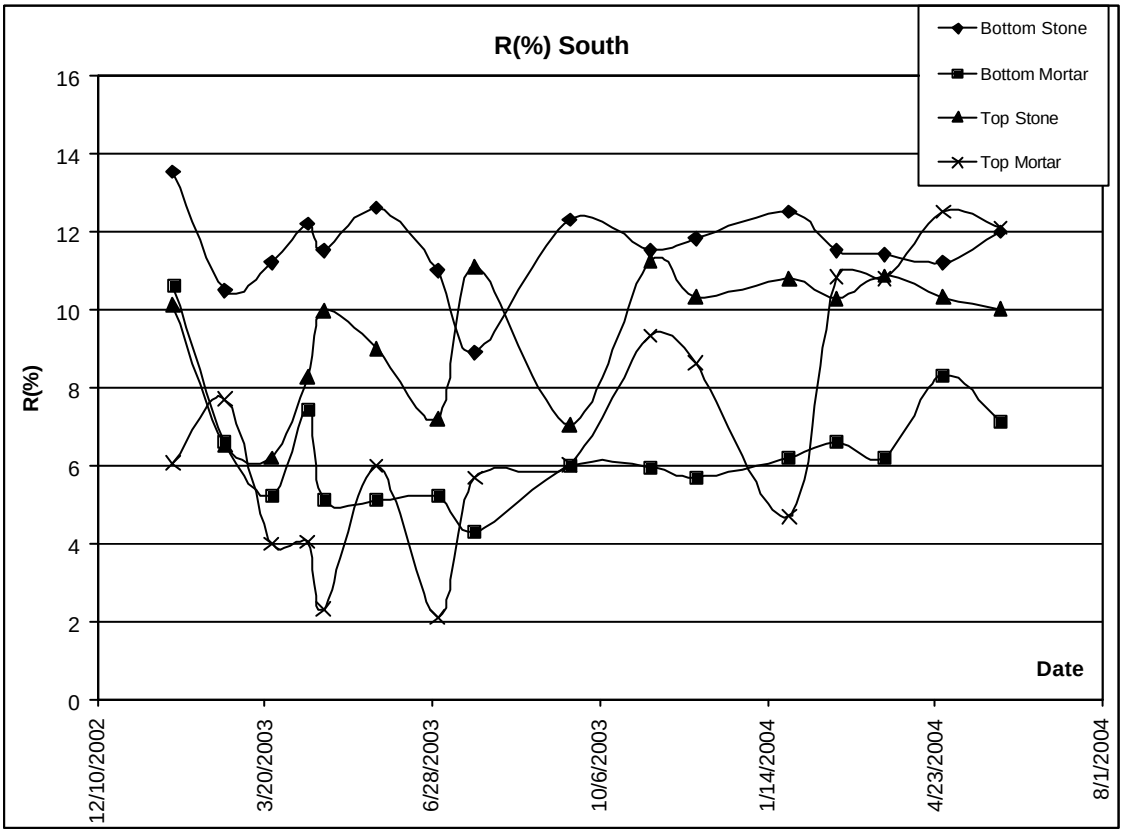

Figure 4.9. Relative moisture at south section

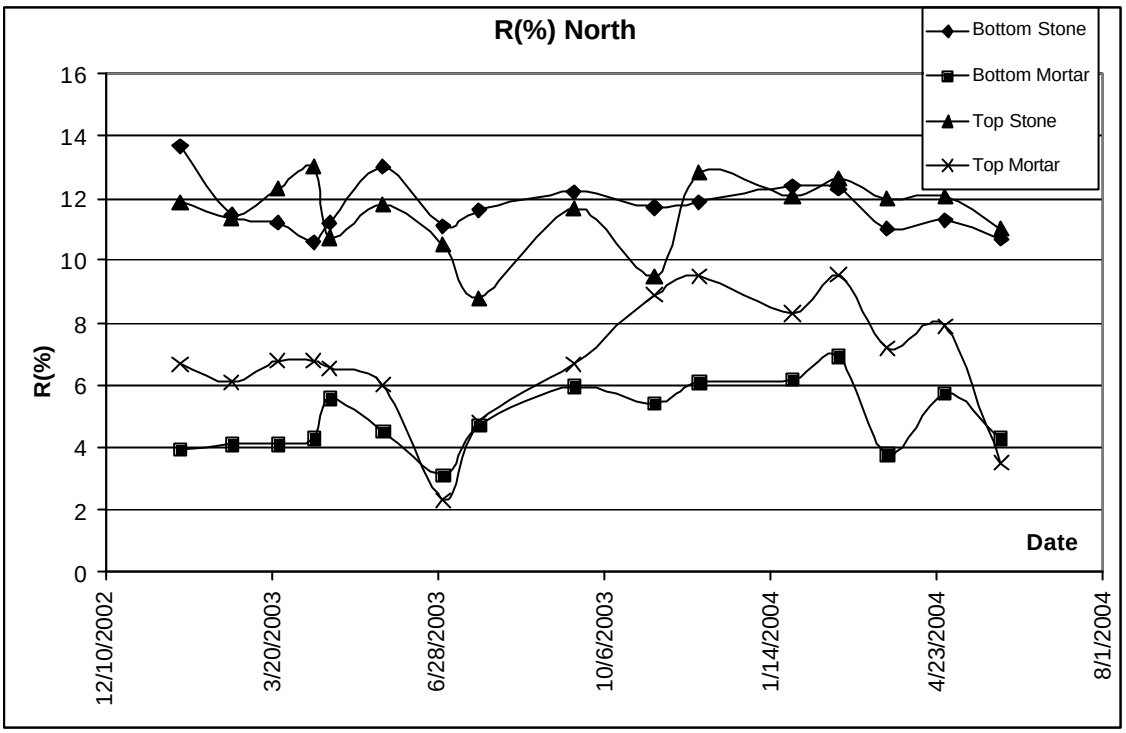

Figure 4.10. Relative moisture at north section

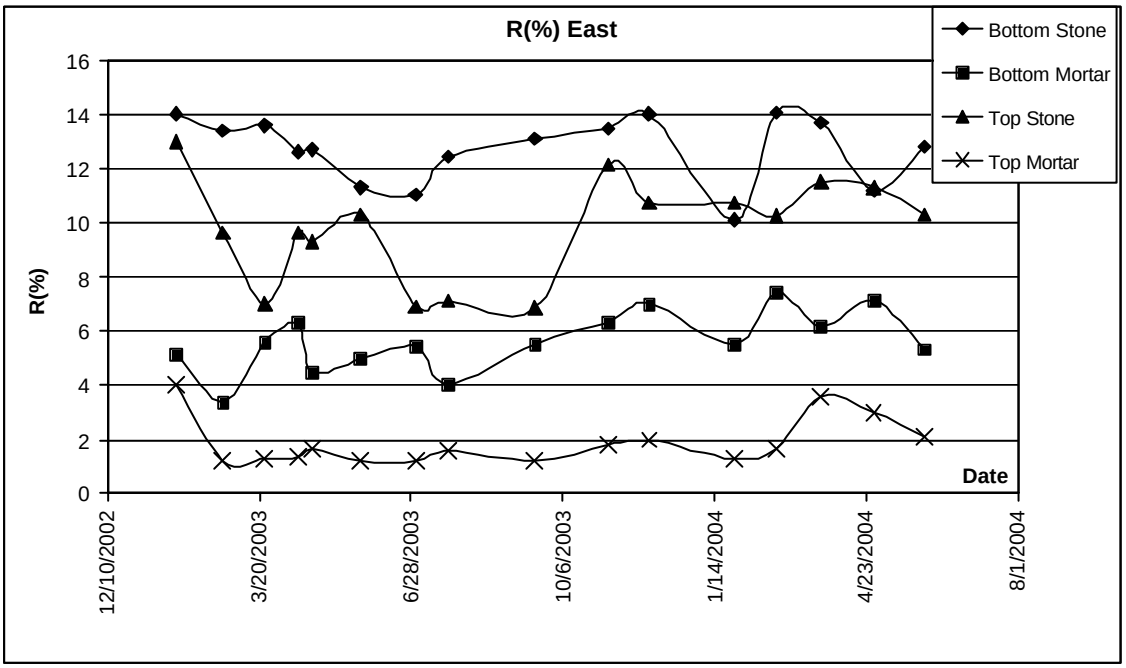

Figure 4.11 Relative moisture at east section

4.3.2. Crack Opening Displacement Observations

The structure has massive cracks at the east and west walls which unite at the key stone of the dome. In order to understand the behavior of the cracks the crack opening displacements have been measured monthly. The measurements have been made on cracks at east and west sections and elevations.

In order to make the measurements a Wykeham Farrance crack measuring gauge has been used which has a precision of 1/100 mm, Figure 4.12. Two studs were attached at opposite sides of a crack by use of epoxy adhesive. By using a calibration bar which has nodes at 10 cm and 5 cm apart, the device has been calibrated to zero with respect to 5cm or 10cm. The distance between the studs has been measured. The other readings were made by calibrating the device by the same value as was made at the beginning for that pair of studs. The differences between the consequent measurements give us the opening-closing of the crack.

The data collected during the observations are given in Table 4.2. As the studs have been subject to out side wheathering, the ones on the east and west elevation had dropped. New studs attached and the observations were taken. Only the east elevation horizontal studs were not attached again after they dropped 2nd time. These information are also available at Table 4.2.

Figure 4.12. Crack measuring device

The calibration values for each observation point are given by R in Table 4.2. On the east elevation, one stud was attached on one side and the other two on the other

in such that one of them makes an almost vertical line and the other makes an almost horizontal line with the stud attached on the other side.

Table 4.2. Crack opening observations (mm).

No	East Section Bottom R: 10cm	East Section Top R:10cm	East Elevation Horizontal R:10cm	East Elevation Vertical R:10cm	West Section R:10cm	West Elevation R:5cm	Date
1	-0.03	0	0	0.08	0.68	0.05	24.12.2003
2	-0.09	-0.07	-0.18	-0.1	0.63	-0.02	10.01.2003
3	-0.08	-0.07	-0.14	-0.14	0.64	stud drop	24.01.2003
4	-0.08	-0.04	-0.14	-0.08	0.69	new stud	24.02.2003
5	-0.09	-0.09	-0.25	-0.13	0.66	0.02	24.03.2003
6	-0.15	-0.19	stud drop	stud drop	0.62	0.1	14.04.2003
7	-0.12	-0.18	new stud	new stud	0.62	0.05	24.04.2003
8	-0.16	-0.22	-38.94	0.37	0.57	0.01	26.05.2003
9	-0.17	-0.21	-39.12	0.42	0.56	0.04	01.07.2003
10	-0.16	-0.2	-38.9	0.44	0.54	0.01	23.07.2003
11	-0.06	-0.06	-38.54	0.67	0.58	0.03	18.09.2003
12	-0.06	-0.05	-38.61	0.72	0.62	0.08	05.11.2003
13	-0.03	-0.05	stud drop	0.73	0.66	0.06	02.12.2003
14	-0.03	-0.03	stud drop	0.58	0.76	0.11	27.01.2004
15	-0.09	-0.1	stud drop	0.49	0.71	0.08	24.02.2004
16	-0.14	-0.17	stud drop	0.41	0.63	0.07	24.03.2004
17	-0.13	-0.16	stud drop	0.45	0.62	0.05	28.04.2004
18	-0.12	-0.15	stud drop	0.39	0.6	0.05	01.06.2004

The east section one and two observations have similar trend. There is a crack closure behavior in summer whereas there is crack opening behavior in winter, see Figure 4.13. This behavior can be seen for the other observations as well. The reason for the crack closure at summer and opening at winter may be because of underground water movements. Also, the calibrating bar used before every measurement may be effected by the varying temperature by means of length. In the summer time, when it is hot, the bar extends and the cracks may seem to be closed whereas in the winter the bar shortens and the cracks may seem to be opened.

In order to over come this malfunctioning due to temperature, the crack measuring gauge can be used without the calibration bar. The digital unit can be closed to one end then calibrated to zero and the measurement can be conducted. Temperature

problem was not foreseen by the researcher so this proposed technique could not be applied at this study.

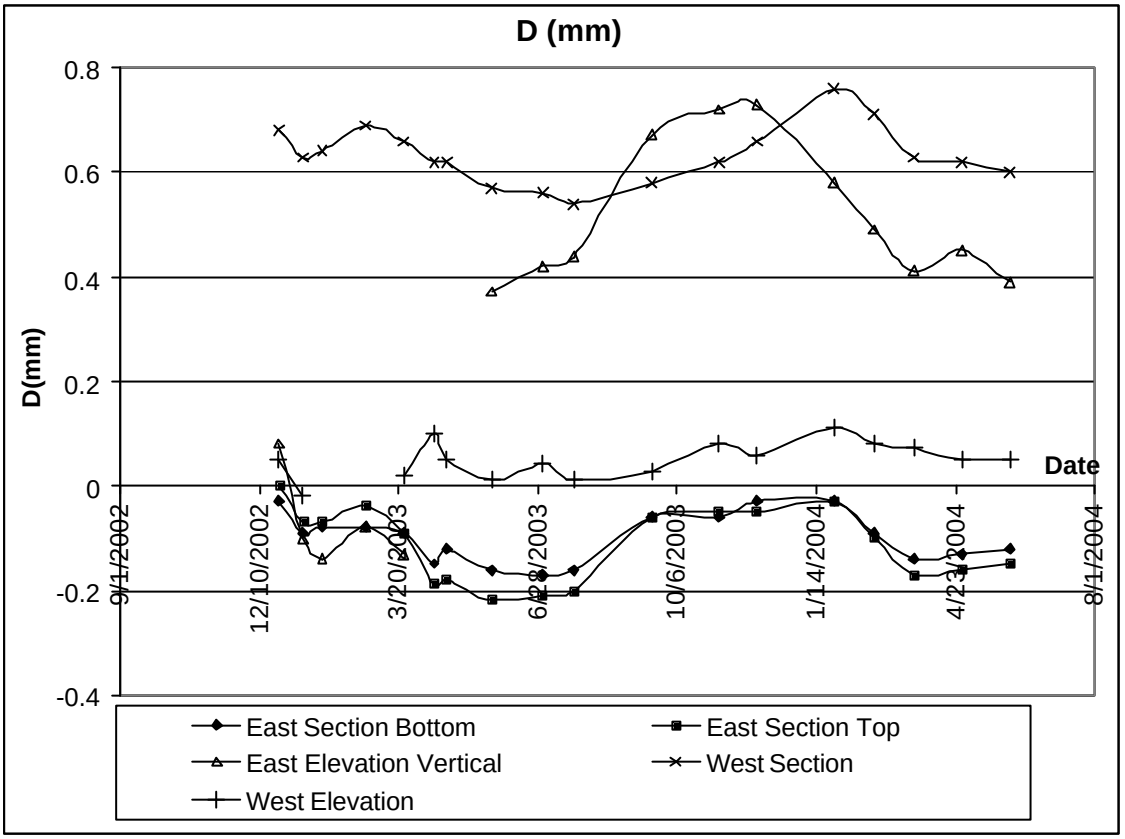

Figure 4.13. Variation of crack opening displacements.

4.3.3 Settlement Observations

The reason of the cracks on the east and west walls have been thought to be differential settlement. In order to observe the behavior of the structure due to settlement, displacements of the walls have been observed.

For displacement observations two studs were attached on opposite sides of the walls by epoxy adhesive. The places of the studs are given in Figure 4.14. By using geodetics techniques, a polygon net was created for the coordinates of the studs. The coordinates of the studs are given in Table 4.3. The Z coordinates represents the height of the studs where the X and Y coordinates are on the horizontal plane.

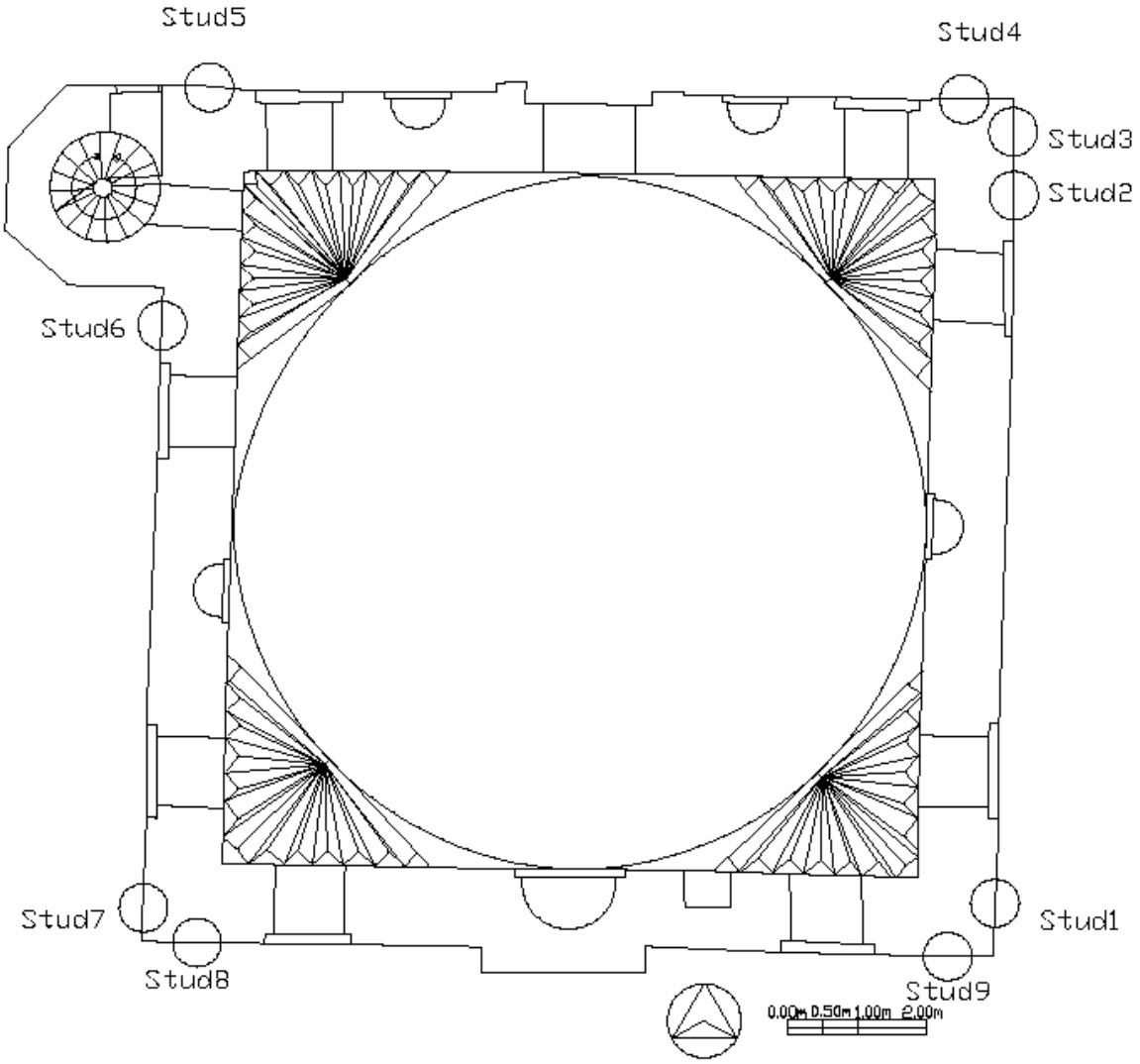

Figure 4.14. Locations of the studs

Table 4.3. Settlement observations.

Stud No (26.05.2003)	Y	X	Z	Distance(m)		Stud No (18.09.2003)	Y	X	Z	Distance(m)
1	135.169	100	97.566			1	135.166	100	97.564	
2	130.072	88.948	96.608	12.1707		2	130.069	88.945	96.606	12.1734
3	130.064	88.939	96.61	12.1822		3	130.062	88.936	96.608	12.1845
4	119.719	100	101.575			4	119.715	100	101.57	
5	117.422	90.273	101.605	9.99454		5	117.42	90.27	101.602	9.997
6	110.116	100	103.527			6	110.114	100	103.525	
7	108.292	91.194	103.637	8.99292		7	108.29	91.196	103.635	8.99096
8	114.848	100	99.206			8	114.846	100	99.203	
9	106.924	91	99.822	11.9912		9	106.923	90.998	99.82	11.9921
Stud No (27.01.2004)	Y	X	Z	Distance(m)		Stud No (1.06.2004)	Y	X	Z	Distance(m)
1	135.167	100	97.565			1	135.168	100.01	97.565	
2	130.07	88.945	96.607	12.1734		2	130.071	88.945	96.608	12.1825
3	130.062	88.935	96.608	12.1859		3	130.063	88.937	96.609	12.1931
4	119.715	100	101.569			4	119.716	100	101.57	
5	117.421	90.271	101.603	9.99579		5	117.421	90.271	101.603	9.99602
6	110.114	100	103.525			6	110.114	99.999	103.526	
7	108.291	91.195	103.634	8.99174		7	108.291	91.195	103.636	8.99076
8	114.846	100	99.2			8	114.846	100	99.204	
9	106.922	90.997	99.821	11.9935		9	106.923	90.999	99.821	11.9913

The distances are found by using Eq. 4.2.

$$D = \sqrt{\left((X_2 - X_1)^2 + (Y_2 - Y_1)^2\right)} \qquad \text{Eq. 4.2}$$

where X and Y values are the coordinates of two studs at the same elevation.

The amounts of separation of the walls are found by taking the differences of the distances at the dates 26.05.2003 and 27.01.2004. In the east wall maximum separation occurs which is approximately 3.6mm. In the north and south walls there are also separations with values 1.25mm and 2.25mm, respectively. For the west wall, there is a 1.18mm contraction observed, Figure 4.15.

When the first and the last observations are compared there are decreases in heights especially for the studs at the north elevation called stud 4 and 5, which means that there is settlement towards north direction, see Figure 4.16. Also the greatest

separation was observed in the east wall as in Figure 4.15 which also may be a sign of settlement at the north wall of the structure.

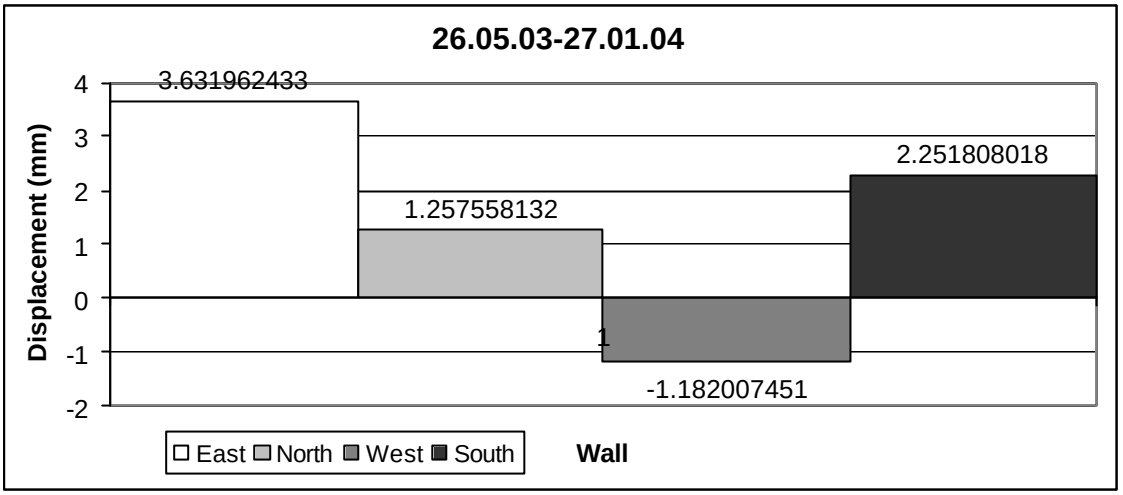

Figure 4.15. The separations of the walls.

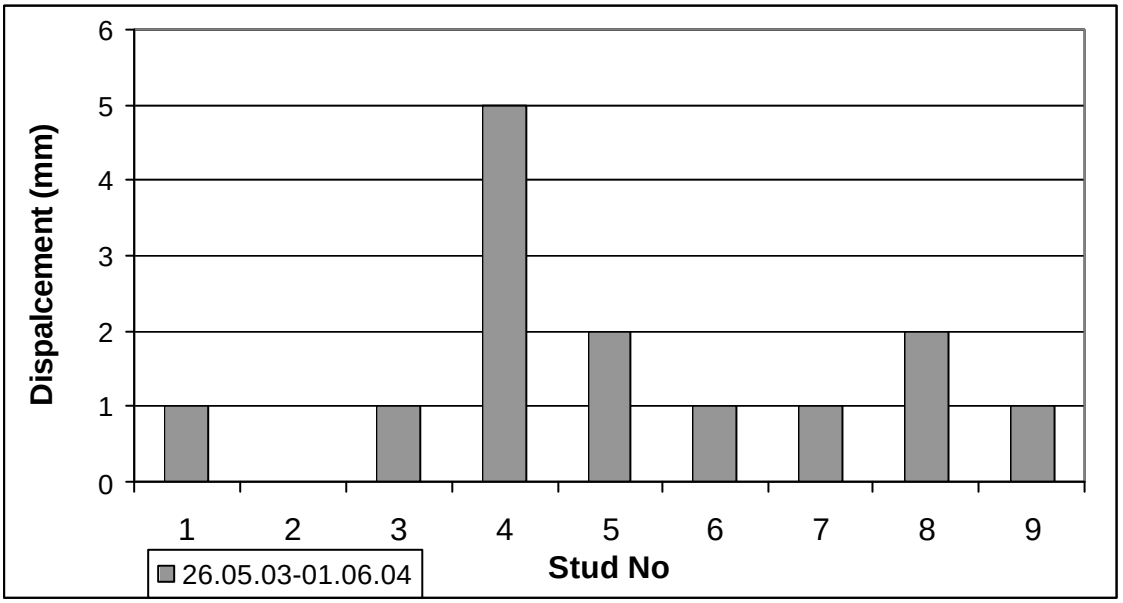

Figure 4.16. The vertical displacement of the studs between 26.05.03-01.06.04

4.4. Material Tests on Stone, Brick and Mortar

In order to determine the parameters needed for finite element modeling, material tests have been applied on constituents of masonry. Nondestuctive and destructive tests have been applied on stone, brick and mortar.

While taking samples from the structure, care was shown in order to comply with the below facts;

- Stones and bricks defining the architectural dimensions which may be used in future surveying works were not taken, i.e. corner stones. In general the fallen stones and bricks which belong to the structure were taken.
- Samples strong enough to cut out core samples were selected. Highly deteriorated samples which will break down during core drilling were left.
- Samples large enough to cut out core samples of diameter D=54mm, height H=15mm for stones and diameter D=25mm for bricks were selected.
- The number of samples were limited in order not to destroy the original materials of the historical structure.

4.4.1. Tests on Stone

The stone used at the construction of the structure is roughly cut limestone. The dimensions of the stones are variable in a range of 15cm to 50cm. The stones used at the west elevation were cut in a more precious way.

Four stones were chosen. The places of the stones in the structure are given in Figure 4.17. The stones were taken to the laboratory and cylinder core samples of diameter D=54mm were drilled out, see Figure 4.18. The heads of the samples were cut with cut of machine. Test samples for indirect tension test with height of H=30-50mm and samples for uniaxial compression test with heights of H=108-120mm were prepared.

The heads of the cylinder core samples were emeried by iron dust in order to have perfect cylinder samples that have heads which are paralel, see Figure 4.19. In Figure.4.20, all of the stone core samples can be seen.

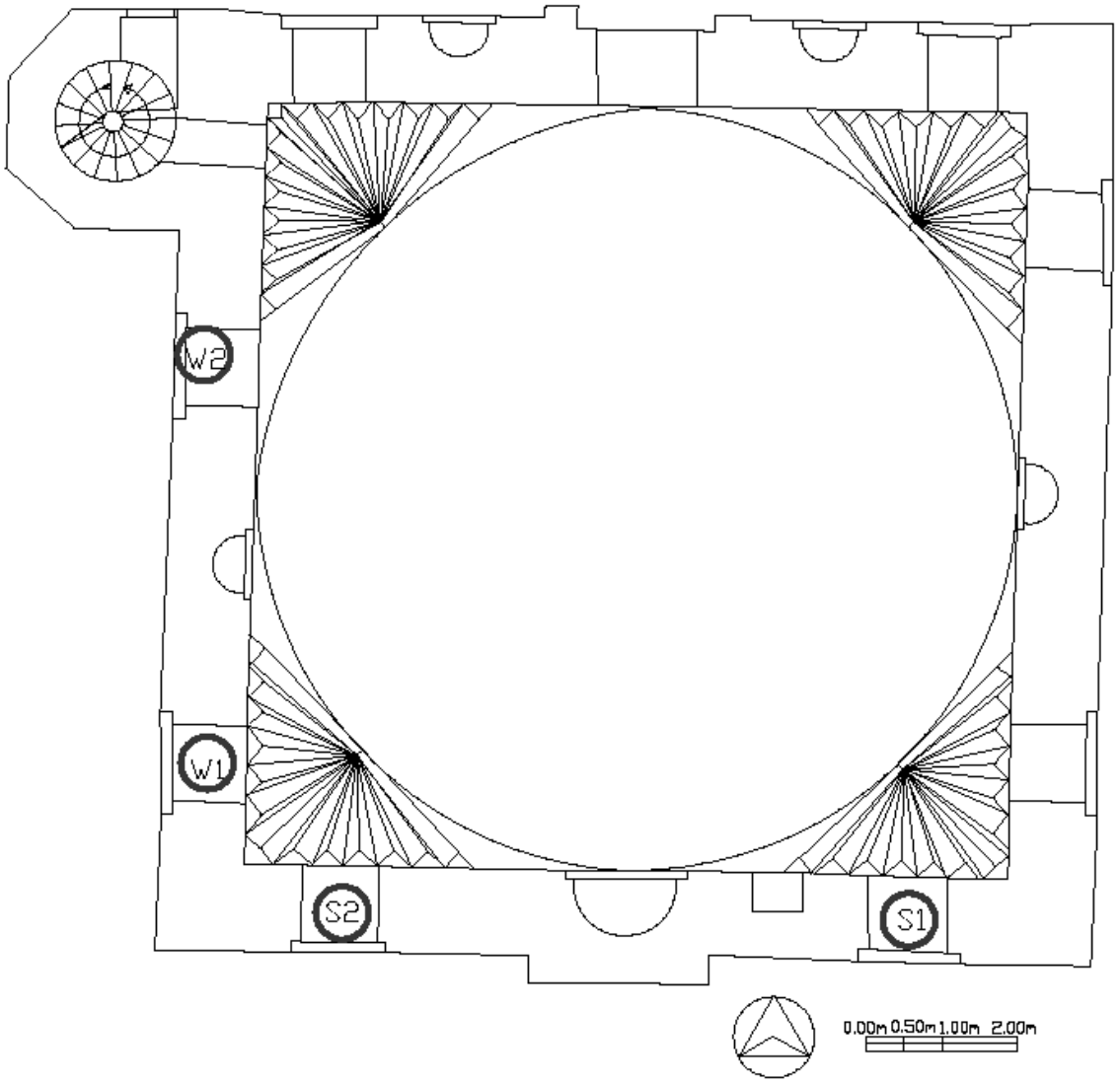

Figure 4.17. Places of the stone samples.

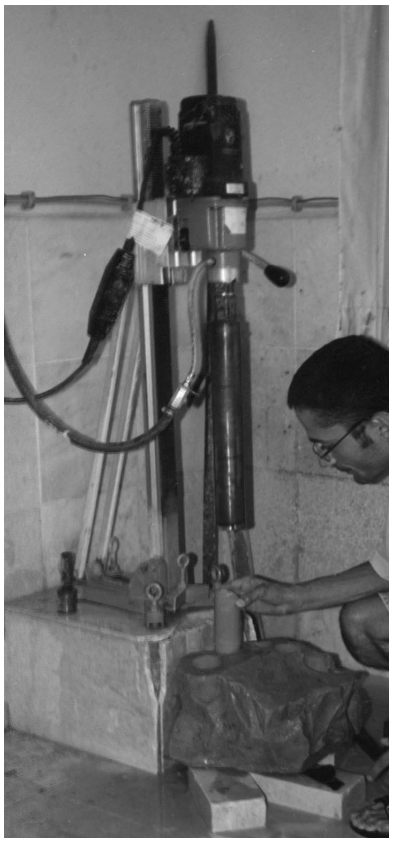

Figure 4.18. Core drilling.

Figure 4.19. Emery machine.

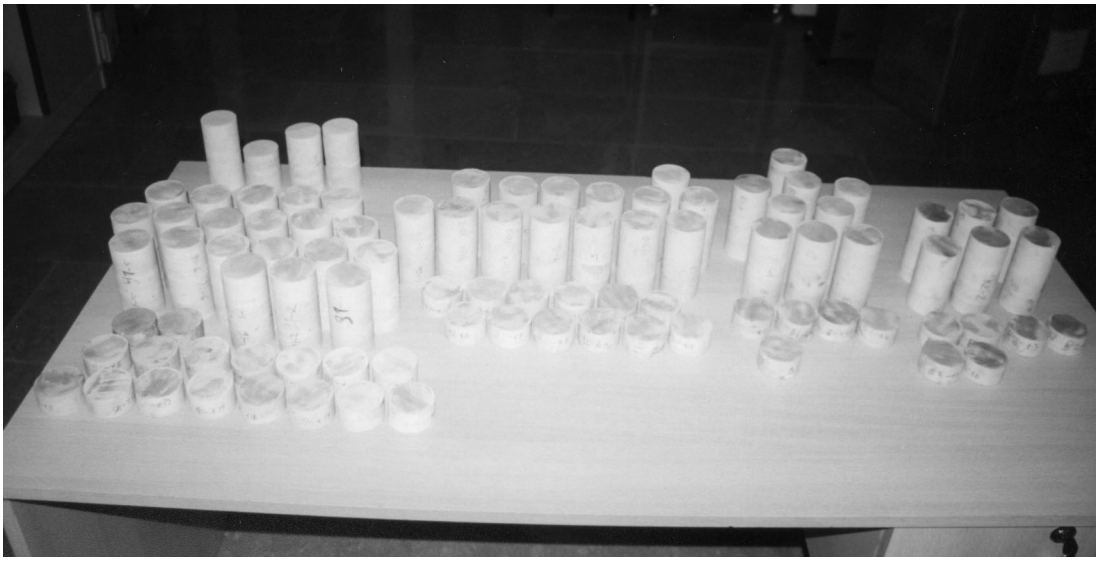

Figure 4.20. Stone core samples.

4.4.1.1. Schmidt Hammer Test

Before taking the stones to the laboratory, Schmidt Hardness test was applied on them in order to find the surface hardness values of the stone samples insitu, as can be

seen in Figure 4.21. L type Proceq Schmidt Hammer which has an impact energy of 0.74Nm was used. Ten impact measurements were applied on each stone. The lowest 5 values were discarded and average of the highest 5 values were determined to be the surface hardness of the stone (Ulusay et al. 2001, p43).

The data obtained are given in Table 4.4. Because of the hammers mechanism, the horizontal impacts give higher hardness values then the vertical impacts. The hardness values of W1 and W2 from west wall are higher than S1 and S2 from south wall, see Table 4.4. The compressive strengths of the stones were determined from their hardness values by use of the Figure 4.22. Altough the chart apsis is subdivided due to impact direction, the horizontal impacts give higher values for uniaxial compressive strength for the same stone, see Table 4.4.

Figure 4.21 Schmidt Hardness tests on stone S1, insitu.

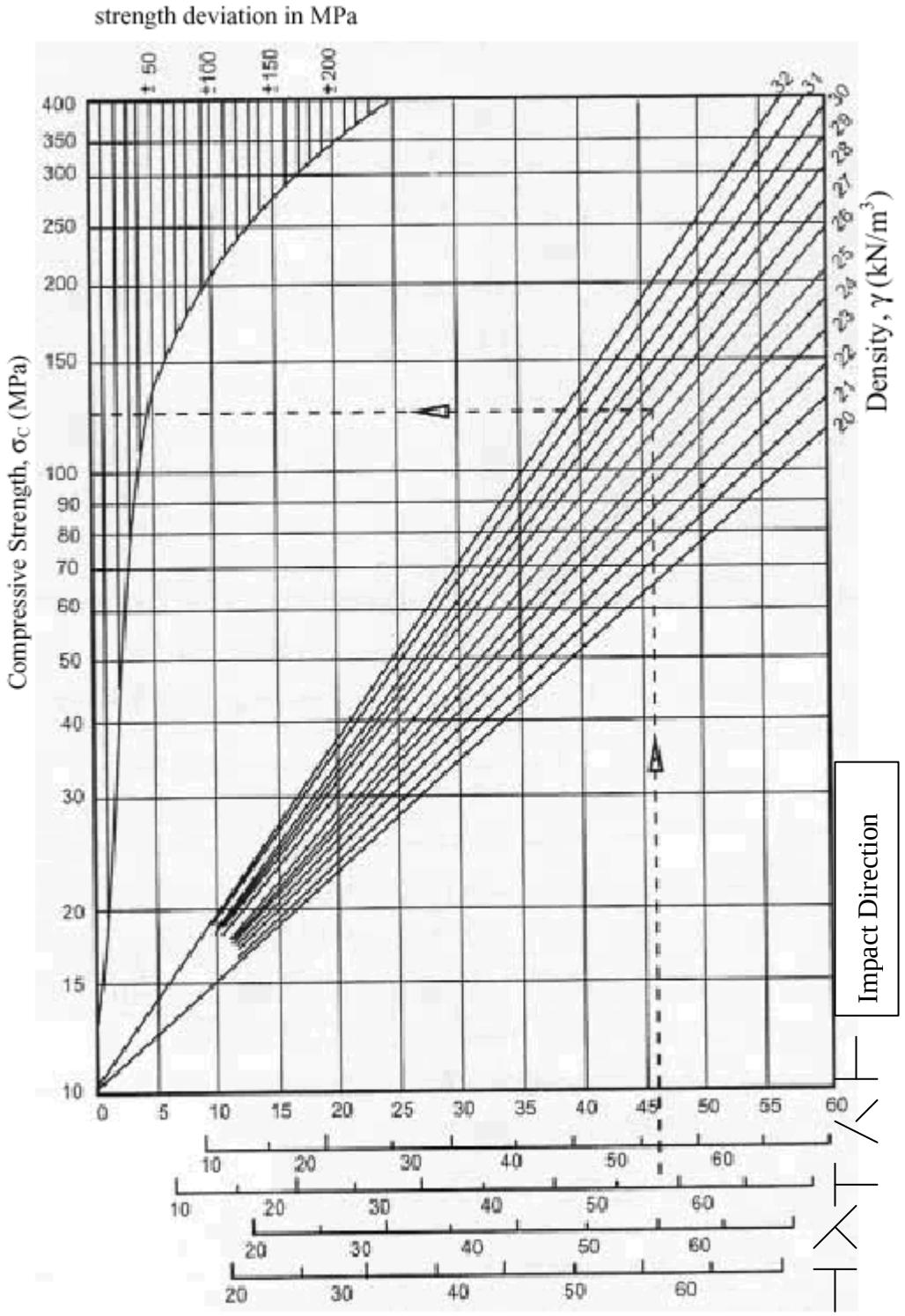

Figure 4.22. Relationship between hardness and compressive strength (Ulusay et al. 2001, p44)

Table 4.4. Insitu Schmidt Hammer test on stone samples.

Sample	S1	S1	S2	S2	W1	W2	W2
Hammer Position	———	|	———	|	|	———	|
Surface Hardness Values	48	30	50	18	42	53	50
	50	34	50	35	52	54	51
	50	34	52	40	53	55	51
	50	34	52	43	54	57	51
	50	36	53	44	54	57	52
	52	36	53	44	54	57	52
	53	36	54	46	56	58	52
	53	36	58	47	57	58	53
	54	37	58	53	58	59	54
	54	38	58	53	59	62	61
Average (R)	53.2	36.6	56.2	48.6	56.8	58.8	54.4
Density (kN/m3)	25	25	25.3	25.3	26	25	25
Comp.Str. (MPa)	125	62	160	120	220	180	155

The uniaxial compressive strengths of the stone samples were determined by destructive test which will be presented in this chapter. The estimated compressive strengths from the hardness are generally higher then the values determined by the destructive test, see Table 4.4 and Table 4.7.

In order to determine the hardness values of stones at different locations of the structure hardness tests was conducted on the structure. The Schmidt Hammer test was conducted at six locations in the structure for every section and elevation, a total of 48 locations. The data collected are presented at Table 4.5. The impacts were made horizontally and the “h” values represent the height of the stone from the ground level.

Table 4.5. Insitu Schmidt Hardness (R) test results.

	Ni 1 h:30cm	Ni2 h:30cm	Ni3 h:30cm	Ni4 h:30cm	Ni5 h:100cm	Ni6 h:110cm	Ni7 h:90cm	No1 h:30cm	No2 h:50cm	No3 h:150cm	No4 h:140cm	No5 h:40cm	No6 h:110cm	Wi1 h:30cm	Wi2 h:30cm	Wi3 h:30	Wi4 h:150cm	Wi5 h:100cm	Wi6 h:60cm
1	38	46	40	43	46	48	44	52	50	50	50	48	40	53	44	44	37	48	38
2	40	47	42	44	46	50	45	52	50	51	52	49	44	54	46	48	38	50	38
3	41	50	43	44	46	50	49	53	50	52	53	51	44	53	47	49	39	50	39
4	44	50	44	49	49	50	50	54	53	52	53	52	44	54	50	50	40	53	39
5	46	50	44	49	49	50	50	54	54	53	54	52	44	57	53	54	42	54	40
6	48	51	44	49	50	52	51	54	54	54	54	52	44	52	53	54	42	54	42
7	48	52	44	50	52	52	51	54	54	54	56	52	46	57	54	55	44	54	43
8	49	52	45	50	52	52	52	56	55	55	56	53	48	49	54	55	44	55	44
9	49	52	48	50	52	52	52	56	56	55	58	53	50	51	55	55	46	56	45
10	50	52	50	52	52	55	52	57	57	58	58	55	52	51	56	55	47	56	46
averages	48.8	51.8	46.2	50.2	51.6	52.6	51.6	55.4	55.2	55.2	56.4	53	48	52	54.4	54.8	44.6	55	44

Continue of Table 4.5.

Wo1 h:30cm	Wo2 h:30cm	Wo3 h:50cm	Wo4 h:40cm	Wo5 h:30cm	Wo6 h:110cm	Si1 h:40cm	Si2 h:20cm	Si3 h:100cm	Si4 h:100cm	Si5 h:100cm	Si6 h:100cm	So1 h:50cm	So2 h:110cm	So3 h:40cm	So4 h:90cm	So5 h:20cm	So6 h:20cm	Ei1 h:0cm
54	42	42	38	47	46	27	48	44	43	42	49	32	52	44	44	49	36	53
55	44	44	38	48	48	28	50	50	44	46	50	46	53	46	46	50	37	53
56	44	44	38	52	50	28	52	53	45	50	51	49	54	48	48	50	37	54
56	46	44	40	52	50	30	52	54	45	51	52	50	54	50	50	52	38	48
56	46	45	41	53	50	30	53	54	45	51	53	51	54	52	50	52	40	53
57	50	45	42	54	51	30	54	54	48	52	54	52	56	52	52	52	41	55
58	52	46	43	54	52	30	54	55	48	54	54	52	56	52	52	52	42	54
60	52	47	45	54	52	30	54	56	48	54	54	53	56	53	53	54	43	56
60	53	47	46	54	52	31	54	57	48	55	54	53	56	54	53	54	44	54
62	54	47	48		53	32	56	59	51	55	55	54	59	56	54	55	48	54
59.4	52.2	46.4	44.8	53.8	52	30.6	54.4	56.2	48.6	54	54.2	52.8	56.6	53.4	52.8	53.4	43.6	54.6

Continue of Table 4.5.

Ei2 h:30cm	Ei3 h:30cm	Ei4 h:40cm	Ei5 h:100cm	Ei6 h:100cm	Eo1 h:60cm	Eo2 h:30cm	Eo3 h:50cm	Eo4 h:100cm	Eo5 h:60cm	Eo6 h:100cm	Wo7 h:30cm	M1 h:30cm	M2 h:40cm	M3 h:20cm
48	50	46	42	44	40	54	50	50	40	50	48	19	18	16
50	52	48	42	50	45	54	52	52	46	53	50	24	20	16
51	52	48	42	50	45	55	52	52	48	54	51	25	24	16
52	54	49	43	52	45	56	52	52	48	54	51	26	28	16
52	54	49	44	52	45	56	53	52	50	54	52	27	29	16
54	54	50	46	52	46	57	54	53	50	54	52	29	30	17
54	54	50	47	53	48	58	54	54	50	56	52	29	34	18
55	54	52	49	53	48	58	54	55	51	56	53	30	38	19
55	55	52	49	54	52	58	56	55	52	57	55	36	40	26
56	55	54	50	56	53	59	56	57	53	58		38	48	29
54.8	54.4	51.6	48.2	53.6	49.4	58	54.8	54.8	51.2	56.2	52.8	32.4	38	21.8

Where Ni1means sample stone at north section number 1, No1 means sample stone at north elevation number 1, Wi1 means sample stone at west section number 1, Wo1, means sample stone at west elevation number 1, and the same coding is valid for south and east walls. M1 means the first stone sample at the minaret. The impact direction for all is horizontal. The averages of the values for each section and elevation are given in Table 4.6.

Table 4.6. Averages of hardness values.

North Section	North Elevation	West Section	West Elevation	South Section	South Elevation	East Section	East Elevation	Minaret
50.4	53.87	50.8	51.43	49.67	52.1	52.87	53.89	30.73

The hardness values for the sections are lower then the ones for the elevations, see Table 4.6. This is probably because of the material deterioration because of moisture, in the structure. In general there is not much difference for the west and south stone's average hardness, see Table 4.6. While applying the test insitu, care was taken to apply the test on stones that will not crack during the test. This results in application of the test on strong stone at its location. The low difference of values may result because of sampling techniques which is restricted by the standards (Ulusay et al. 2001, p.41).

The Schmidt Hammer test was applied on cylinder core samples of stone by use of a cradle which is used to mount the core samples during the test, see Figure 4.23.

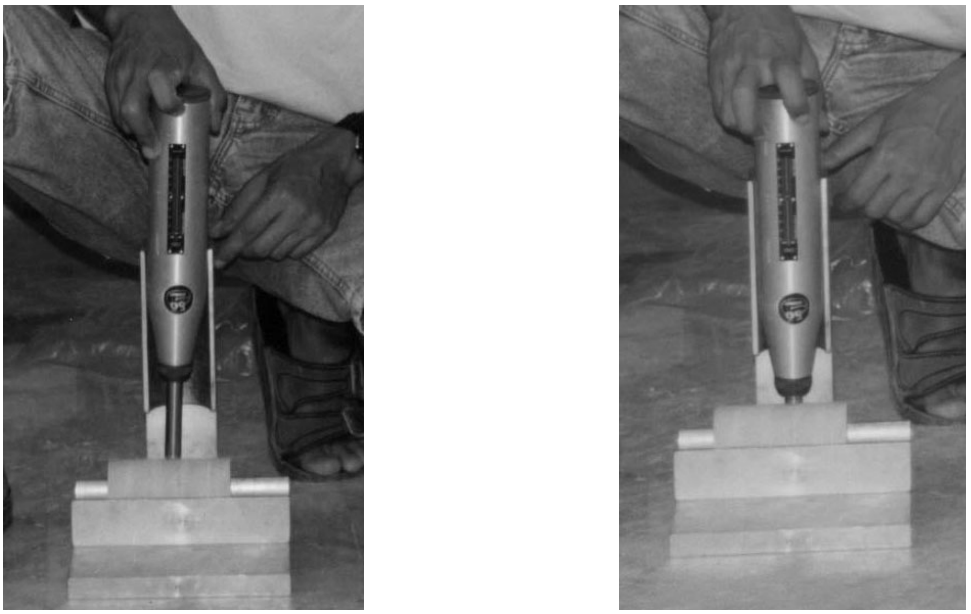

a. Before impact b. After impact

Figure 4.23. Schmidt Hammer test for cylinder samples.

The results of the Schmidt Hammer test of core samples are given in Table 4.7. The compressive strength of the core samples were determined from their hardness values by use of Figure 4.21. The compressive strengths determined from hardness values are lower then the ones determined by destructive tests, see Table 4.7.

The density values used for determining the compressive strengths from the hardness values are determined for the indirect tensile test core samples, see Table 4.

Table 4.7. Test results of compressive test core samples.

1	2	3	4	5	6	7	8	9	10	11	12	13	14
No:	Name:	Length L: (mm)	Surface Hardness R:	sc from R (Mpa)	Ultra. Time µsec	Ultra. V (m/sec)	Rel. Moist. (%)	P (kN)	sc (MPa)	Elasticity Mod. E (MPa)	E from V:(MPa)	Fracture Energy Fc (KJ/m^3)	Shape
1	S1-1	116.00	33.0	50	36.2	3204.42	10.8	143.07	62.47	8568.26	25650.56	348.83	y
2	S1-2	116.00	32.6	50	34.5	3362.32	12.3	169.97	74.21	9824.77	28240.72	429.45	y
3	S1-3	110.00	27.6	43	32.7	3363.91	12.5	159.43	69.61	9328.00	28267.53	342.47	y
4	S1-4	110.00	31.4	46	33.7	3264.09	14.0	155.40	67.85	9328.00	26614.82	342.47	y
5	S1-5	108.00	31.2	46	33.1	3262.84	13.8	158.79	69.33	9931.40	26594.36	338.42	y
6	S1-6	115.50	30.4	45	34.4	3357.56	14.2	158.52	69.22	10004.30	28160.81	355.39	y
7	S1-7	109.30	28.8	44	34.7	3149.86	12.2	143.52	62.67	8725.85	24784.45	312.38	y
8	S1-8	107.50	29.2	45	32.6	3297.55	12.6	137.42	60.00	9580.40	27163.12	297.95	y
9	S1-9	109.20	29.8	45	34.6	3156.07	12.7	146.93	64.15	9096.14	24882.33	372.14	y
10	S1-10	109.00	29.6	45	34.6	3150.29	12.0	109.88	47.98	7783.45	24791.27	165.54	y
11	S1-11	109.30	30.0	45	32.8	3332.32	10.5	169.81	74.15	10392.42	27738.99	389.50	y
12	S1-12	115.50	28.6	44	36.0	3208.33	12.0	153.38	66.97	9565.68	25713.25	329.96	y
13	S1-13	109.40	31.6	46	33.2	3295.18	11.8	155.36	67.84	10285.60	27124.17	340.63	y
14	S1-14	109.30	31.6	46	32.0	3415.63	12.0	152.57	66.62	9837.94	29143.28	271.09	y
15	S1-15	116.00	32.4	47	36.1	3213.30	11.5	156.52	68.34	9965.24	25792.86	426.71	y
16	S1-16	109.90	31.6	46	32.3	3402.48	11.9	166.85	72.85	10269.47	28919.34	351.60	y
17	S1-17	109.90	31.2	46	32.4	3391.98	12.6	173.21	75.63	10587.80	28741.10	418.12	y
18	S1-18 wet	109.67	32.6	47	33.2	3303.31	12.8	106.24	46.39	6726.30	27258.22	212.07	y
19	S1-19 wet	109.69	30.2	45	32.4	3385.49	12.4	123.73	54.03	7906.45	28631.36	240.86	y
20	S1-20 wet	112.10	32.2	47	34.0	3297.06	13.2	98.89	43.18	6722.76	27155.10	179.55	y

Continue of Table 4.7 Test results of compressive test core samples.

1	2	3	4	5	6	7	8	9	10	11	12	13	14
No:	Name:	Length L: (mm)	Surface Hardness R:	sc from R (Mpa)	Ultra. Time µsec	Ultra. V (m/sec)	Rel. Moist. (%)	P (kN)	sc (MPa)	Elasticity Mod. E:(MPa)	E from V:(MPa)	Fracture Energy Fc (KJ/m^3)	Shape
21	S2-1	116.30	32.0	47	32.6	3567.48	12.8	164.97	72.031475	11216.00	32220.11128	388.25	y
22	S2-2	115.30	33.2	50	34.2	3371.35	12.1	166.37	72.642333	9574.68	28774.5943	362.24	y
23	S2-3	116.00	33.0	50	35.9	3231.20	11.9	181.58	79.28405	9701.63	26431.99162	447.83	y
24	S2-4	116.70	32.8	49	35.8	3259.78	11.6	144.82	63.234071	8058.49	26901.62196	276.92	y
25	S2-5	115.80	28.4	44	35.1	3299.15	11.9	77.71	33.931223	6257.00	27555.33483	141.79	n
26	S2-6	116.00	29.8	45	32.6	3558.28	12.2	192.41	84.015471	11090.68	32054.09982	415.66	y
27	S2-7	114.50	31.2	46	31.5	3634.92	11.6	202.59	88.456527	12543.35	33449.7343	424.58	y
28	S2-8	116.20	32.6	47	35.1	3310.54	12.2	119.27	52.075759	8444.60	27746.02861	318.12	y
29	S2-9	115.40	30.2	45	33.1	3486.40	11.0	144.23	62.9782	11093.94	30772.19223	245.41	n
30	S2-10	114.00	32.6	47	33.0	3454.55	12.1	161.33	70.442109	9068.19	30212.35851	288.79	n
31	S2-11	115.00	32.2	47	34.7	3314.12	12.3	188.20	82.173291	9193.30	27806.06527	479.28	y
32	S2-12 wet	116.68	32.2	47	32.5	3590.15	13.6	98.31	42.925988	7522.40	32630.89048	131.18	y
33	S2-13 wet	115.58	31.6	46	32.0	3611.88	13.0	119.64	52.239499	7276.40	33026.93185	216.54	y
34	S2-14 wet	116.17	31.4	46	31.4	3699.68	12.8	136.71	59.692928	8424.92	34652.25401	260.78	y
35	W1-1 n.f.	114.60	39.4	79	22.0	5209.09	11.4	359.05	156.77351	30549.90	70444.53362	0.00	y
36	W1-2 n.f.	114.90	40.2	80	22.2	5175.68	11.5	351.20	153.34677	32199.85	69543.65836	0.00	y
37	W1-3 n.f.	115.50	39.4	79	22.2	5202.70	11.8	245.00	106.97657	29909.06	70271.85924	0.00	y
38	W1-4 n.f.	114.50	40.0	80	22.1	5181.00	11.8	309.96	135.34065	30921.78	69686.69222	0.00	y
39	W1-5 n.t.	115.50	39.2	79	22.4	5156.25	10.1	300.19	131.07294	0.00	69022.60664	0.00	y
40	W1-6 n.t.	115.90	40.4	80	22.0	5268.18	7.9	310.00	135.35637	0.00	72051.8166	0.00	y
41	W1-7 n.t.	115.90	39.6	79	22.4	5174.11	11.0	196.20	85.668587	0.00	69501.51314	0.00	y
42	W1-8 wet	115.60	39.2	79	22.3	5183.86	15.9	266.83	116.50928	0.00	69763.67765	0.00	y
43	W1-9 wet	116.00	40.0	80	22.6	5132.74	16.4	296.26	129.35957	0.00	68394.71194	0.00	y
44	W2-1	99.20	35.8	56	17.5	5668.57	8.9	245.00	106.97657	31185.39	80826.92	226.14	y
45	W2-2	116.00	38.4	68	22.1	5248.87	6.3	199.95	87.3038	22969.00	69301.11	179.82	n
46	W2-4	115.60	39.2	72	20.7	5584.54	7.6	221.18	96.575394	27580.99	78448.34	250.54	y
47	W2-5 no test	115.00	39.2	72	20.8	5528.85	3.4	378.67	165.34037	0.00	76891.40	0.00	y
48	W2-6 wet	108.00	36.8	60	19.3	5595.85	14.4	83.39	36.409149	0.00	78766.52	0.00	n
49	W2-7 wet	108.40	38.6	68	19.4	5587.63	14.0	326.67	142.6382	0.00	78535.12	0.00	y

Table 4.8. Test results of indirect tensile test core samples.

1	2	3	4	5	6	7	8	9	10	11	12	13	14	15
NO:	Name :	Length L (mm)	Ultra. Time µsec	Ultra V (m/sec)	Wrdy (gr)	Wwet (gr)	Warc (gr)	Apparent Density ?a (kg/m3)	Real Density ?r (kg/m3)	% porosity	Rel Moisture (%)	P (kN)	Tensile Str. st (MPa)	E from V (GPa)
1	S1-t1	30.0	10.1	2970.30							12.09	12.58	4.94	0.00
2	S1-t2	30.0	11.0	2727.27							12.16	11.86	4.66	0.00
3	S1-t3	30.0	9.9	3030.30	142.71	153.02	84.58	2085.18	2455.01	15.06	12.50	17.30	6.79	22.54
4	S1-t4	30.0	8.8	3409.09	154.63	163.13	94.94	2267.63	2590.55	12.47	12.39	17.41	6.84	30.11
5	S1-t5	30.0	10.8	2777.78	137.67	150.24	82.46	2031.13	2493.57	18.55	12.48	15.44	6.06	19.24
6	S1-t6	29.0	11.5	2521.74							12.38	7.91	3.21	0.00
7	S1-t7*	29.5	9.7	3041.24	138.67	151.69	84.69	2069.70	2568.91	19.43	11.82	0.00	0.00	23.76
8	S1-t8	30.1	9.6	3135.42	142.44	154.51	86.09	2081.85	2527.77	17.64	12.60	13.17	5.15	24.85
9	S1-t9	30.0	10.2	2941.18	139.93	152.03	84.13	2060.82	2507.71	17.82	12.68	14.83	5.82	21.69
10	S1-t10	30.0	7.4	4054.05	150.98	158.28	90.24	2218.99	2485.68	10.73	11.95	20.42	8.02	40.85
11	S1-t11	30.0	8.3	3614.46							11.41	19.79	7.77	0.00
12	S1-t12	29.0	12.0	2416.67	131.66	143.25	77.20	1993.34	2417.55	17.55	12.05	12.91	5.24	14.12
13	S1-t13	29.5	10.9	2706.42							11.80	8.80	3.51	0.00
14	S1-t14	29.2	15.0	1946.67							11.70	10.10	4.07	0.00
15	S1-t15	29.9	10.5	2847.62							12.10	14.88	5.86	0.00
16	S1-t16*	28.9	8.7	3321.84	137.26	147.41	82.07	2100.70	2487.04	15.53	12.05	0.00	0.00	27.44
17	S1-t17	29.7	8.3	3579.52	145.96	153.98	86.30	2156.62	2446.53	11.85	10.69	19.75	7.83	31.35

Continue of Table 4.8. Test results of indirect tensile test core samples.

1	2	3	4	5	6	7	8	9	10	11	12	13	14	15
NO:	Name :	Length L (mm)	Ultra. Time µsec	Ultra V (m/sec)	Wrdy (gr)	Wwet (gr)	Warc (gr)	Apparent Density ?a (kg/m3)	Real Density ?r (kg/m3)	% porosity	Rel Moisture (%)	P (kN)	Tensile Str. st (MPa)	E from V (GPa)
18	S2-t1	30.0	8.3	3608.43	150.28	160.22	92.23	2210.33	2588.80	14.62	11.86	17.69	6.96	33.71
19	S2-t2	29.8	7.5	3970.67							11.60	19.44	7.69	0.00
20	S2-t3	29.6	7.9	3751.90	152.78	160.26	92.81	2265.09	2547.61	11.09	11.94	20.55	8.17	35.86
21	S2-t4	29.3	7.6	3852.63	151.73	158.91	91.89	2263.95	2535.59	10.71	11.95	20.82	8.37	37.64
22	S2-t5	30.3	7.9	3832.91	155.10	162.65	93.61	2246.52	2522.36	10.94	12.15	18.86	7.34	37.06
23	S2-t6	29.4	8.0	3677.50	148.96	157.85	91.00	2228.27	2570.05	13.30	11.67	14.57	5.83	34.76
24	S2-t7	29.8	7.7	3874.03	152.74	159.43	91.83	2259.47	2507.63	9.90	12.13	16.39	6.47	37.63
25	S2-t8	29.7	7.8	3808.97							12.32	23.45	9.30	0.00
26	S2-t9	29.7	7.0	4235.71	153.95	159.76	91.98	2271.32	2484.27	8.57	11.57	20.31	8.07	44.57
27	S2-t10	29.0	6.7	4332.84	150.94	156.80	90.58	2279.37	2500.66	8.85	11.15	24.73	10.03	46.95
28	S2-t11	24.8	6.6	3760.61	124.66	131.63	75.49	2220.52	2535.29	12.42	11.15	9.46	4.49	35.85
29	S2-t12	28.5	6.9	4124.64	146.58	153.34	88.51	2260.99	2524.19	10.43	12.00	15.11	6.25	42.94
30	W1-t1	28.9	4.1	7036.59	167.33	168.85	102.92	2537.99	2597.89	2.31	10.30	25.10	10.25	128.63
31	W1-t2	29.6	4.3	6879.07	168.79	170.35	103.69	2532.10	2592.78	2.34	10.56	24.88	9.91	122.69
32	W1-t3	29.5	4.6	6419.57	169.88	171.28	104.28	2535.52	2589.63	2.09	10.44	19.38	7.73	106.72
33	W1-t4	29.2	4.2	6945.24	169.52	170.97	104.38	2545.73	2602.39	2.18	9.47	19.36	7.82	125.53
34	W1-t5	29.0	4.3	6744.19	168.42	169.81	103.59	2543.34	2597.87	2.10	8.80	16.67	6.77	118.16
35	W2-t1	27.9	3.6	7738.89	159.15	159.84	96.47	2511.44	2539.09	1.09	8.40	22.06	9.33	152.07
36	W2-t2	28.0	3.8	7368.42	158.46	158.95	95.61	2501.74	2521.24	0.77	6.25	22.23	9.35	136.89
37	W2-t3	28.8	3.9	7371.79	163.50	163.93	98.38	2494.28	2510.75	0.66	5.72	19.24	7.88	136.44
38	W2-t4	29.5	4.0	7367.50	166.60	167.00	100.28	2497.00	2512.06	0.60	5.24	23.96	9.58	136.35
39	W2-t5	29.6	3.7	8000.00	168.42	168.80	101.75	2511.86	2526.17	0.57	6.06	30.92	12.30	161.68
40	W2-t6	27.6	3.9	7084.62	154.75	155.40	92.43	2457.52	2483.15	1.03	4.59	25.47	10.86	124.63

For easiness of comparing the results of stone samples S1, S2, W1 and W2, the average values of the test results are given in Table 4.9.

Table 4.9. Average values of the tests for stone core samples.

Sample	Number of Total Cores	Surface Hardness R:	Ultra Velocity V (m/sec)	Apparent Density ?a (kg/m3)	Real Density ?r (kg/m3)	porosity (%)	Compressive Str. sc (Mpa)	Tensile Str. st (Mpa)	Modulus of Elasticity E (MPa)	E from V (MPa)
S1	37	30.8	3290.7	2106	2498	15.66	64.17	5.72	9221	27068
S2	26	31.7	3456.4	2250	2531	11.08	65.44	7.41	9247	30302
W1	14	39.7	5187.1	2538	2596	2.202	127.82	8.49	30895	69853
W2	12	38	5535.7	2495	2515	0.786	105.87	9.88	27245	77128

The surface hardness values of the W1 and W2 stone core samples are higher then the values for S1 and S2, see Table 4.9.

4.4.1.2. Ultrasonic Pulse Velocity Test

The ultrasonic pulse velocity test was applied by CNS Farnell Electronic's Pundit type equipment. The equipment was used under 500V EHT voltage and 10pps (pulse per second). As the cores were emeried their surfaces were smooth but again lubricating grease was used on the surfaces of the cores in very little amounts as can be seen from Figure 4.24.

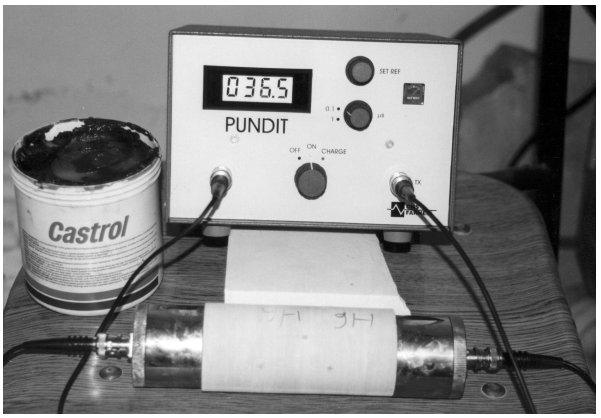

Figure 4.24. Ultrasonic Pulse Velocity Test

The test was applied on both uniaxial compression test and indirect tension test core samples. The pundit digital unit gives us the time needed for the ultrasonic waves to

pass through the specimen in micro-seconds. From the distance between the probes (the height of the core), the ultra velocity of the specimen is found in meter/second as can be seen in Eq.4.2. The average ultra velocities of the stone samples are given on Table 4.9. The ultra velocity values of the W1 and W2 are higher then the values for S1 and S2, see Table 4.9.

$$V = \frac{H}{t} \qquad \text{Eq.4.2}$$

where H and t are the distance between probes and the time needed for the ultrasonic wave to pass through the specimen, respectively.

The modulus of elasticity values of stone samples were also determined by Eq.4.3 (ASTM 1997, C597) and presented at Table 4.9.

$$E = V^2 \times r \times (1+m) \times \frac{(1-2m)}{(1-m)} \qquad \text{Eq.4.3}$$

where V (m/sec), ? (kg/m^3) and m are ultrasonic pulse velocity, density and Poisson's ratio, respectively. The Poisson's ratio is taken as 0.18 for the lime stone. The estimated modulus of elasticity values by use of ultra velocity are higher then the values determined by destructive tests, see Table 4.7 and Table 4.9.

4.4.1.3. Density-Porosity Test

Density-porosity tests were applied on tensile strength core samples. The testing procedure is presented in 2.5.3. The results of the test are given in Table 4.8 and the averages for each stone sample are given in Table 4.9. The difference between apparent and real densities for S1 and S2 samples are higher than the differences for W1 and W2 samples. The porosity of W1 and W2 are lower then the porosity of S1 and S2. The porosity of S1 is approximately 20 times the porosity of W2, see Table 4.9.

4.4.1.4. Uniaxial Compression Test

The testing procedure is presented in 2.5.4. The dimensions and relative moisture of each sample are measured. The diameter of each sample is D=54mm, while their lengths vary. The perfectly shaped cylinder core samples have a “y” while the ill shaped ones have a “n” on the “shape” column of Table. 4.7. The test was conducted by use of mechanical testing machine Shimadzu AG1 which has a capacity of 250kN. The machine reads the stroke from the head with respect to applied load and time. The loading rate was taken as 0.2mm/minute which satisfied the condition of failure time between 5 to 10 minutes. Generally all the samples were failed at 10 minute. The stone samples have a brittle type of fracture, see Figure 25 a-b.

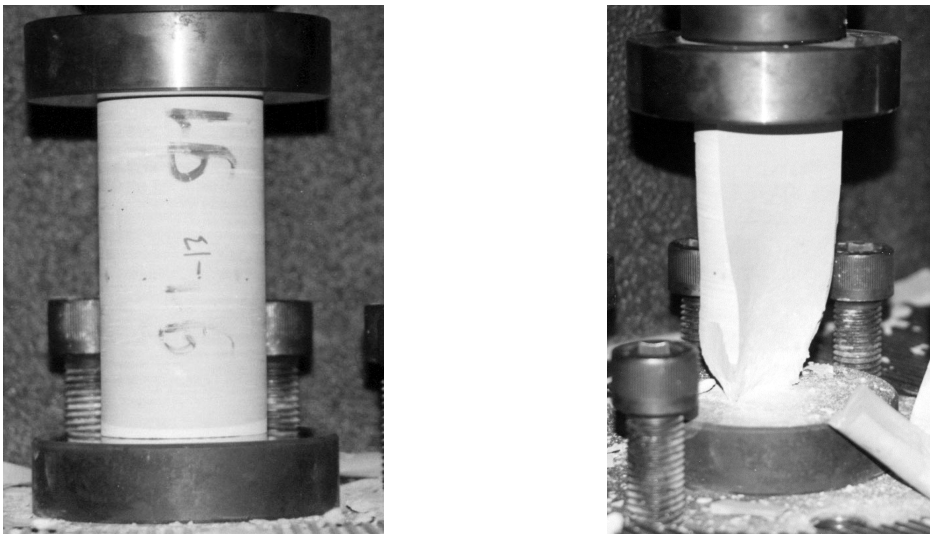

a. Loaded sample b. Failed sample

Figure 4.25 a-b. Compression Test

The brittle type of failure can also be seen at Figure 4.26 where stress-strain graphs of S1, S2, W1 and W2 are given.

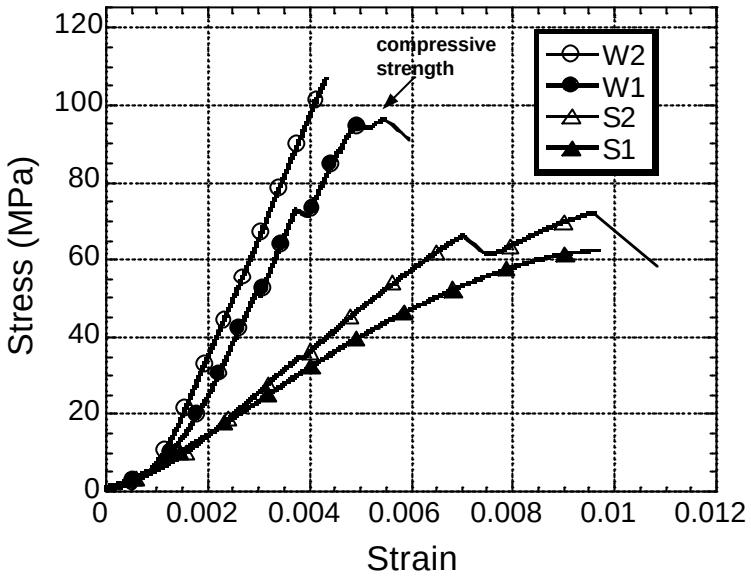

Figure 4.26. Stress-strain graph of stone samples.

The compressive strength values for W1 and W2 are approximately 2 times the values for S1 and S2.

The modulus of elasticity values of stone core samples were found by use of stress-strain graphs and presented at Table 4.7. The average of modulus of elasticity values for stone samples is presented in Table.4.9. The modulus of elasticity values for W1 and W2 are approximately three times the values for S1 and S2, see Table 4.9. The fracture energy of the core samples were determined by the area under the stress-strain curve and are presented in Table 4.7.

Some of the core samples for each stone were put in water for one week and tested immediately after taken out of the water in order to determine the durability of the stone samples.

The durability of stone samples was determined according to Winkler (Tuncoku 2001, p.42) by Eq. 4.4.

$$D = \frac{s_{cwet}}{s_{cdry}} \times 100 \qquad \text{Eq.4.4.}$$

where D, σ_{cwet}, σ_{cdry} are durability factor, compressive strength of wet samples and compressive strength of dry samples, respectively.

The classification of rocks by durability factor is made by following data;

- D:100-80 Excellent durability
- D:80-70 Very good durability

- D:70-60 Fair durability
- D:60-50 Poor durability

The durability of four stone samples determined from their average core compressive strengths are presented in Table 4.10.

Table 4.10 Durability of Stone Samples

Sample	Durability D (%)
S1	75
S2	79
W1	96
W2	85

The stone samples S1 and S2 are in the range of very good while W1 and W2 are excellent for durability, see Table 4.10.

Some of the core samples of W1 did not fail under maximum load 250kN and tested again with a 300tons of press designed for concrete testing which can not give stroke. These samples have “n.f.” (means “no fracture”) within their name at Table 4.7. Some of the core samples were tested with only the 300tons test press and have “n.t” (means “no test with 250kN press”) within their name at Table 4.7.

4.4.1.5. Indirect Tension Test

The test procedure is given in part 2.5.5. The diameter of the core samples was D=54mm. The test was conducted by use of mechanical testing machine Shimadzu AG1 which has a capacity of 250kN. The machine reads the stroke from the head with respect to applied load and time. The loading rate applied was 1mm/min. Generally all the core samples failed at 30 seconds which complies with the 15-30 second rule for duration (Ulusay et al.2001, p.71).

The stone core samples failed in a brittle type of fracture see Figure 4.27 a-b.

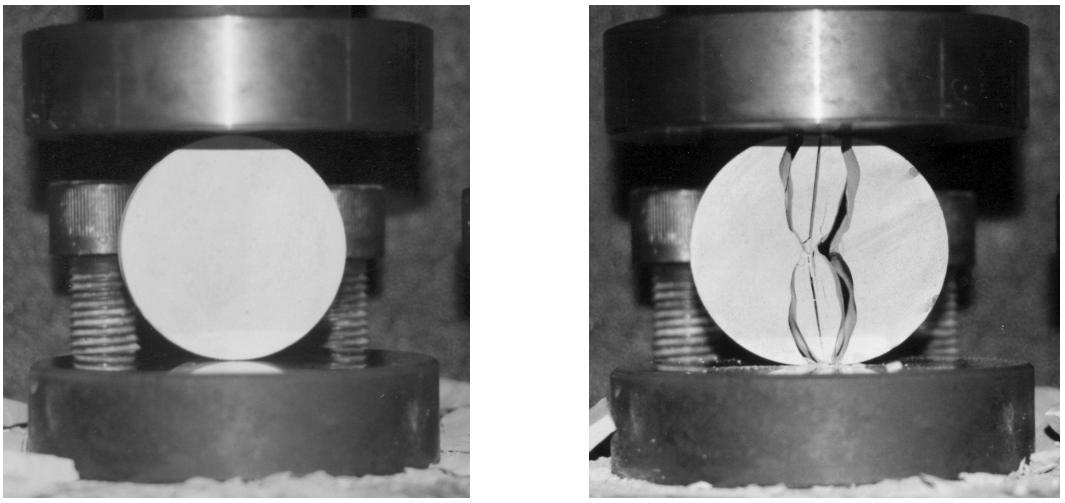

a. Loaded sample b. Failed sample

Figure 4.27. a-b. Indirect tension test.

The brittle fracture can also be seen from load–displacement curve at Figure 4.28. The tensile strength of W1 and W2 samples are higher then the values for S1 and S2, see Table 4.9. The core samples S1-t7 and S1-t16 were failed at preloading.

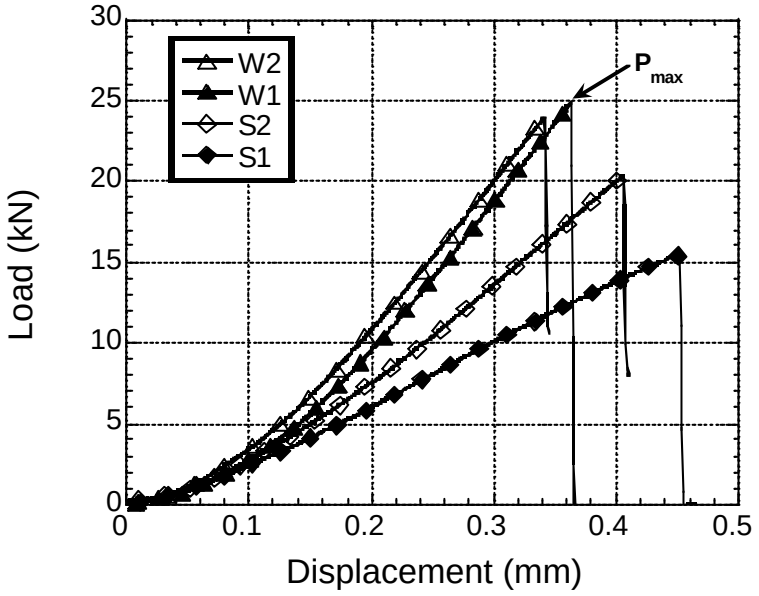

Figure 4.28. Load-displacement graphs of indirect tension test.

4.4.1.6. SEM, XRD and EDX Analyses

Microstructural analyses of stones were made by use of Philips XL30-SFEG scanning electron microscope. The mineralogical composition of stones was determined

by use of Philips X-Pert X-Ray diffraction (XRD). The compositional analysis was conducted using an Energy Dispersive X-ray (EDX) analyzer.

Microstructural analyses showed that all stone samples were composed of micritic calcite crystals, 2µ in size, see Figure 4.29.

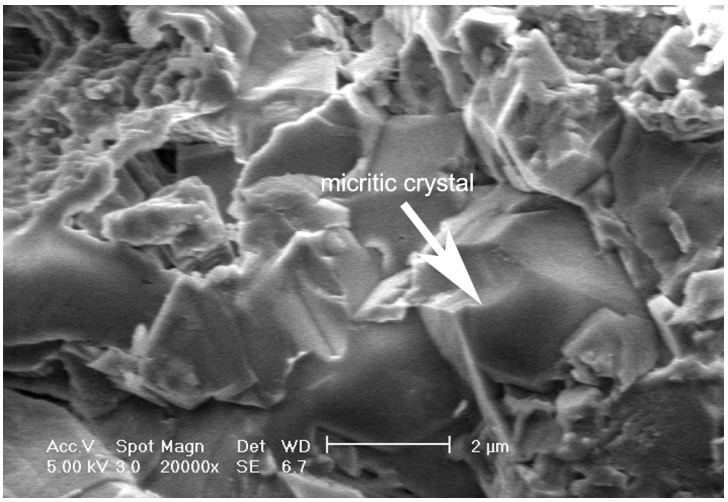

Figure 4.29.Typical SEM micrographs of W-stone samples showing micritic crystals.

The S1 and S2 stone samples from the south wall contain circular diatomer fossil shells, 5-10 µm in outer diameter, see Figure 4.30. On the other hand, the W1 and W2 samples do not have fossils.

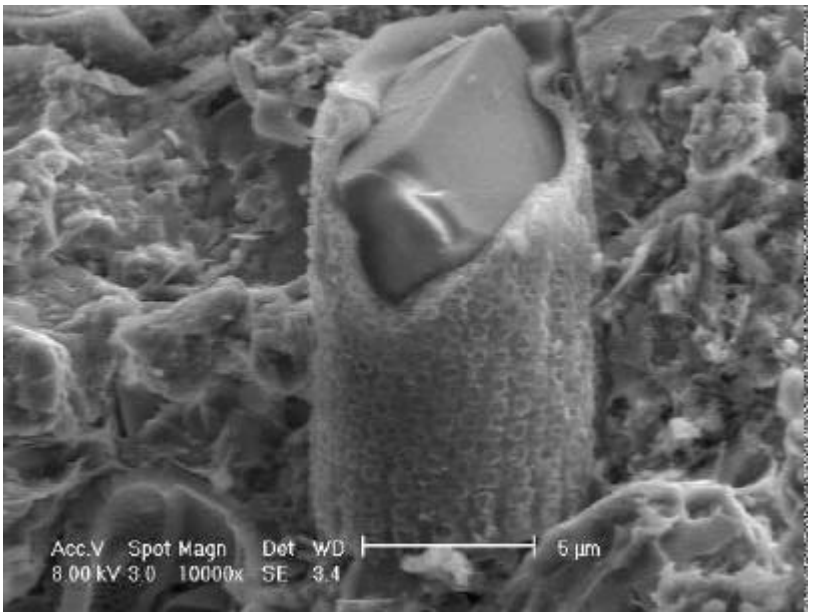

a. Fossil in stones S.

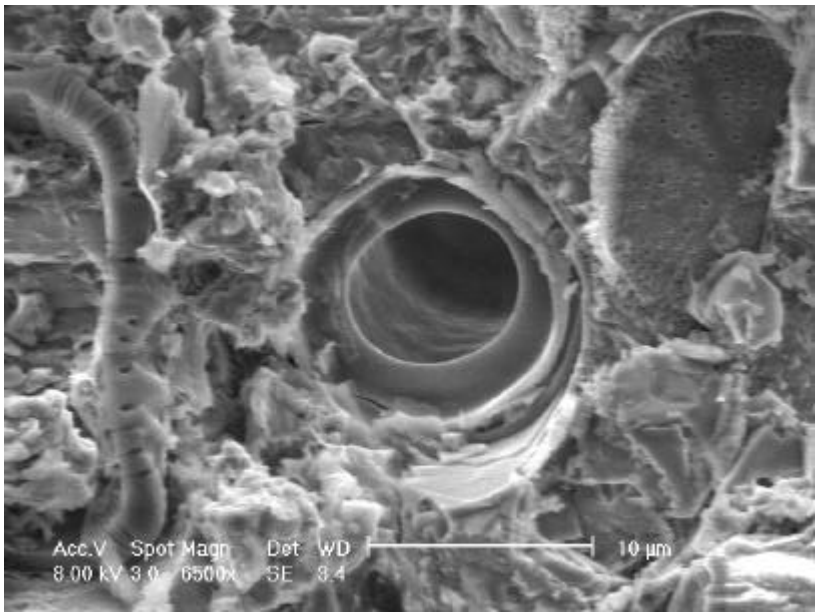

b. Fossils in stones S.

Figure 4.30. a-b. Fossils in stones S.

The core of and around the fossils are not filled leading to a relatively high porosity for S stones with respect to W stones, see Table 4.9 and Figure 4.30b.

The results of semi quantitative elemental analysis conducted on six different areas (0.65 mm^2) of W- and S-stone samples showed a marked difference between the silica contents of W and S samples, see Table 4.11. The silica content of S samples is more than two times that of W samples. The higher concentration of silica in S-samples

is due to the siliceous skeleton of fossils, which was further confirmed by the elemental analysis as shown in Figure 4.31.

Table 4.11 Elemental compositions of the lime stones.

Sample	Na_2O (%)	K_2O (%)	MgO(%)	CaO(%)	Al_2O_3(%)	SiO_2(%)
W Stones	3.52± 1.39	1.35±0.18	3.87±1.07	72.64±4.53	5.79±1.17	12.83±1.47
S Stones	0.99± 0.19	1.59±0.53	1.90±0.58	58.77±0.66	6.34±0.51	30.42±1.74

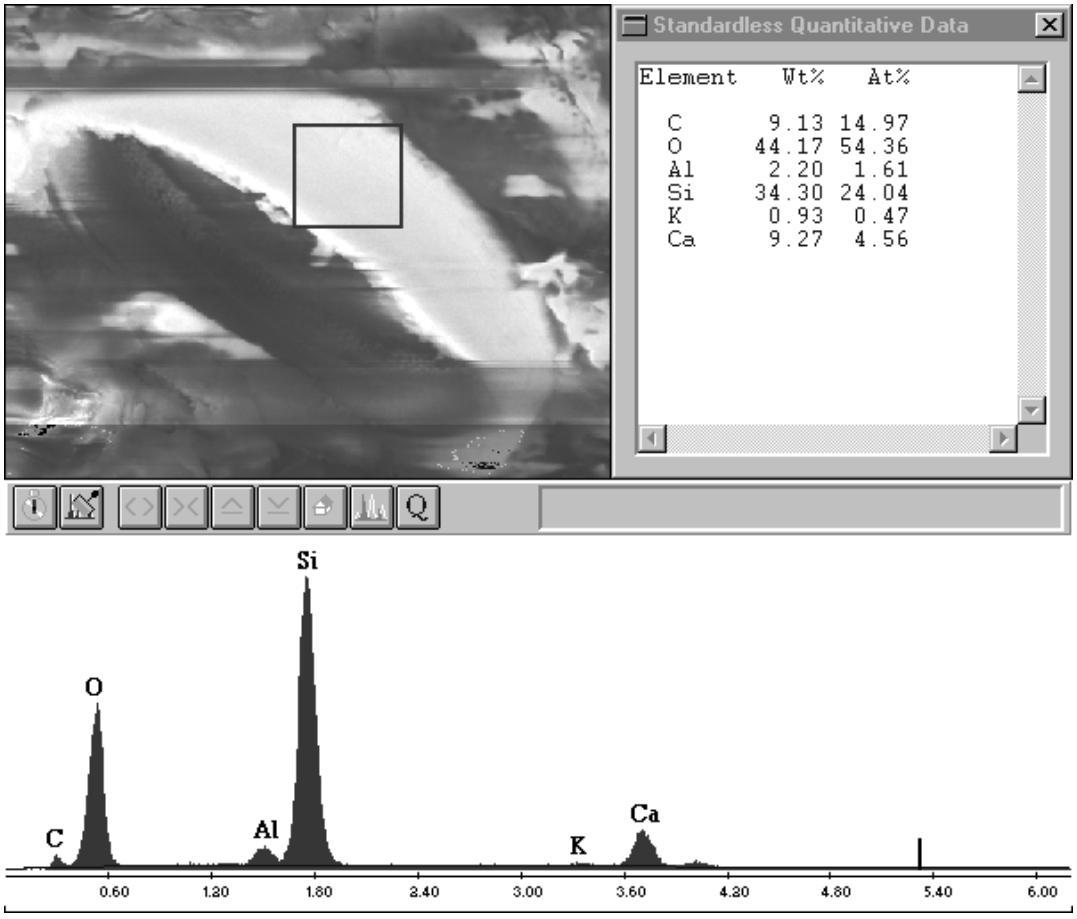

Figure 4.31 Elemental analysis of fossil skeleton in S samples.

The XRD analyses of stone samples showed that they are formed of $CaCO_3$ and they are limestone, see Figure 4.32.

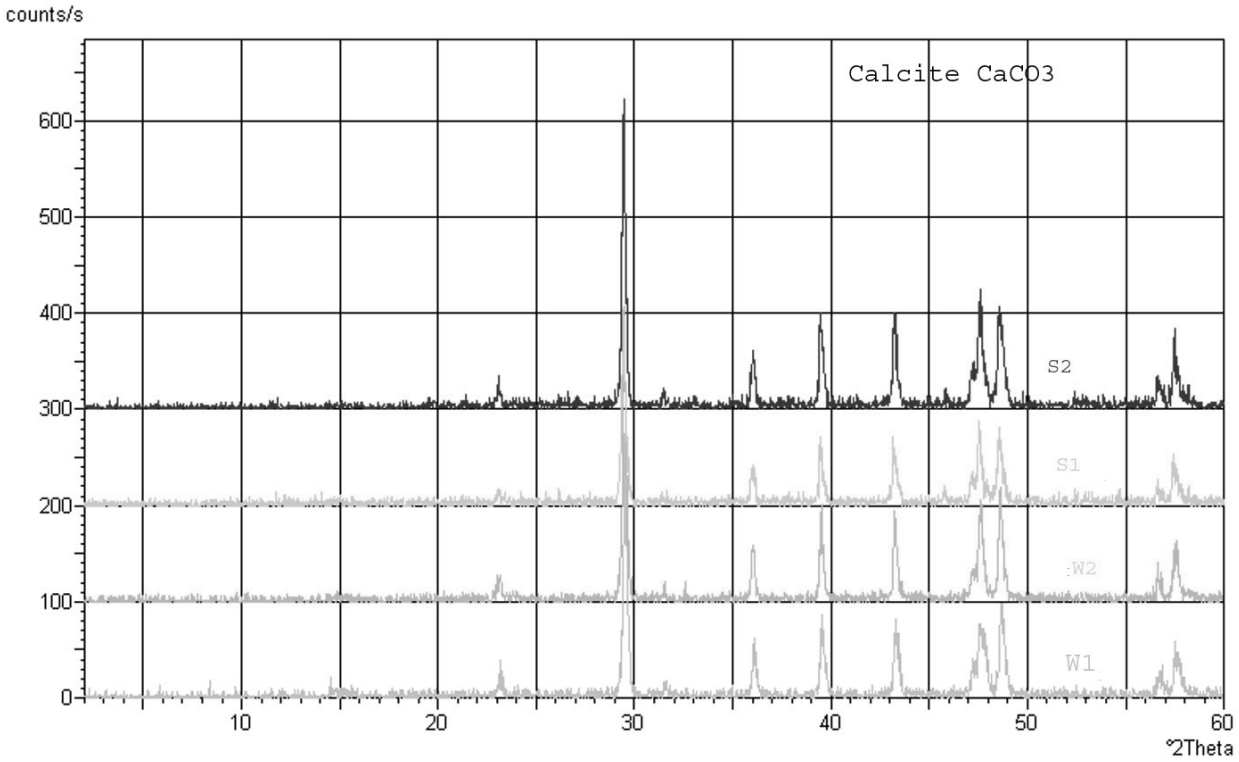

Figure 4.32. XRD analyses of stone samples.

The destructive tests led to a brittle type of fracture as the cleavage type of fracture of micritic crystals can be seen in Figure 4.33.

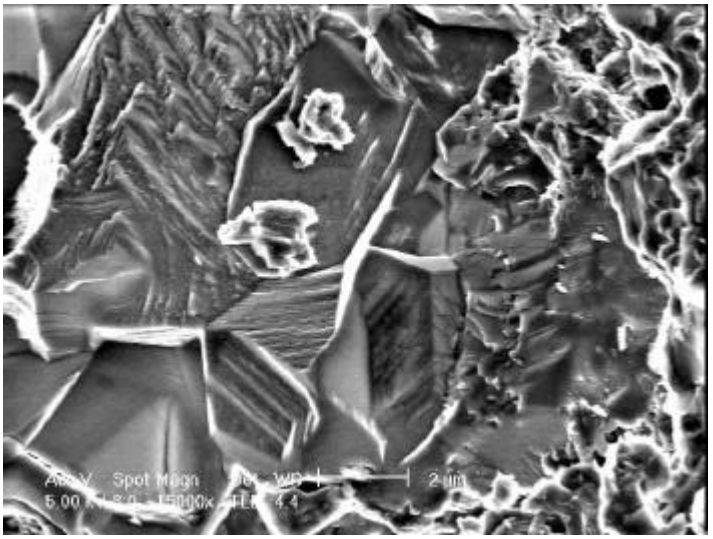

Figure 33. Fracture surface of W sample showing the cleavage type fracture of micritic crystal

4.4.1.7. Relationships Between Tests Results

While working on historical structures, the number of material samples that can be taken from the structure is generally limited, at least for conservation purposes. Moreover, it is not practical to get samples from every wall, every section and elevation, every structural element etc. and conduct tests. Some times there can be no chance of getting any sample either. In order to overcome such difficulties nondestructive tests can be used.

Although density-porosity tests are slightly destructive, their relations with other results will also be presented. In addition, relationship between two destructive tests will be presented incase some destructive tests are easier to conduct then to some others by means of equipment etc.

In this study, nondestructive tests of Schmidt Hammer test and ultrasonic pulse velocity tests were conducted. The Schmidt Hammer test was applied on stone samples insitu, on stones at different parts of the structure and on cylinder core samples of stone. The ultra velocity test was applied on cylinder core samples.

The strength of W1 and W2, from west wall, are higher then the strength of S1 and S2, from south wall, by all means, see Table 4.9. Also, non-destructive test results of W1 and W2 are higher then the results for S1 and S2. The main reason for these differences seems to be the porosity difference, see Table 4.9. Porosity is related to tensile strength, see Figure 4.34. As the porosity increases, tensile strength decreases.

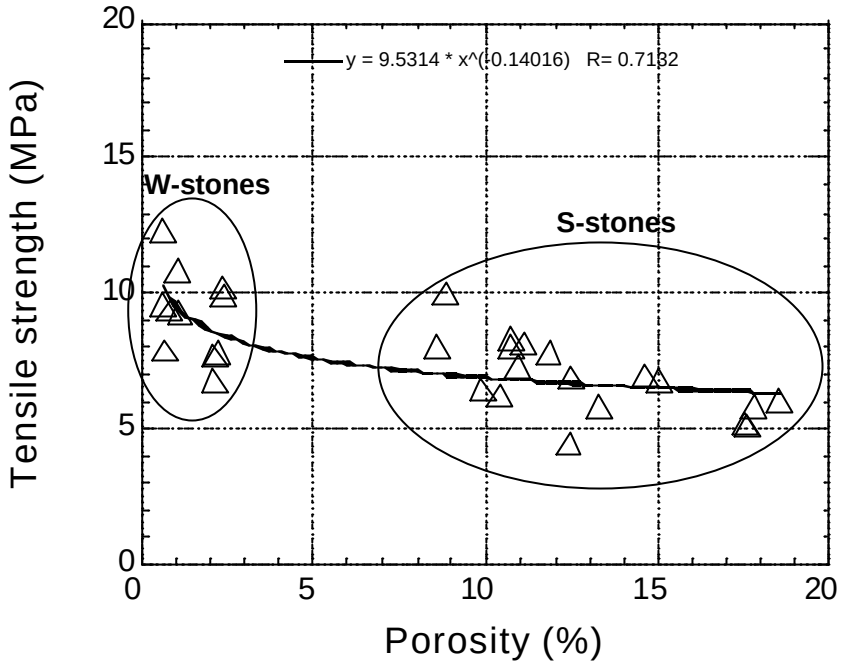

Figure 4.34. Relationship between porosity and tensile strength.

The ultrasonic pulse velocity has also a close relationship with the porosity, see Figure 4.35. As the porosity increases, wave velocity decreases.

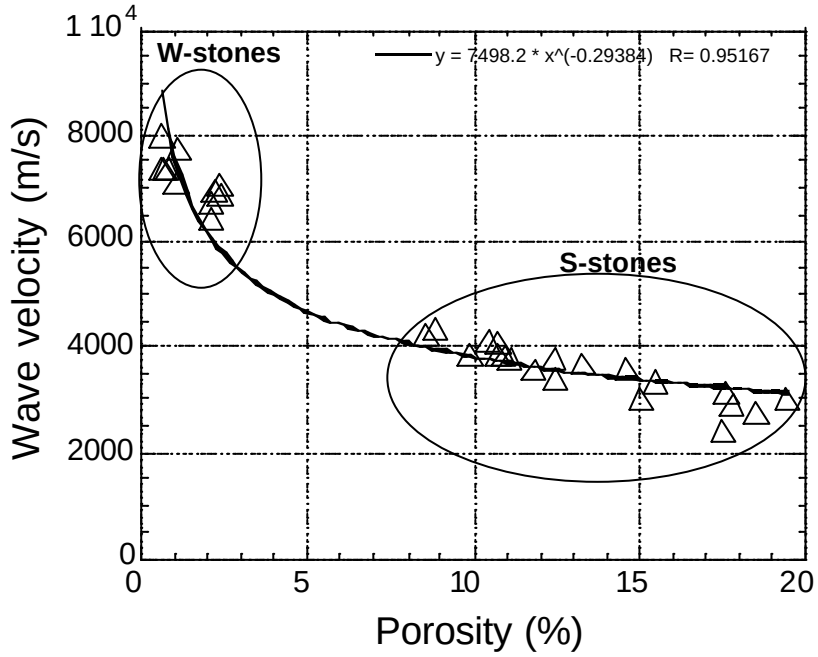

Figure 4.35. Relationship between porosity and pulse velocity.

Wave velocity has a relationship between the compressive strength. As the wave velocity increases, compressive strength increases, see Figure 4.36.

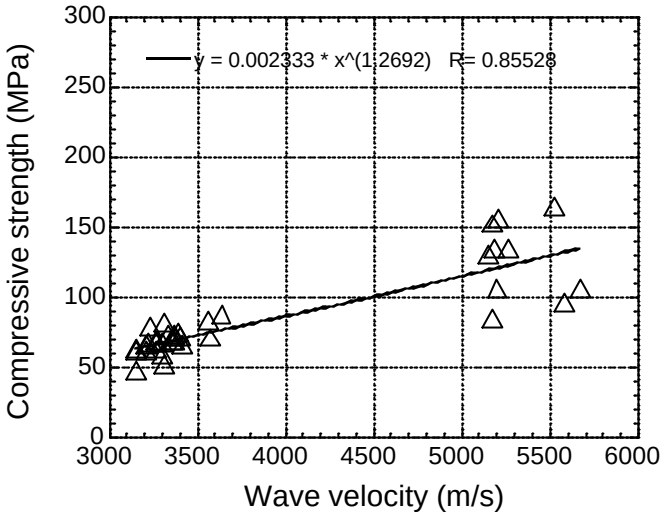

Figure 4.36. Relationship between wave velocity and compressive strength.

Also as the wave velocity increases, the tensile strength and the modulus of elasticity increases, see Figure 4.37 and Figure 4.38.

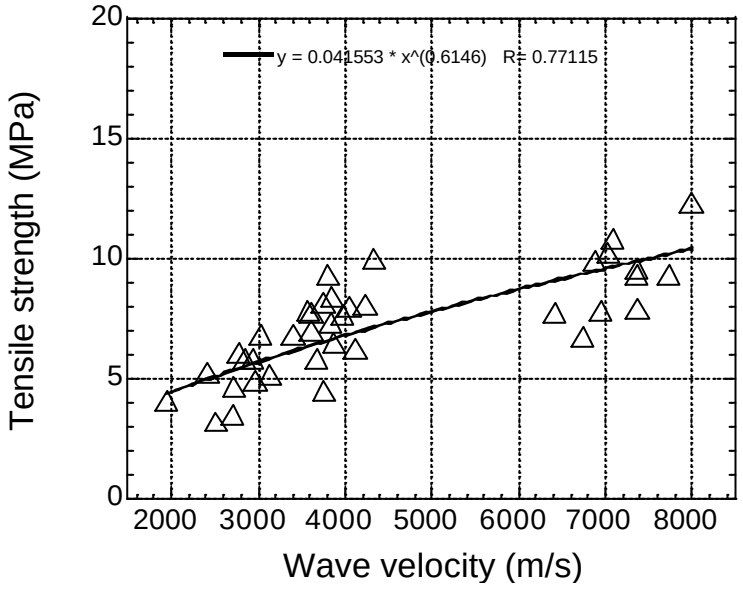

Figure 4.37. Relationship between wave velocity and tensile strength.

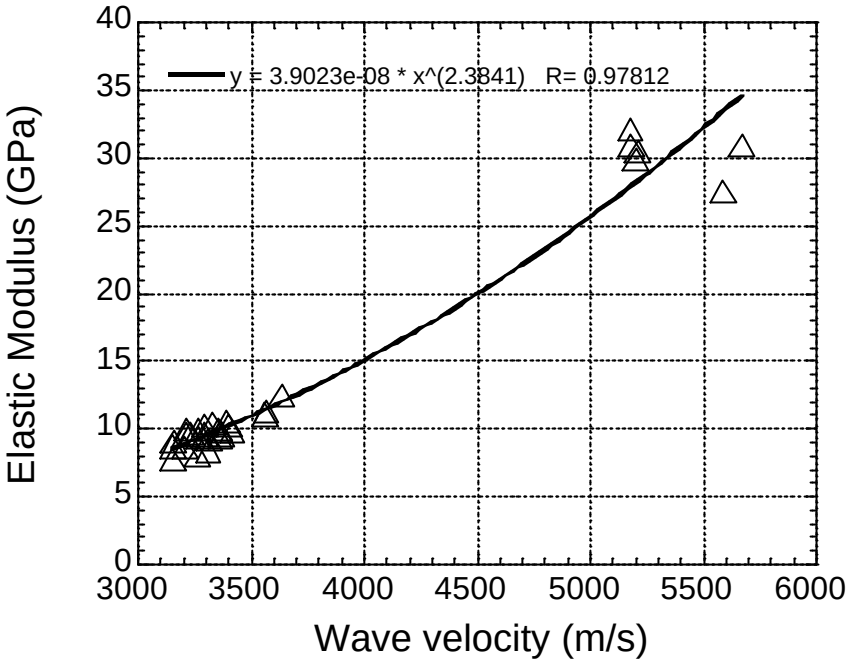

Figure 4.38. Relationship between wave velocity and modulus of elasticity.

There is a close relationship between surface hardness and compressive strength, tensile strength and modulus of elasticity. As the surface hardness increases compressive strength, tensile strength and modulus of elasticity increases, see Figure 4.39, Figure 4.40, Figure 4.41.

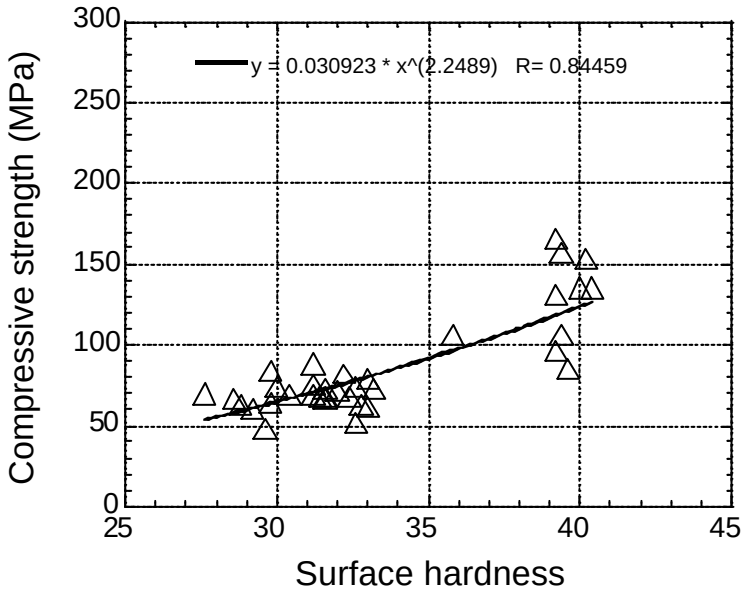

Figure 4.39. Relationship between surface hardness and compressive strength.

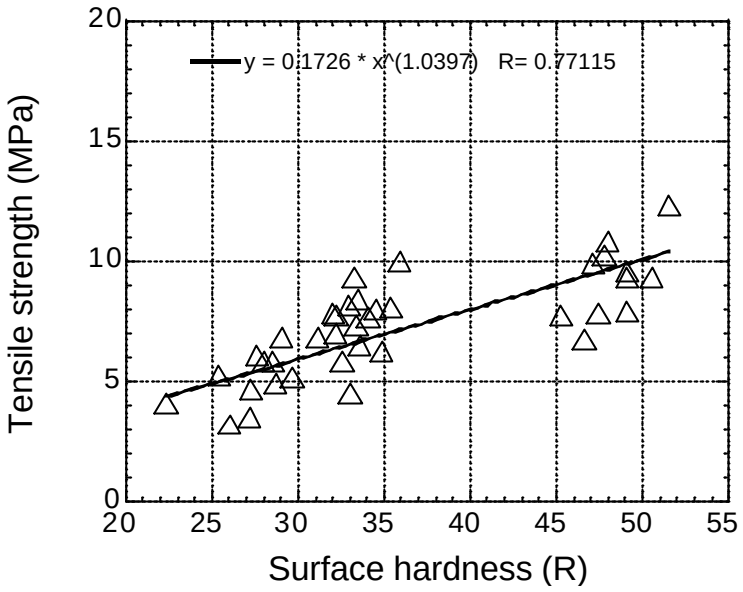

Figure 4.40. Relationship between surface hardness and tensile strength.

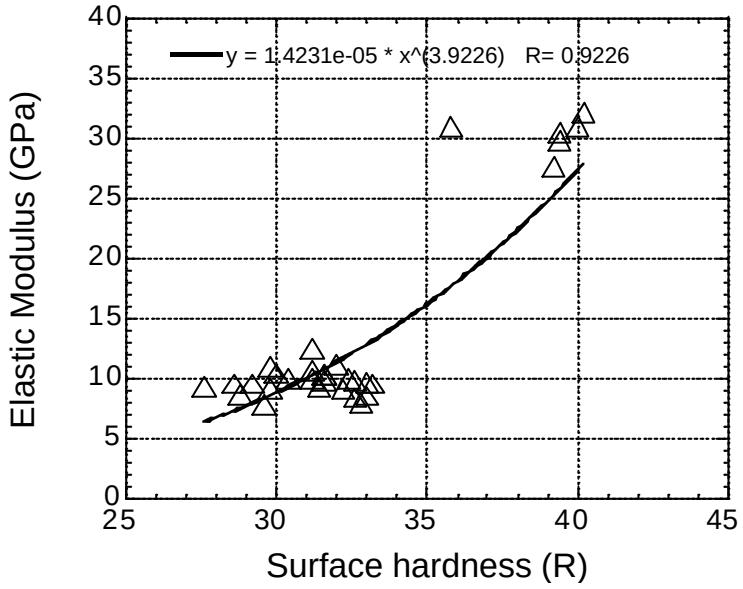

Figure 4.41. Relationship between surface hardness and modulus of elasticity.

The experimental set up of uniaxial compression test is far easier then the set up for test defining the modulus of elasticity especially incase when the strain gauges are used to determine the deformation. Because of that, the relationship between the compressive strength and the modulus of elasticity is given in Figure 4.42. The modulus of elasticity increases as the compressive strength increases, see Figure 4.42.

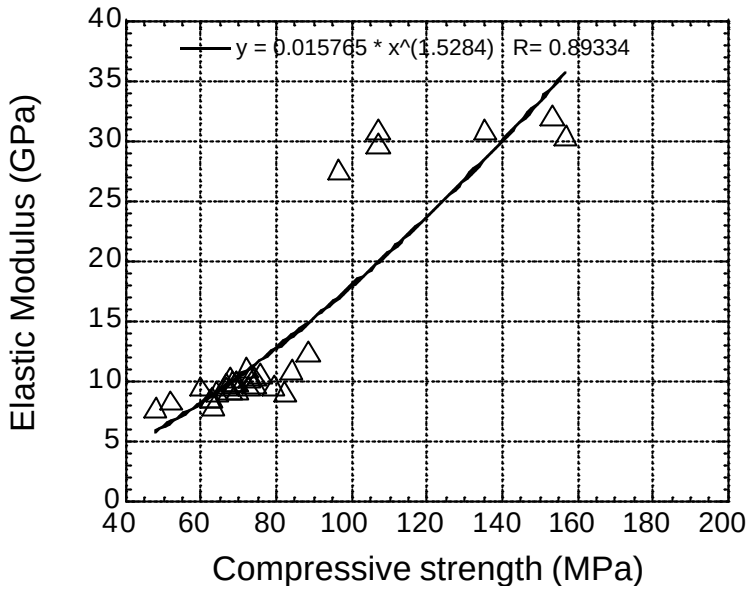

Figure 4.42. Relationship between the compressive strength and modulus of elasticity.

The compressive strength is also related to tensile strength as the compressive strength increases, tensile strength increases, see Figure 4.43.

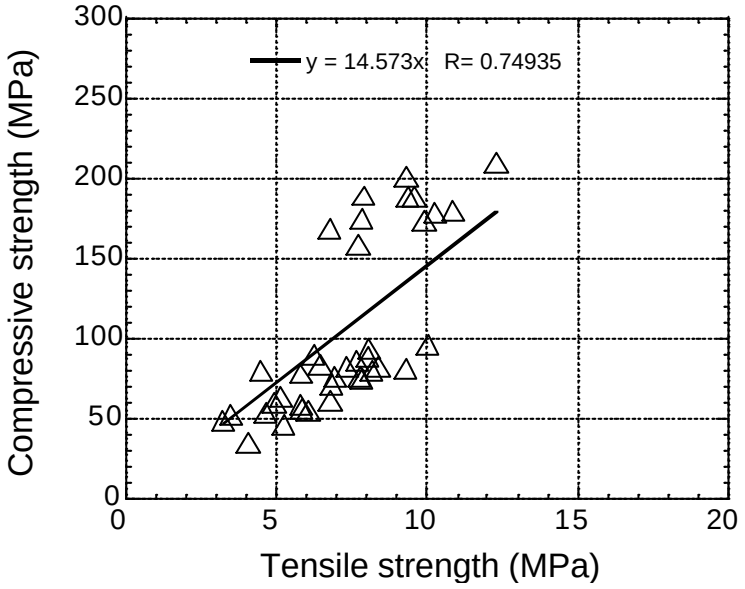

Figure 4.43. Relationship between the compressive strength and tensile strength.

Limestone has been a widely used construction material through centuries. Because of that, these relationships may help other researchers working on historical structures who do not have the chance to conduct such variety of tests and who are in

need of relationships given here. Lots of other relationships can be derived by use of data given in this chapter for limestone.

One important point is that, the relationships including porosity can be increased so that by use of only a small amount of stone sample, i.e. 100 grams, and determining its density and porosity by Archimedes principal, the strength values of the stone can be estimated.

4.4.2. Tests on Bricks

Bricks were used in the construction of dome, trompes, window arches and the west wall out leaf. Other then these, brick pieces were used with mortar on some regions of the walls irregularly.

Thirteen bricks were taken from the structure in which most of them were fallen bricks. Ultrasonic pulse velocity test was conducted on the brick samples before core drilling, see Table 4.12 and Table 4.13. The ultrasonic pulse velocity test was applied by CNS Farnell Electronics' Pundit type equipment. The equipment was used under 500V EHT voltage and 10pps (pulse per second). As the surfaces of the bricks were not smooth pulse velocity measurements contain some error.

Cylinder core samples of diameter D=25.6mm were drilled out that have varying height. Some of the core samples were used for uniaxial compression test while others were used for indirect tension test.

4.4.2.1. Uniaxial Compression Test

The testing procedure is presented in 2.5.4. The perfectly shaped cylinder core samples have a "y" while the ill shaped ones have a "n" on the "shape" column of Table. 4.12. The test was conducted by use of mechanical testing machine Shimadzu AG1 which has a capacity of 250kN. The machine reads the stroke from the head with respect to applied load and time. The loading rate was taken as 0.2mm/minute which satisfied the condition of failure time between 5 to 10 minutes. Generally all the samples were failed at 10 minute. The compressive strength value at Table 4.14 is the average of the good shaped cores given in Table 4.12 having "y" on the shape column.

The modulus of elasticity values were determined by the use of stress-strain curve of the test and the slope of the linear portion of the curve is evaluated. The modulus of elasticity values are given at Table 4.12 and an average value for all bricks is given in Table 4.14.

Fracture energy of the samples was determined by evaluating the area under stress- strain diagram. Fracture energy values are given at Table 4.12.

Table 4.12. Test results of compression test core samples for bricks.

No:	Name:	Diameter D: (mm)	Length L (mm)	Area A (mm2)	P (kN)	Compressive Strength (MPa)	Modulus of Elasticity E:(MPa)	Fracture Energy (KJ/m3)	Ultra. Time µsec	Thickness for Ultra.V (mm)	Ultra. V (m/sec)	Shape
1	t1-1	25.6	32.16	514.72	4.52	8.78	526.59	78.28	20.5	33	1609.76	n
2	t1-2	25.6	29.42	514.72	7.10	13.79	1239.79	94.17	20.5	33	1609.76	n
3	t1-3	25.6	29.95	514.72	6.24	12.12	861.62	83.51	20.5	33	1609.76	n
4	t2-1	25.6	28.89	514.72	7.55	14.67	1995.00	82.91	25.8	36	1395.35	n
5	t2-2	25.6	25.88	514.72	7.73	15.02	838.89	175.56	25.8	36	1395.35	y
6	t2-3	25.6	23.56	514.72	10.35	20.11	1386.50	274.24	25.8	36	1395.35	y
7	t2-4	25.6	27.20	514.72	5.66	11.00	798.70	122.68	25.8	36	1395.35	y
8	t2-5	25.6	25.97	514.72	8.45	16.42	1196.88	144.67	25.8	36	1395.35	y
9	t2-6	25.6	30.70	514.72	3.38	6.57	394.60	90.09	25.8	36	1395.35	n
10	t3-1	25.6	30.40	514.72	5.09	9.89	789.34	78.62	33.0	34	1030.30	n
11	t3-2	25.6	27.29	514.72	4.97	9.66	589.30	125.92	33.0	34	1030.30	n
12	t3-3	25.6	23.83	514.72	7.23	14.05	1008.08	174.36	33.0	34	1030.30	n
13	t4-1	25.6	35.90	514.72	4.88	9.48	1470.96	38.53	22.3	32	1434.98	n
14	t4-2	25.6	27.11	514.72	8.64	16.79	0.00	0.00	22.3	32	1434.98	y
15	t4-3	25.6	30.97	514.72	6.60	12.82	1021.18	86.72	22.3	32	1434.98	y
16	t4-4	25.6	29.02	514.72	8.67	16.84	2465.36	71.34	22.3	32	1434.98	y
17	t4-5	25.6	27.18	514.72	4.13	8.02	1270.01	30.85	22.3	32	1434.98	n
18	t4-6	25.6	26.40	514.72	7.22	14.03	1709.37	67.94	22.3	32	1434.98	n
19	t4-7	25.6	27.70	514.72	7.23	14.05	994.27	131.95	22.3	32	1434.98	n
20	t5-1	25.6	29.78	514.72	5.34	10.37	697.00	97.74	38.8	35	902.06	y
21	t6-1	25.6	27.27	514.72	4.73	9.19	1225.44	37.00	21.0	34	1619.05	n
22	t6-2	25.6	27.66	514.72	5.61	10.90	1479.92	65.31	21.0	34	1619.05	n
23	t6-3	25.6	29.39	514.72	6.07	11.79	1271.79	153.14	21.0	34	1619.05	n
24	t6-4	25.6	21.38	514.72	6.85	13.31	1174.50	209.13	21.0	34	1619.05	n
25	t7-1	25.6	24.70	514.72	6.22	12.08	971.20	106.27	32.0	30	937.50	n
26	t7-2	25.6	23.27	514.72	5.14	9.99	646.17	159.10	32.0	30	937.50	n
27	t7-3	25.6	21.99	514.72	5.40	10.49	702.28	316.84	32.0	30	937.50	n
28	t8-1	25.6	26.99	514.72	4.89	9.50	890.37	93.93	19.0	32	1684.21	n
29	t8-2	25.6	25.36	514.72	4.10	7.97	375.37	181.05	19.0	32	1684.21	n
30	t8-3	25.6	24.40	514.72	6.30	12.24	392.00	156.38	19.0	32	1684.21	y
31	t8-4	25.6	24.06	514.72	4.45	8.65	699.22	115.12	19.0	32	1684.21	n
32	t8-5	25.6	24.25	514.72	8.57	16.65	1653.88	129.55	19.0	32	1684.21	n

Continue of Table 4.12. Test results of compression test core samples for bricks.

No:	Name:	Diameter D (mm)	Length L (mm)	Area A (mm2)	P (kN)	Compression Strength (MPa)	Modulus of Elasticity E:(MPa)	Fracture Energy (KJ/m3)	Ultra. Time µsec	Thickness for Ultra.V (mm)	Ultra. V (m/sec)	Shape
33	t8-6	25.6	26.80	514.72	3.96	7.69	731.35	129.70	19.0	32	1684.21	n
34	t8-7	25.6	24.00	514.72	5.48	10.65	709.54	146.61	19.0	32	1684.21	y
35	t8-8	25.6	25.81	514.72	4.78	9.29	346.40	208.70	19.0	32	1684.21	y
36	t8-9	25.6	26.36	514.72	3.91	7.60	1338.08	22.60	19.0	32	1684.21	n
37	t8-10	25.6	27.03	514.72	7.27	14.12	1568.97	161.04	19.0	32	1684.21	y
38	t9-1	25.6	27.58	514.72	3.56	6.92	1068.87	65.56	25.0	33	1320.00	n
39	t9-2	25.6	27.64	514.72	3.23	6.28	236.49	178.01	25.0	33	1320.00	n
40	t9-3	25.6	28.07	514.72	4.95	9.62	739.35	114.16	25.0	33	1320.00	n
41	t9-4	25.6	29.76	514.72	4.98	9.68	1083.40	54.71	25.0	33	1320.00	y
42	t9-5	25.6	27.13	514.72	6.38	12.40	907.83	104.74	25.0	33	1320.00	n
43	t9-6	25.6	28.70	514.72	4.16	8.08	545.65	190.39	25.0	33	1320.00	n
44	t10-1	25.6	29.04	514.72	3.53	6.86	806.58	29.54	21.0	36	1714.29	n
45	t10-2	25.6	29.36	514.72	6.62	12.86	1803.23	99.82	21.0	36	1714.29	n
46	t10-3	25.6	25.83	514.72	5.31	10.32	1369.72	46.61	21.0	36	1714.29	y
47	t10-4	25.6	26.79	514.72	7.45	14.47	882.99	192.20	21.0	36	1714.29	n
48	t10-5	25.6	25.36	514.72	5.79	11.25	684.74	155.83	21.0	36	1714.29	n
49	t11-1	25.6	32.41	514.72	2.78	5.40	309.41	64.91	39.2	39	994.90	y
50	t11-2	25.6	30.25	514.72	1.97	3.83	190.42	60.66	39.2	39	994.90	y
51	t11-3	25.6	32.26	514.72	1.69	3.28	126.30	52.56	39.2	39	994.90	n
52	t11-4	25.6	32.06	514.72	3.16	6.14	432.50	49.91	39.2	39	994.90	y
53	t11-5	25.6	32.31	514.72	2.70	5.24	447.00	40.29	39.2	39	994.90	y
54	t12-1	25.6	23.62	514.72	4.88	9.48	241.88	180.56	29.2	30	1027.40	n
55	t12-2	25.6	24.60	514.72	2.05	3.98	155.79	151.27	29.2	30	1027.40	n
56	t13-1	25.6	25.88	514.72	5.45	10.59	458.34	153.93				n
57	t13-2	25.6	24.90	514.72	5.89	11.44	0.00	0.00				n
58	t13-3	25.6	25.98	514.72	4.08	7.93	484.90	131.08				n
59	t13-4	25.6	23.10	514.72	8.08	15.70	718.40	146.62				y

For t4-2 and t13-2 the data (stress-strain) for evaluating the modulus of elasticity and fracture energy was lost.

For coding, ti-j means ith brick sample, jth core sample from the ith brick sample.

4.4.2.2. Indirect Tension Test

The test procedure is given in part 2.5.5. The test was conducted by use of mechanical testing machine Shimadzu AG1 which has a capacity of 250kN. The machine reads the stroke from the head with respect to applied load and time. The loading rate applied was 1mm/min. Generally all the core samples failed at 15 seconds which complies with the 15-30 second rule for duration (Ulusay et al. 2001, p.69). The data obtained by indirect tension test are given at Table 4.13. The average values for brick samples are given at Table 4.14.

Table 4.13. Test results of indirect tension test core samples for bricks.

No:	Name :	Diameter D (mm)	Length L (mm)	Area A (mm2)	P (kN)	Tensile Strength (MPa)	Ultra. V. (m/sec)	Loading Rate (mm/min)
1	t1-t1	25.6	23.42	514.72	1.86	1.973	1609.75	1
2	t1-t2	25.6	22.87	514.72	1.91	2.075	1609.75	1
3	t2-t1	25.6	21.42	514.72	1.49	1.728	1395.35	1
4	t2-t2	25.6	20.22	514.72	1.23	1.511	1395.35	1
5	t4-t1	25.6	19.31	514.72	2.43	3.126	1434.98	1
6	t5-t1	25.6	19.81	514.72	1.66	2.082	902.06	1
7	t7-t1	25.6	20.14	514.72	1.39	1.715	937.50	1
8	t8-t1	25.6	17.63	514.72	1.27	1.790	1684.21	1
9	t8-t2	25.6	26.13	514.72	1.05	0.998	1684.21	1
10	t8-t3	25.6	20.03	514.72	1.22	1.513	1684.21	1
11	t8-t4	25.6	24.38	514.72	2.28	2.323	1684.21	1
12	t9-t1	25.6	22.49	514.72	2.05	2.265	1320.00	1
13	t10-t1	25.6	27.31	514.72	2.60	2.365	1714.29	1
14	t10-t2	25.6	28.03	514.72	3.07	2.721	1714.29	1
15	t11-t1	25.6	29.49	514.72	1.09	0.918	994.89	1
16	t12-t1	25.6	19.24	514.72	0.60	0.775	1027.39	1

Table 4.14.Average values for brick test.

	Compressive Strength (MPa)	Tensile Strength (MPa)	Modulus of Elasticity E (MPa)
Bricks	11.68	1.867	866.5

According to a study conducted by Architectural Restoration Department of IZTECH on bricks of Urla Kamanli Bath which belongs to the same structural group

with the Kamanli Mosque, the porosity and density of bricks are %p=29.45 , ?=1800kg/m^3 respectively. All of the brick core samples are given in Figure 4.44.

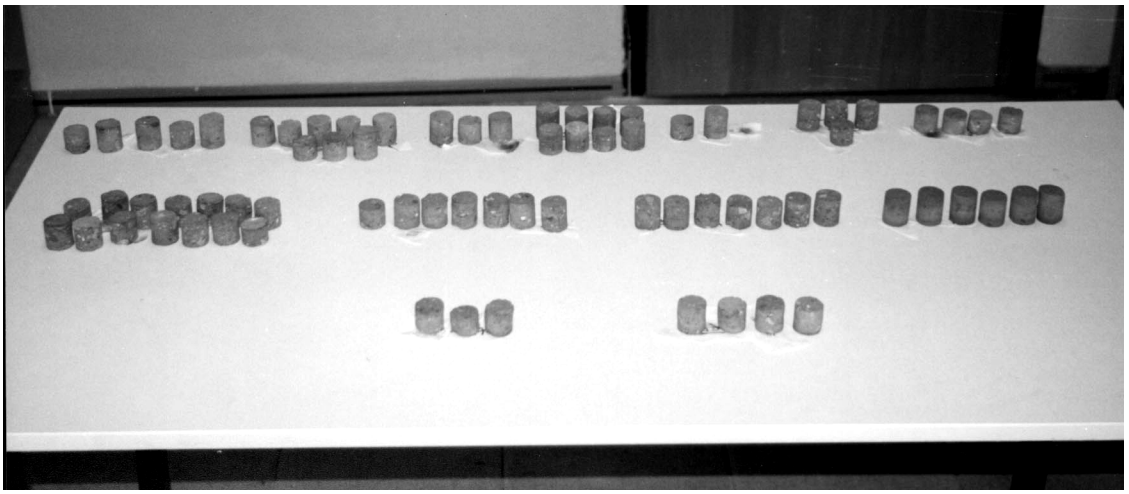

Figure 4.44. Brick core samples.

4.4.3. Tests on Mortars

The mortar samples were taken from inside the structure and outside the structure, from the walls of the gate wall. The mortar samples obtained from Kamanli Mosque were weak for core drilling so only point load test could be applied. The testing procedure is presented at part 2.5.6. The point load test was applied on arbitrary shape samples. The moisture of the samples was also measured by use of James Instruments Moisture Meter. By use of point load index, the uniaxial compressive strength of mortars were estimated, see Table 4.15. The average uniaxial compressive strength of mortar samples taken from inside the structure is σ_c=19.9MPa. These samples are shown in grey cells on Table 4.15.

Table 4.15. Point load test results on mortar.

No:	Name:	Rel.Moist.	Width W (mm)	Diameter D(mm)	Eq.Diameter De2 (mm2)	P (kN)	Is (Mpa)	F	Is(50) (Mpa)	Comp.Str.Mpa
1	h1	0.87	44.4	22.4	1264.89	0.02	0.0158	4.279	0.0677	3.194
2	h2	0.76	48.5	30.0	1852.56	0.10	0.0540	5.081	0.2743	5.394
3	h3	0.75	67.0	47.0	4009.43	0.30	0.0748	7.192	0.5381	8.203
4	h4	0.61	50.0	47.0	2992.11	0.18	0.0602	6.305	0.3793	6.512
5	h5	0.48	40.0	34.5	1757.07	0.05	0.0285	4.962	0.1412	3.977
6	h6	0.66	50.0	35.0	2228.17	0.35	0.1571	5.521	0.8673	11.708
7	h7	0.61	47.0	44.0	2633.06	0.10	0.0380	5.952	0.2261	4.880
8	h8	0.49	46.0	18.0	1054.24	0.20	0.1897	3.943	0.7480	10.437
9	h9	0.45	32.5	13.5	558.63	0.20	0.3580	2.963	1.0607	13.766
10	h10	0.53	37.0	28.5	1342.63	0.20	0.1490	4.396	0.6548	9.445
11	h11	0.87	53.0	28.0	1889.49	0.06	0.0318	5.126	0.1628	4.207
12	h12	0.40	47.0	40.0	2393.69	0.12	0.0501	5.702	0.2859	5.517
13	h13	0.56	37.0	30.0	1413.30	0.07	0.0495	4.499	0.2228	4.846
14	h14	0.66	51.0	34.0	2207.80	0.20	0.0906	5.499	0.4981	7.777
15	h15	0.59	41.0	45.0	2349.13	0.06	0.0255	5.654	0.1444	4.011
16	h16	0.53	28.0	31.0	1105.17	0.00	0.0000	4.027	0.0000	2.474
17	h17	3.80	43.0	27.3	1494.66	0.04	0.0268	4.613	0.1235	3.788
18	h18	2.75	36.5	37.5	1742.75	0.06	0.0344	4.943	0.1702	4.286
19	h19	4.92	35.0	39.5	1760.25	0.10	0.0568	4.966	0.2821	5.477
20	h20	4.92	43.0	18.0	985.49	0.05	0.0507	3.825	0.1941	4.540
21	h21	1.18	36.5	26.0	1208.30	0.00	0.0000	4.192	0.0000	2.474
22	h22	0.95	105.5	34.8	4674.57	0.56	0.1198	7.706	0.9232	12.303
23	h23	0.91	53.0	39.0	2631.79	0.33	0.1254	5.951	0.7462	10.418
24	h24	0.91	42.5	36.0	1948.06	0.25	0.1283	5.197	0.6670	9.575
25	h25	0.91	43.0	30.0	1642.48	0.25	0.1522	4.813	0.7326	10.274
26	h26	0.91	27.0	27.0	928.19	0.20	0.2155	3.723	0.8022	11.015
27	h27	0.91	24.0	36.5	1115.36	0.03	0.0269	4.044	0.1088	3.632
28	h28	0.75	46.0	37.5	2196.34	0.50	0.2277	5.486	1.2488	15.770
29	h29	0.55	27.0	37.0	1271.97	0.18	0.1415	4.290	0.6071	8.938
30	h30	0.63	49.5	36.0	2268.91	0.45	0.1983	5.566	1.1040	14.228
31	h31	0.63	33.0	32.0	1344.54	0.35	0.2603	4.399	1.1450	14.665
32	h32	0.63	32.0	35.0	1426.03	0.10	0.0701	4.517	0.3167	5.846
33	h33	1.06	92.5	21.0	2473.27	1.00	0.4043	5.787	2.3397	27.385
34	h34	0.93	44.0	21.0	1176.47	2.80	2.3800	4.142	9.8583	107.436
35	h35	0.91	48.0	23.0	1405.66	1.25	0.8893	4.488	3.9906	44.962
36	h36	0.96	46.0	24.0	1405.66	0.36	0.2561	4.488	1.1493	14.710
37	h37	0.96	34.0	21.0	909.09	0.50	0.5500	3.688	2.0286	24.072
38	h38	0.76	88.0	18.0	2016.81	1.20	0.5950	5.279	3.1411	35.917
39	h39	0.74	40.0	22.0	1120.45	0.70	0.6247	4.052	2.5316	29.428
40	h40	0.75	49.0	23.5	1466.14	0.60	0.4092	4.573	1.8716	22.401
41	h41	0.85	63.0	23.0	1844.92	0.80	0.4336	5.072	2.1992	25.889

Continue of Table 4.15. Point load test results on mortar.

No:	Name:	Rel.Moist.	Width W (mm)	Diameter D(mm)	Eq. Diameter De2 (mm2)	P (kN)	Is (Mpa)	F	Is(50) (Mpa)	Comp.Str. Mpa
41	h41	0.85	63.0	23.0	1844.92	0.80	0.4336	5.072	2.1992	25.889
42	h42	0.70	73.0	28.0	2602.50	2.00	0.7685	5.921	4.5502	50.920
43	h43	0.76	40.0	21.0	1069.52	1.80	1.6830	3.968	6.6785	73.581
44	h44	0.76	34.0	29.0	1255.41	0.20	0.1593	4.265	0.6795	9.708
45	h45	0.71	22.0	32.0	896.36	0.73	0.8144	3.665	2.9848	34.253
46	h46	0.71	61.0	48.0	3728.05	1.30	0.3487	6.960	2.4271	28.315
47	h47	0.59	60.0	35.0	2673.80	0.60	0.2244	5.993	1.3449	16.793
48	h48	1.64	100.0	38.0	4838.31	1.50	0.3100	7.827	2.4265	28.308
49	h49	0.97	50.0	41.0	2610.14	1.20	0.4597	5.929	2.7257	31.495
50	h50	0.95	50.0	37.0	2355.49	1.00	0.4245	5.661	2.4034	28.062
51	h51	0.95	50.0	43.0	2737.47	1.70	0.6210	6.057	3.7616	42.524
52	h52	1.83	33.0	36.0	1512.61	0.60	0.3967	4.638	1.8398	22.062
53	h53	1.05	39.0	34.5	1713.14	1.40	0.8172	4.905	4.0087	45.155
54	h54	1.30	92.0	47.0	5505.49	1.50	0.2725	8.295	2.2600	26.537
55	h55	1.92	55.0	36.0	2521.01	1.00	0.3967	5.837	2.3152	27.124
56	h56	1.28	55.0	30.0	2100.85	0.35	0.1666	5.377	0.8958	12.011
57	h57	1.37	36.0	32.0	1466.77	0.30	0.2045	4.574	0.9356	12.435
58	h58	2.03	52.0	46.0	3045.59	1.25	0.4104	6.355	2.6083	30.244
59	h59	1.11	49.0	24.0	1497.33	0.50	0.3339	4.617	1.5417	18.889
60	h60	0.70	56.0	59.0	4206.78	0.75	0.1783	7.349	1.3102	16.424
61	h61	1.11	57.0	32.0	2322.39	1.00	0.4306	5.625	2.4221	28.262
62	h62	1.15	60.0	33.0	2521.01	0.70	0.2777	5.837	1.6207	19.729
63	h63	0.78	60.0	33.0	2521.01	0.15	0.0595	5.837	0.3473	6.171
64	h64	1.05	104.0	33.0	4369.76	0.70	0.1602	7.476	1.1976	15.225
65	h65	0.87	59.0	38.0	2854.60	0.50	0.1752	6.172	1.0811	13.985
66	h66	0.84	32.0	32.0	1303.80	0.19	0.1457	4.338	0.6322	9.205
67	h67	0.84	42.0	32.0	1711.23	0.10	0.0584	4.903	0.2865	5.524
68	h68	0.76	44.0	33.0	1848.74	0.50	0.2705	5.076	1.3729	17.091
69	h69	1.05	72.0	35.0	3208.56	0.60	0.1870	6.506	1.2166	15.427
70	h70	2.29	36.0	40.0	1833.46	0.40	0.2182	5.058	1.1034	14.221
71	h71	1.04	57.0	36.0	2612.69	0.35	0.1340	5.931	0.7946	10.933
72	h72	0.90	35.0	35.0	1559.72	0.30	0.1923	4.703	0.9045	12.104
73	h73	0.69	32.0	30.0	1222.31	0.35	0.2863	4.214	1.2067	15.321
74	h74	0.97	33.0	32.0	1344.54	0.25	0.1859	4.399	0.8179	11.182
75	h75	1.37	44.0	43.0	2408.97	0.15	0.0623	5.719	0.3561	6.265
76	h76	1.11	42.0	27.0	1443.85	0.05	0.0346	4.542	0.1573	4.148
77	h77	1.11	28.0	30.0	1069.52	0.00	0.0000	3.968	0.0000	2.474
78	h78	1.17	42.0	33.0	1764.71	0.15	0.0850	4.971	0.4226	6.973
79	h79	0.86	43.0	25.0	1368.73	0.00	0.0000	4.434	0.0000	2.474
80	h80	0.77	85.0	51.0	5519.49	2.30	0.4167	8.305	3.4606	39.319
81	h81	0.77	71.0	48.0	4339.20	1.50	0.3457	7.452	2.5762	29.903
82	h82	0.77	63.0	44.0	3529.42	1.50	0.4250	6.791	2.8861	33.203
83	h83	0.77	52.0	56.0	3707.67	1.60	0.4315	6.943	2.9962	34.375

The Architectural Restoration Department of IZTECH had conducted research on mortar of Urla Kamanli Bath, which belongs to the same group of structure with Kamanli Mosque. Mortar samples were taken from the stone masonry wall and brick masonry of the structure. These samples were strong enough to cut out core samples and

were core drilled. Density-porosity test was applied on the remaining samples while uniaxial compression and indirect tension tests were applied on core samples by use of mechanical testing machine Shimadzu AG1 which has a capacity of 250kN. The machine reads the stroke from the head with respect to applied load and time. The modulus of elasticity was also determined by use of stress-strain curve. The data gathered is presented in Table 4.16.

Table 4.16. Tests results of Kamanli Bath mortar.

	Compressive Strength σc (MPa)	Tensile Strength σt (MPa)	Modulus of Elasticity E (MPa)	Density ? (kg/m3)	porosity (%)
MS	4.19	0.73	110.5	1690	32.796
MB	8.75	0.95	264.38	1400	43.458

The MS represents stone masonry mortar while MB represents brick masonry mortar. The porosity of MB is higher then the porosity of MS. The density of MB is lower then the density of MS. On the other hand, the strength of MB is higher then the strength of the MS, see Table4.16. The constructers of the structure were sensible for the mortar of brick masonry which was used for the dome that it is lighter but stronger then the stone masonry mortar.

The compressive strength estimated by point load test is higher then the values obtained by conventional tests.

4.5. Seismic Risk and Soil Survey

The seismic risk and local soil conditions of the region were investigated.

Izmir city is under high seicmic risk as can be seen on the earthquake zone map, on Figure 4.45 (WEB_3). The red zones show the regions with highest risk where as the white zones show the regions with least seismic risk at Figure 4.45.

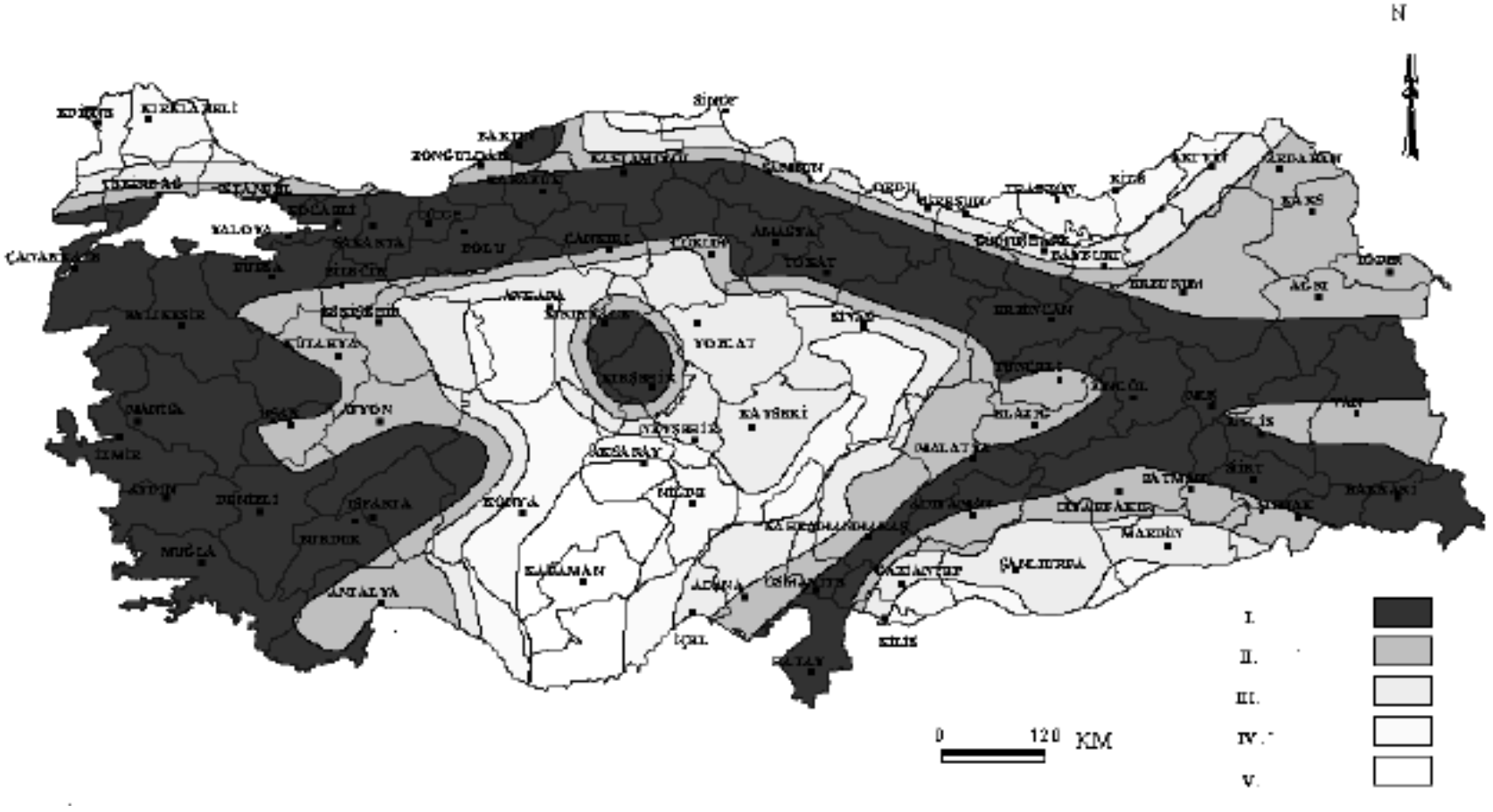

Figure 4.45. Seismic risk zones of Turkey (WEB_3).

In its history, Izmir have had strong seismic actions and the city had almost completely corrupted several times (WEB_4). The strong earthquakes in the 20th century are presented in Figure 4.46. These earthquakes have magnitudes up to 7.

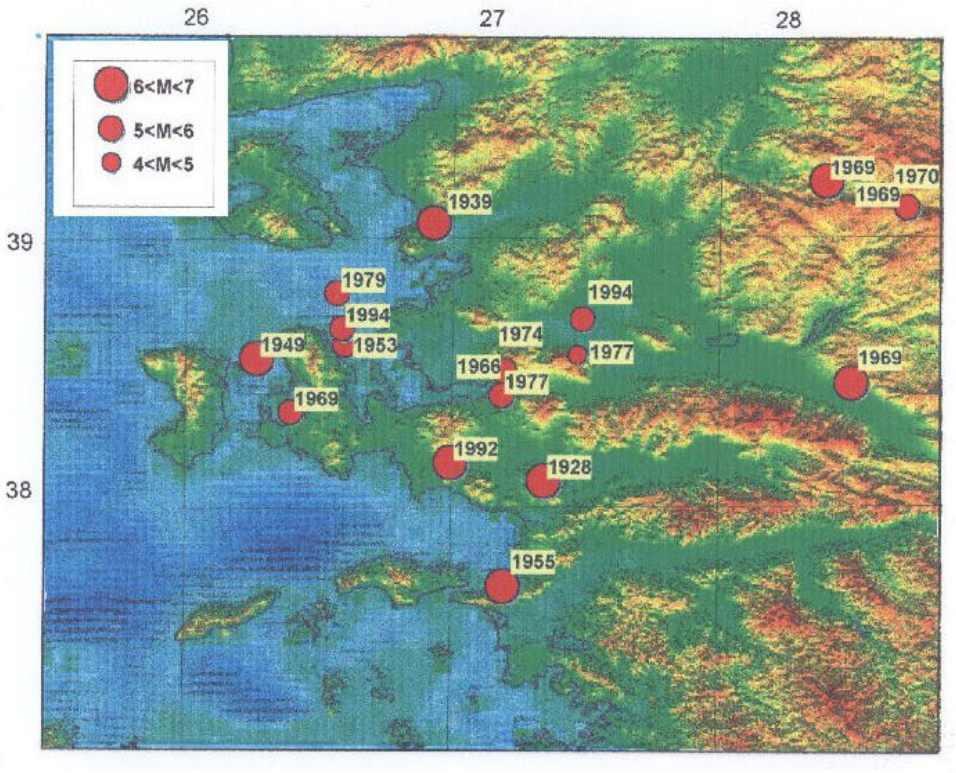

Figure 4.46. Strong earthquakes occured in Izmir and vicinity in 20th century (WEB_5).

Other then strong motions, micro seismic activity has been continuing in Izmir. In Figure 4.47, the micro seismic activity with strong motions are given that occured after 1980, the region of Kamanli Mosque is shown by a star. The region of the structure has been active by means of seismicity, see Figure 4.47. The seismic source zones for Izmir with the faults are presented at Figure 4.48. The star is the place of the Kamanli Mosque, in Urla, Izmir. As can be seen in Figure 4.48, there are two major faults passing from the east and west of the region of the Kamanli Mosque.

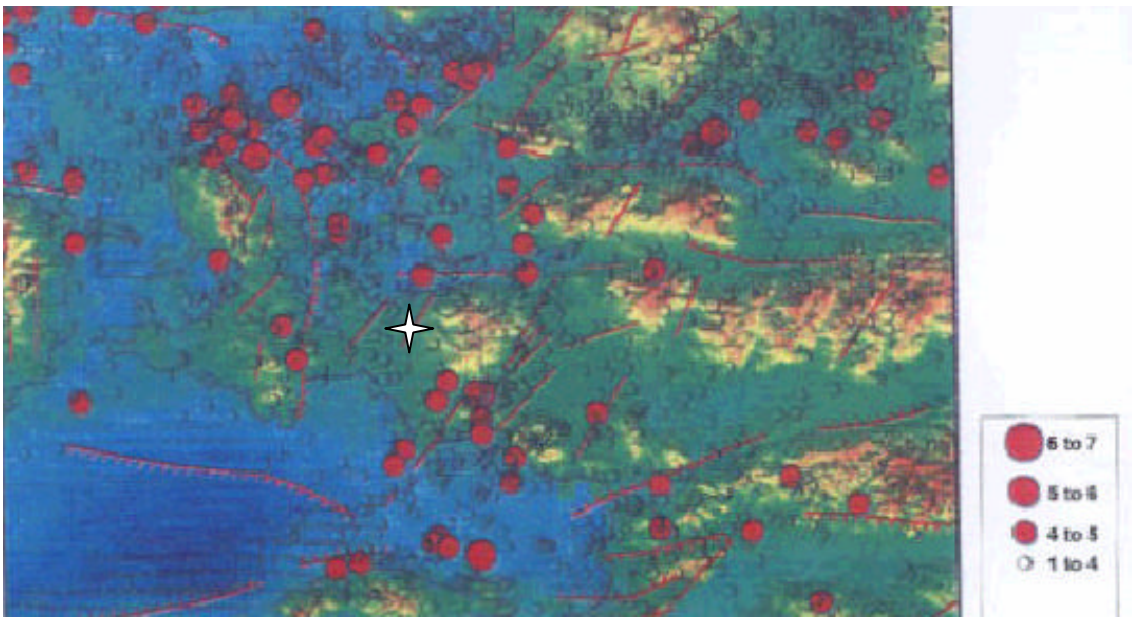

Figure 4.47. The epicentres and distribution of all the earthquakes occured in Izmir and its vicinity (WEB_4).

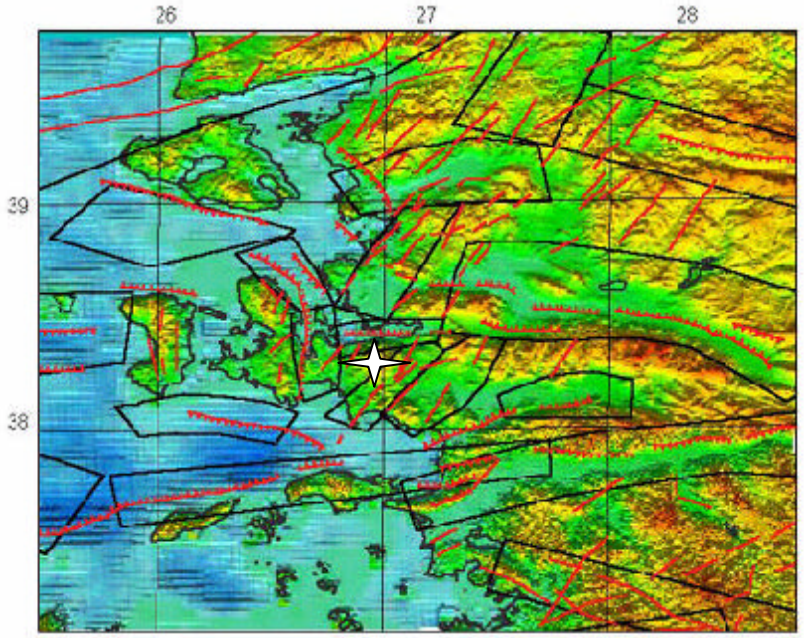

Figure 4.48. Faults near the Kamanli Mosque (WEB_4).

The expected earthquake intensity for a return period of 475 years is approximately 7.5 for the region of the structure which is shown by a star, see Figure 4.49.

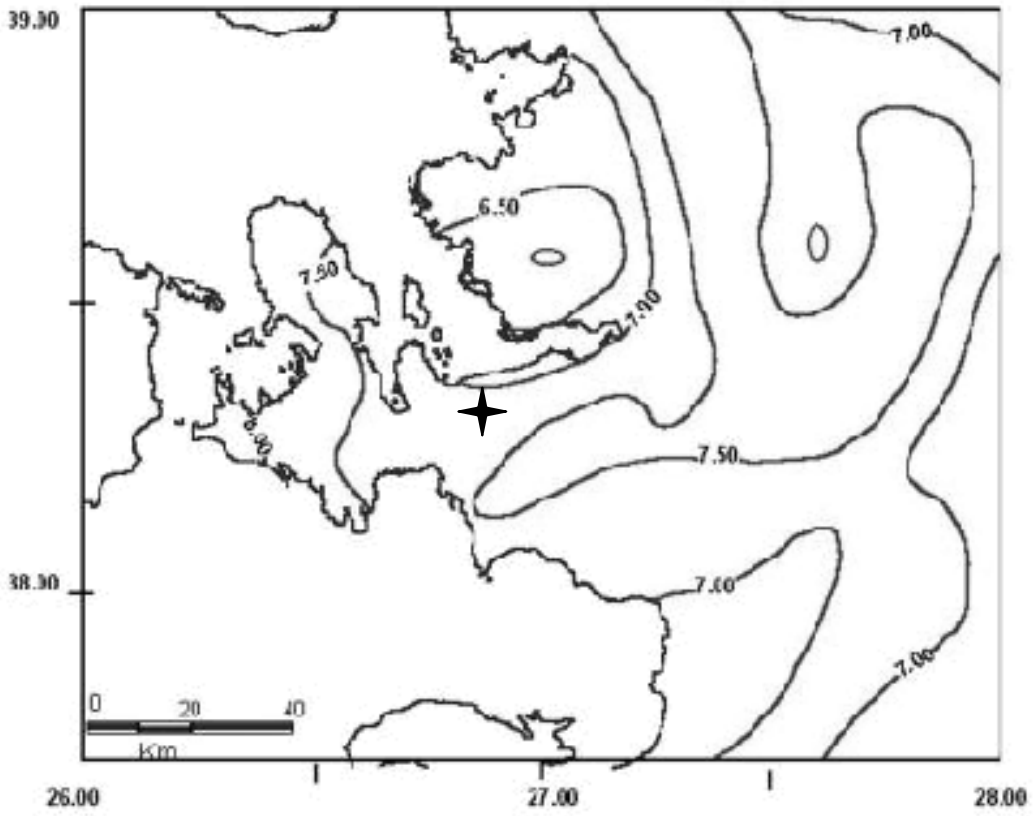

Figure 4.49. Expected MSK intensity for a return period of 475 years (WEB_4).

The expected peak ground acceleration for soft soils for a return period of 475 years is given in Figure 4.50 for Izmir region and its vicinity. The region of the structure is marked by a star and the ground acceleration is approximately 0.4g for the region of the structure.

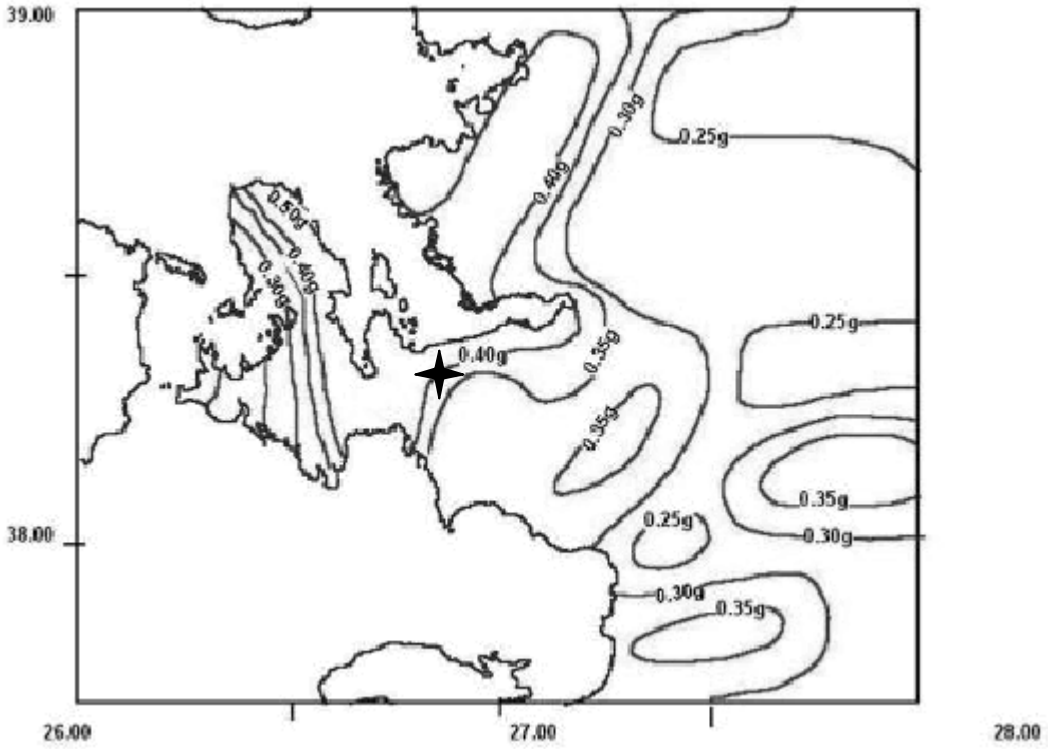

Figure 4.50. Expected peak ground acceleration for soil site for a return period of 475 years (WEB_4).

In order to investigate the local soil conditions, two geological reports which belong to neighboring parcels of the Kamanli Mosque were obtained from Urla Municipality. The region of the structure is composed of Miocene old limestone, clay stone, marl, and volcanic ash. The dominant is limestone. The first 30cm to 1.5m is composed of organic soil (Alkan 1994, p7).

The region is under effect of Alpine tectonics so is in 1st order seismic zone (Ispir 2000, p.3). The period of soil is estimated to be Tc=0.15-0.20sec in the region of the structure (Ispir 2000, p.4). The soil allowable stress is estimated to be Zs=29.7N/cm^2 (Ispir 2000, p.6).

The under ground water level is stated to be at 20m (Alkan 1994, p.8) and at 90m (Ispir 2000, p3) so it can be concluded that the underground water level is not a risk.

There are two wells in the gate of the structure, one of them is just 4 meters and the other is approximately 10 meters apart from the structure. These wells are not used at the time and the one which is 10m apart is open that no water was observed in it. On the other hand the mouth of the nearer well is closed by heavy rocks and any

observation could not be made about its situation. It is suspected that the second well can cause unbalanced seepage in the rainy seasons leading to the differential settlement.

4.6. Finite Element Analyses of Urla Kamanli Mosque

The data gathered up to this section are used for finite element (FE) analyses of Kamanli Mosque. The measurement survey data are used for defining the 3D geometry, the material tests data are used for defining elastic and inelastic material properties, the long term observations give clues about loading.

Finite element analyses of Kamanli Mosque have been performed in order to determine the causes of the structural cracks which challenge the structure. Also the safety of the structure under dead load and seismic load has been investigated.

A commercial FE program, LUSAS (London University Stress Analysis System) which has been developed by FEA Ltd. (in England) has been used for FE modeling. LUSAS can solve linear, nonlinear stress, dynamics, composite and thermal engineering analyses problems. The program has sub menus for Analyst, Composite, Civil and Structural and Bridge in order to make the applications easier for specific groups.

LUSAS has been used for analyses of historical masonry structures by other researchers. Prof. Dr. Ahmet Çakmak had used LUSAS for analyses of Hagia Sophia, see Figure 4.51 (WEB_6). Dr. Ali Koçak used LUSAS for linear and nonlinear analyses of Kucuk Ayasofya Cami (former Sergius and Bacchus Church) (Koçak 1999).

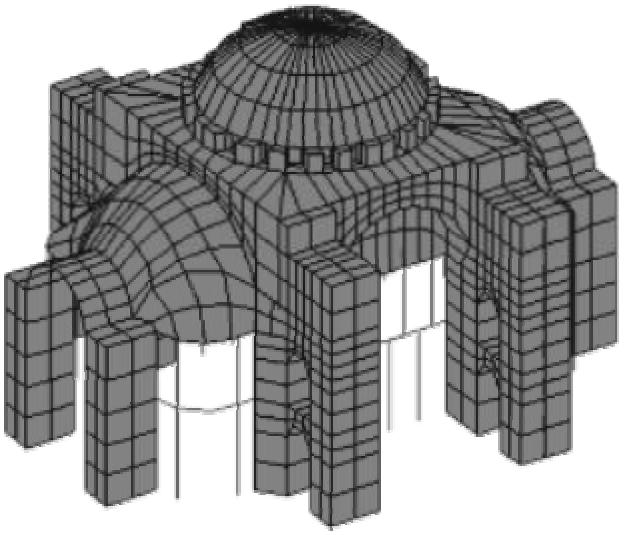

Figure 4.51. FE model of Hagia Sophia by Cakmak et al (WEB_6).

While modeling the structure, two kinds of elements were used, hexahedral (HX8M) and pentahedral (PN6). The HX8M has accuracy in coarse mesh and the element does not suffer from locking in the nearly incompressible limit (FEA Ltd.b, p107). The shape function of HX8M is given in Eq. 4.5 (FEA Ltd.b, p107).

$$\overline{N}_1(x)=\frac{1}{2}\left(1-x^2\right),\overline{N_2}(h)=\frac{1}{2}\left(1-h^2\right),\overline{N_3}(z)=\frac{1}{2}\left(1-z^2\right) \qquad \text{Eq.4.5}$$

The nodal configurations for HX8M element are given in Figure 4.52 (FEA Ltd.b, p117).

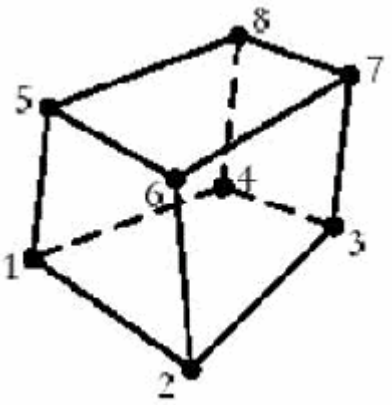

Figure 4.52 The HX8M element (FEA Ltd. b 2002, p. 105).

Translational degrees of freedoms U, V and W are defined at every node.

PN6 elements are used at the top of the dome in order to avoid excessive aspect ratio at the key stone region of the dome. The element shape is given in Figure 4.53.

The strain-displacement relationship for HX8M and PN6 which is developed for 3D space, is given in Eq.4.6. The isotropic and orthotropic elastic modulus matrices are given in Eq.4.7 and Eq.4.8, respectively. The element results of direct and shear stresses and strains can be obtained at both element nodes and Gauss points. Principal stress and strains and corresponding direction cosines can be obtained. The sign convention for stress and strains are given in Figure 4.54.

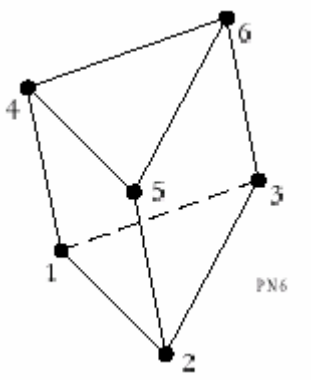

Figure 4.53. The PN6 element (FEA Ltd. b 2002, p. 105).

$$e_x = \frac{\partial U}{\partial X},\ e_y = \frac{\partial V}{\partial Y},\ e_z = \frac{\partial U}{\partial Z},\ g_{xy} = \frac{\partial U}{\partial Y} + \frac{\partial V}{\partial X},\ g_{yz} = \frac{\partial V}{\partial Z} + \frac{\partial W}{\partial Y},\ g_{xz} = \frac{\partial U}{\partial Z} + \frac{\partial W}{\partial X}$$

Eq.4.6.

$$\underline{\underline{D}} = \frac{E}{(1-n)(1-2n)} \begin{bmatrix} (1-n) & n & n & 0 & 0 & 0 \\ n & (1-n) & n & 0 & 0 & 0 \\ n & n & (1-n) & 0 & 0 & 0 \\ 0 & 0 & 0 & \frac{(1-2n)}{2} & 0 & 0 \\ 0 & 0 & 0 & 0 & \frac{(1-2n)}{2} & 0 \\ 0 & 0 & 0 & 0 & 0 & \frac{(1-2n)}{2} \end{bmatrix} \quad \text{Eq.4.7.}$$

$$\underline{\underline{D}} = \begin{bmatrix} \frac{1}{E_x} & -n_{yx}E_y & -n_{zx}E_z & 0 & 0 & 0 \\ \frac{-n_{xy}}{E_x} & \frac{1}{E_y} & \frac{-n_{zy}}{E_z} & 0 & 0 & 0 \\ \frac{-n_{xz}}{E_x} & \frac{-n_{yz}}{E_y} & \frac{1}{E_z} & 0 & 0 & 0 \\ 0 & 0 & 0 & \frac{1}{G_{xy}} & 0 & 0 \\ 0 & 0 & 0 & 0 & \frac{1}{G_{yz}} & 0 \\ 0 & 0 & 0 & 0 & 0 & \frac{1}{G_{xz}} \end{bmatrix} \quad \text{Eq.4.8}$$

Where ν is the Poisson's ratio and E is the modulus of elasticity. ν_{yx}, ν_{zx} and ν_{zy} are defined by Eq.4.9 to maintain the symmetry.

$$n_{yx} = n_{xy}\frac{E_y}{E_x} \qquad n_{zx} = n_{xz}\frac{E_z}{E_x} \qquad n_{zy} = n_{yz}\frac{E_z}{E_y} \qquad \text{Eq.4.9.}$$

In order to define a valid material, inequalities in Eq. 4.10 should be satisfied.

$$n_{xy} < \left(\frac{E_x}{E_y}\right)^{\frac{1}{2}} \qquad n_{xz} < \left(\frac{E_x}{E_z}\right)^{\frac{1}{2}} \qquad n_{yz} < \left(\frac{E_y}{E_z}\right)^{\frac{1}{2}} \qquad \text{Eq.4.10.}$$

The 3D elements can be used in;

1. Material nonlinear analyses using elastoplastic constitutive laws.
2. Geometrical nonlinear analyses.
3. Geometrical and material nonlinear analyses.
4. Nonlinear dynamics using nonlinear material laws.
5. Linear eigen-buckling analyses (FEA Ltd. b 2002, p.103).

There are a total of 3793 HX8M and 24 PN6 element used in the model. The element size was determined to be 3 to 4 times the dimensions of the constituents of masonry, stone or brick and mortar (Koçak 1999, p.172). Taking in to account the computational time, the sensitivity of the system and the fact referred above, the mesh dimension was determined to be 50cm. In some parts where the geometry restricts, deviations of up to ±20cm from 50cm were applied.

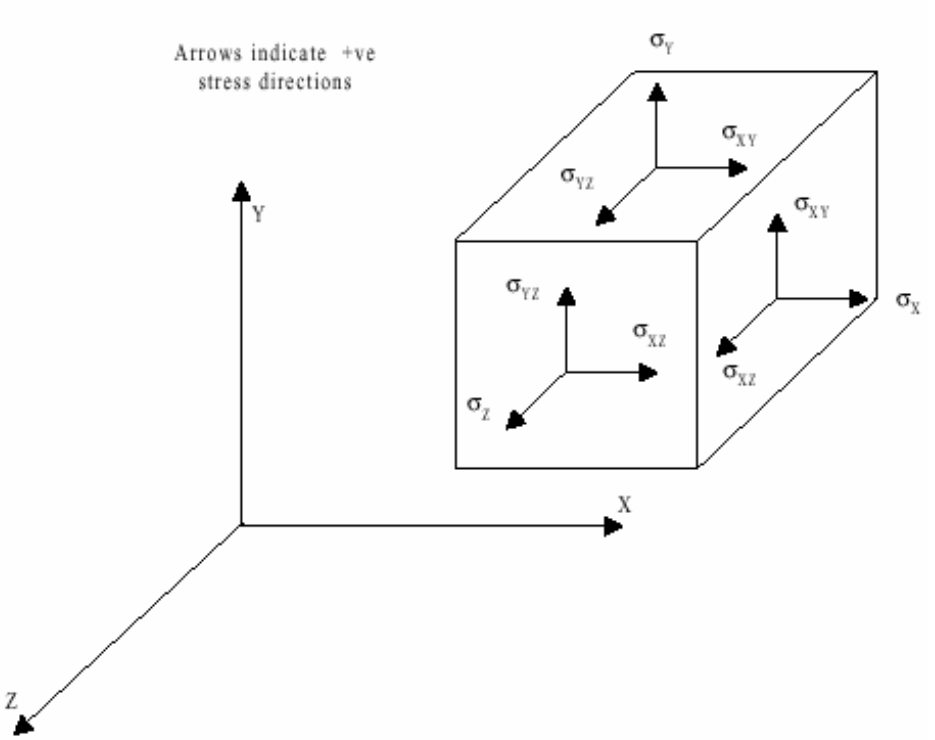

Figure 4.54. Sign convention for stress and strains (FEA Ltd. b 2002, p.106).

The FE program, LUSAS, does not permit to add up volumes and mesh them all together. While creating the model with fidelity to the 3D dimensions obtained from measurement survey, surfaces formed which touches each other. The relationship between the nodes at neighboring surfaces was achieved by use of constraint equations. There are different constraint equation options defined at LUSAS while some of them also have sub alternatives to be defined. The basic types of constraint equations are listed below (FEA Ltd. a, p182);

1.Displacement control,

2.Geometric,

3.Cyclic,

4.Tied mesh.

Tied mesh constraint equation was used for constructing up the model and only this constraint equation will be presented in details here.

The tied mesh can be defined by two ways; specified or normal. The specified tied mesh can be used by defining two points to be tied together which need not to be match geometrically.

The normal tied mesh, which is used in the model, is defined by selecting one surface as slave and the other as master. The nodal variables, i.e. displacements of the master surface nodes are distributed over the nodes of the slave surface with respect to the distances between nodes of master and slave surfaces. For example, if node 1 is on master surface, nodes 2 and 3 are on slave surface and the distance between 1 to 2 and 3 are 0.4m and 0.6m respectively, the displacement of node 1 is shared between nodes 2 and 3 by a ratio of 0.6 and 0.4, respectively. In other words, the closer the node to master node, the higher it takes on from master node, in an inverse proportion with its distance. This constraint approach prevents the model to be over stiffed while maintaining the bonds between the parts of the structure. For constructing up the whole model, 93 normal tied mesh constraint equations was used.

The geometry of the model was constructed up by use of graphical user interface. LUSAS has easy-to-use menus for defining the geometry. Facilities like mirroring, copying, sweeping, moving, with different sub alternatives like translate, rotate, matrix rotation etc. makes 3D modeling available.

As if constructing up the real structure, the model was generated from the bottom step by step. The volume components of the structure were constructed by sweeping the surfaces which were generated generally by sweeping lines and lines were constructed by sweeping points. In order to follow the results easily, the parts of the structure were labeled due to their directions and grouped. The groups can be made invisible for legibility of results or selected individually for assigning different properties. The mesh, material properties, loads etc. are all assigned to geometric features; which are points, lines, surfaces and volumes.

All of the geometrical details like door and window openings, window arches, the tromps, the drum and the embellishment niches in the walls which decreases the cross sections of the walls, were modeled. The empty places of the wooden lintels were modeled by decreasing the wall sections from 110 cm by an amount of 15cm from both sides to 80cm. The wooden lintels were surrounding the walls at two levels, H=1.92m and H=4.5m from the ground level, from inside and outside. In Figure 4.55, the south bottom part volume (S1) is given with the reduction in wall cross section because of lintel places, the embellishment niche at the south section and the black-lined surfaces which are master-slave to each other for a tied mesh constraint.

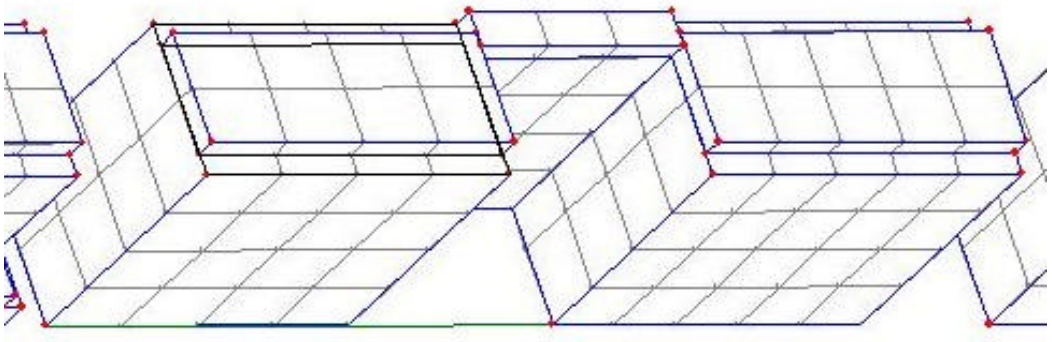

Figure 4.55. South S1 volume with niche and lintel places.

The step by step construction of the model by necessary codes for result evaluation is given through Figure 4.56 to Figure 4.60. The coding was made in regard to the directions. The parts on the west have codes beginning with "W" and same rule is valid for the other directions. In Figure 4.56, the 1st lintel places, the niches at S1, E2, W2, N1 and N2 can be seen. In Figure 4.57, the 2nd lintel places can be seen with the highlighted buttress to support the weak section of the south niche. The transmission from the walls to the dome is achieved by tromps, one of them highlighted in Figure 4.58. Also the window openings can be seen in Figure 4.58. The octagon drum was used to support the dome, see Figure 4.59. The whole model can be seen in Figure 4.60.

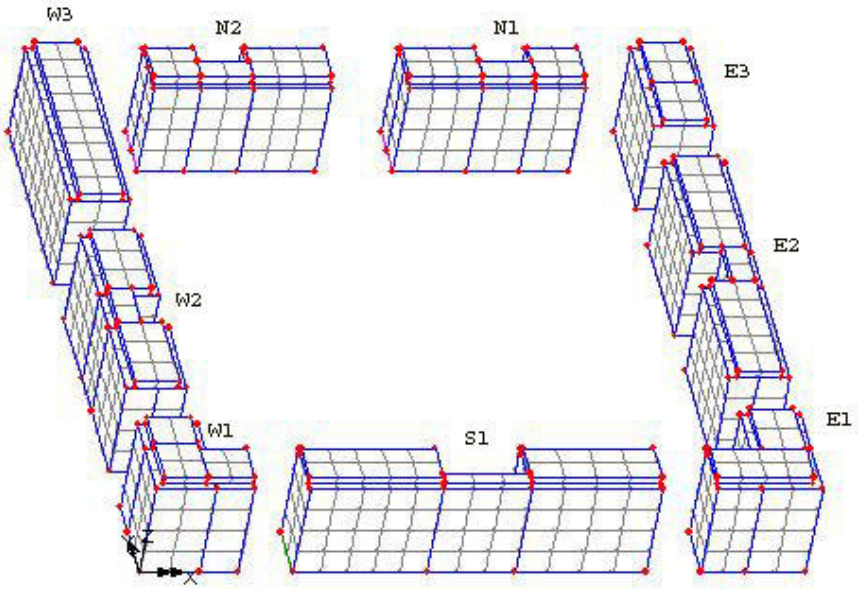

Figure 4.56. The 1st level of the model, H=2.07m.

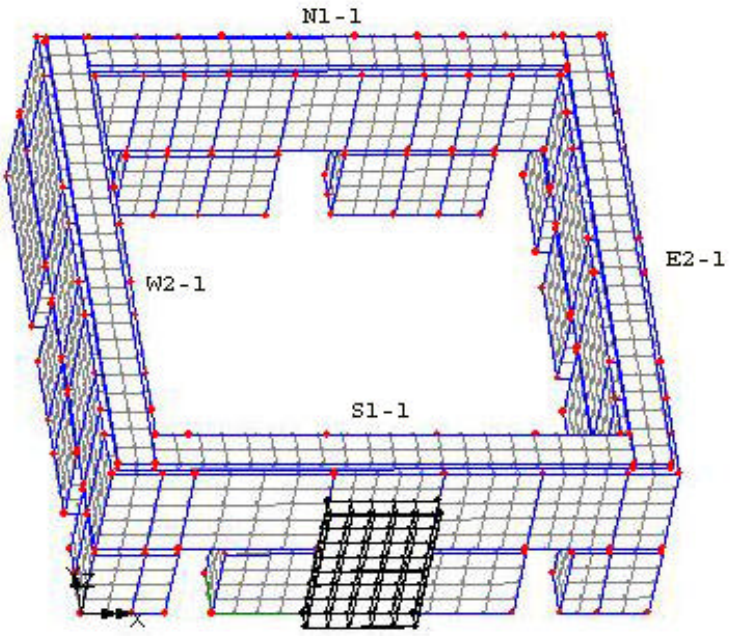

Figure 4.57. The 2nd level of the model H=4.65m.

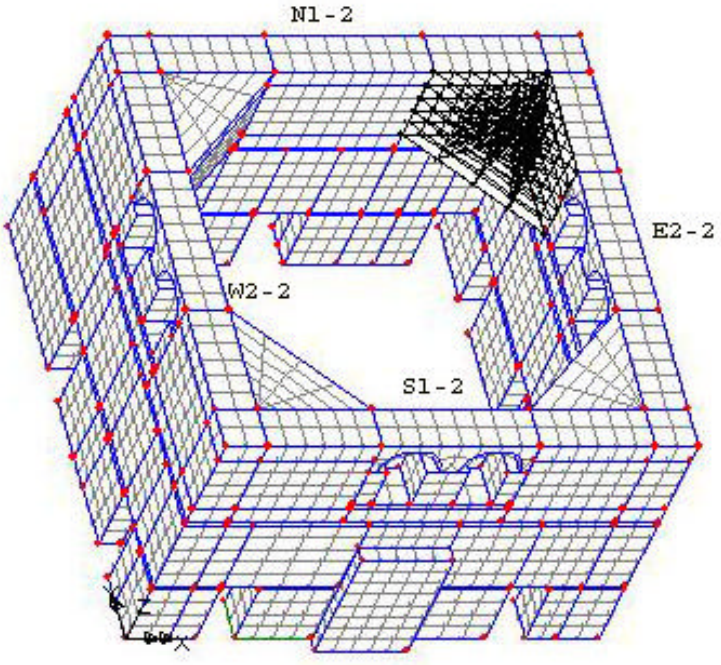

Figure 4.58. The 3rd level of the model H=7.66m.

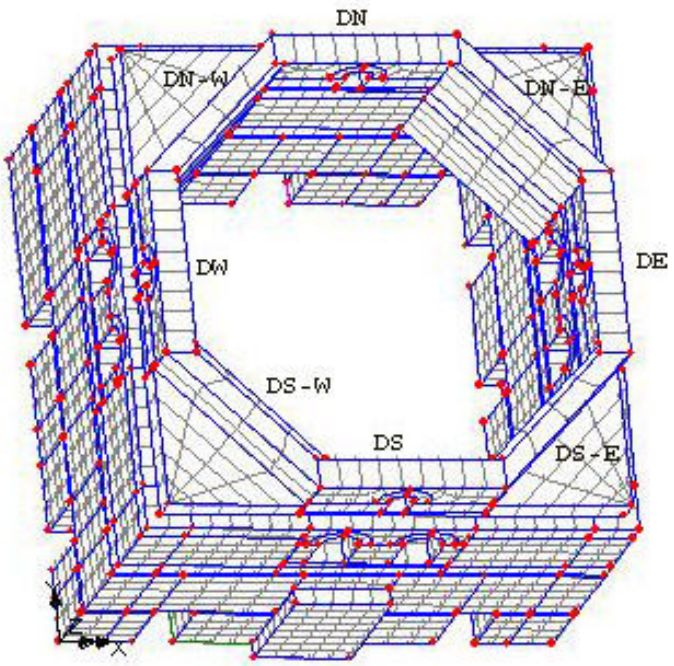

Figure 4.59. The drums H=9.46m.

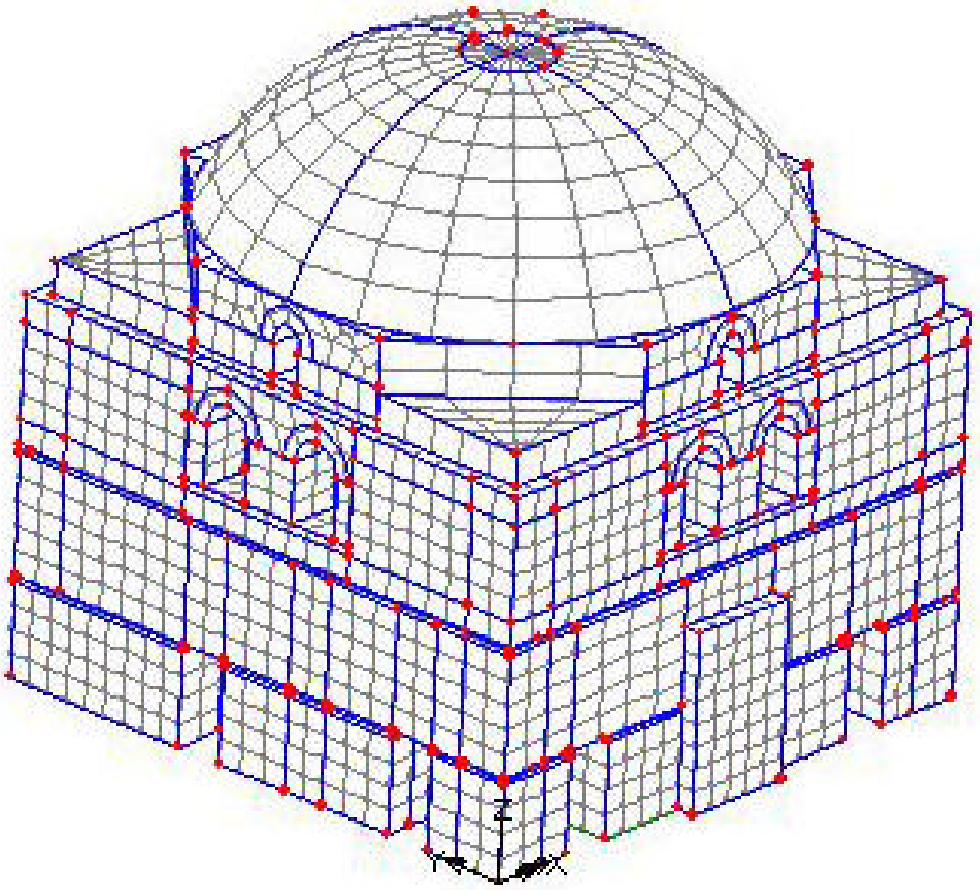

Figure 4.60. Whole model H=12.66m.

4.6.1 Determination of Material Parameters for FE Model

The masonry composite media has been modeled by use of homogenization approach. In this approach, the behavior of individual constituents (stone and mortar) is discarded and an over all behavior of the composite media has been taken into account. While determining the elastic parameters of masonry media, the homogenization equations which depend on the strength parameters of constituents were used.

The compressive strength of masonry is determined by Eq. 4.11 (European Committee for Standardization 1995, p. 51).

$$f_k = K \times f_b^{0.65} \times f_m^{0.25} \qquad \text{Eq. 4.11}$$

where K is a constant, f_b is the compressive strength of unit (stone or brick), f_m is compressive strength of mortar. K is in the range of 0.6 to 0.4 with 0.05 variations. The value of K depends on the morphology of the masonry (European Committee for Standardization 1995, p. 51). In this study K is taken as 0.5. All of the units should be in N/mm^2 (MPa). There are different relationships for compressive strength of different kinds of masonry which are not presented here (European Committee for Standardization 1995).

The modulus of elasticity of masonry is determined by use of Eq.4.12 (Lourenco 2001, p.669).

$$E = \frac{t_m + t_u}{\frac{t_m}{E_m} + \frac{t_u}{E_u}} \times r \qquad \text{Eq.4.12.}$$

where t_m, t_u, E_m and E_u are the thickness of mortar and height of the unit (stone), and modulus of elasticity of mortar and unit, respectively. The coefficient ? varies with the bond between mortar and unit and taken 0.5 for this study (Lourenco 2001, p.669). Also Eq.4.13 could be used for determining the modulus of elasticity of masonry (European Committee for Standardization 1995, p.61).

$$E = 1000 \times f_k \qquad \text{Eq.4.13}$$

The shear modulus can be taken 40% of the modulus of elasticity (European Committee for Standardization 1995, p.62).

The tensile strength of masonry can be taken as 10% of compressive strength (Kocak 1999, p.215).

The elastic parameters of brick masonry (BM, composed of brick and mortar) and stone masonry (SM, composed of stone and mortar) are defined separately.

4.6.1.1. Parameters of Stone Masonry (SM)

The elastic parameters of stone masonry were found by use of the strength values of south stones which are weaker then the west stones. The average of the compressive strength value of S1 and S2 stones is found by use of values at Table 4.9 and Eq.4.14.

$$f_{average} = \frac{64.17 + 65.44}{2} = 64.8MPa \qquad \text{Eq.4.14.}$$

The compressive strength value at Table 4.16 is used which is f_m=4.19MPa.

The compressive strength of stone masonry is determined by Eq.4.15.

$$f_{ksm} = 0.5 \times 64.8^{0.65} \times 4.19^{0.25} = 10.77MPa \qquad \text{Eq.4.15.}$$

The tensile strength of stone masonry is determined by Eq.4.16.

$$f_{tsm} = 0.1 \times f_{ksm} = 0.1 \times 10.77 = 1.077MPa \qquad \text{Eq.4.16.}$$

In order to determine the modulus of elasticity of stone masonry, the average value of south stone samples (S1 and S2) were used at Table 4.9 and put into Eq. 4.17.

$$E_{average} = \frac{9.22 + 9.24}{2} = 9.23GPa \qquad \text{Eq.4.17}$$

The modulus of elasticity of stone masonry mortar is taken from Table 4.16, E_m=0.11GPa.

The modulus of elasticity of stone masonry is determined by Eq. 4.18.

$$E_{sm} = \frac{0.01 + 0.25}{\frac{0.01}{0.11} + \frac{0.25}{9.23}} \times 0.5 = 1.1GPa \qquad \text{Eq.4.18.}$$

where 0.01m is the thickness of mortar and 0.25m is the average height of the stone.

The shear modulus of stone masonry is found by Eq.4.19.

$$G_{sm} = 1.1 \times \frac{40}{100} = 0.44GPa \qquad \text{Eq.4.19.}$$

The density of the stone masonry is taken ?=2200kg/m^3 which is a reasonable value between the densities of stones (2500kg/m^3) and mortar (1690kg/m^3).

4.6.1.2. Parameters of Brick Masonry (BM)

The compressive strength of brick masonry is determined by Eq. 4.20.

$$f_{kbm} = 0.5 \times 11.68^{0.65} \times 8.75^{0.25} = 4.25 MPa \qquad \text{Eq.4.20}$$

where 11.68 and 8.75 are compressive strengths of brick and brick masonry mortar, respectively.

The tensile strength of brick masonry is determined by Eq.4.21.

$$f_{tbm} = 0.1 \times 4.25 = 0.425 MPa. \qquad \text{Eq.4.21}$$

The modulus of elasticity of brick masonry is determined by Eq.4.22.

$$E_{bm} = \frac{0.01 + 0.03}{\frac{0.01}{0.26} + \frac{0.03}{0.87}} \times 0.5 = 0.27 GPa \qquad \text{Eq.4.22}$$

The shear modulus of brick masonry is determined by Eq. 4.23.

$$G_{bm} = 0.4 \times 0.27 = 0.11 GPa \qquad \text{Eq.4.23}$$

The density of brick masonry is taken as ?=1700kg/m^3 which is a reasonable value between the density of brick (1800kg/m^3) and density of brick masonry mortar (1400kg/m^3). The Poisson's ratio is taken as 0.17 for masonry (Kocak 1999, p.214). The elastic material parameters are presented at Table 4. 17.

Table 4.17. Elastic material parameters for masonry.

	Stone Masonry	Brick Masonry
Compressive Strength (MPa)	10.77	4.25
Tensile Strength (MPa)	1.077	0.425
Modulus of Elasticity (GPa)	1.1	0.27
Shear Modulus (GPa)	0.44	0.11
Density (kg/m3)	2200	1700
Poisson's Ratio	0.17	0.17

The material parameters determined for stone masonry have been assigned to walls while the parameters for the brick masonry have been assigned to window arches, tromp and dome of the structure.

The analyses results will be presented in ongoing parts. The directions will also be used with the coding of the parts of the structure. The global X axis lays parallel to the south elevation and point towards east. The global Y axis lays parallel to the west

elevation and points towards north. The Z axis points towards up to the structure, see Figure 4.60. Units of N, kg, m, sec are used during the analyses.

4.6.2. Linear Elastic Self Weight Analysis

Linear elastic self weight analysis of the structure has been conducted in order to understand the safety of the structure under its self weight. Also, the relationship between stress state under self weight and the existing cracks has been investigated.

The material parameters of modulus of elasticity, density and porosity presented at Table 4.17 have been used for the analysis. The dead load has been acted on the structure by applying acceleration equal to 9.81m/sec^2 in global -Z direction.

The contour plot of the global Z direction displacements (DZ) is given in Figure.4.61.

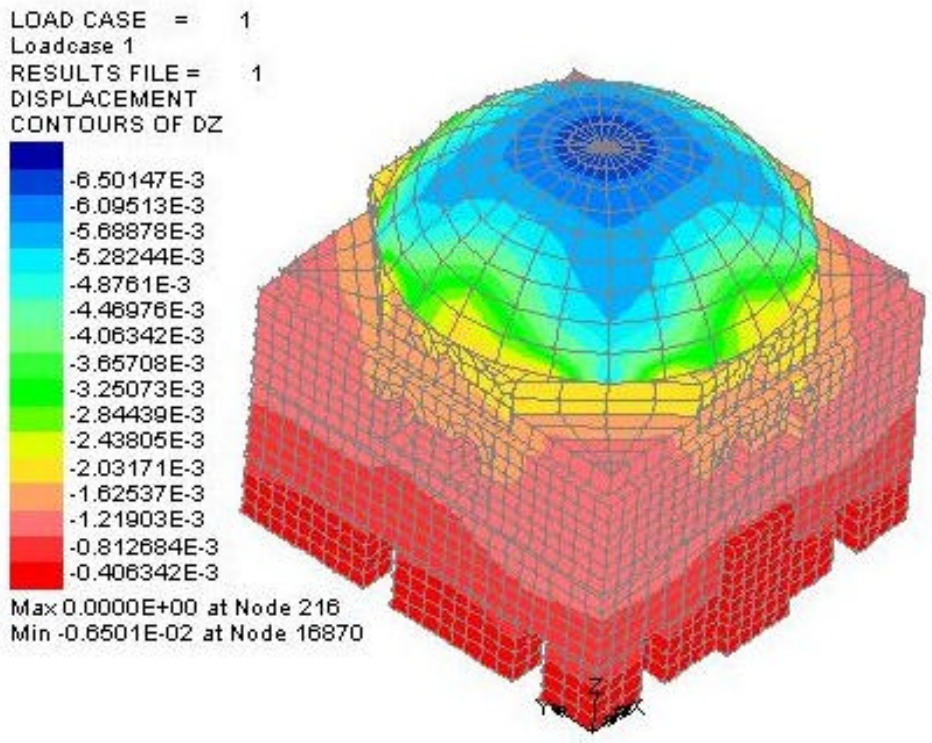

Figure 4.61. DZ displacement contours of self weight analysis.

In the self weight analysis, the displacements DZ in the vertical direction increases (by means of their absolute value), to the higher points as expected, see Figure 4.61. The portions of the dome resting on the corners (supported by the tromps) sag more then the portions resting on the drum which is supported by the walls, see Figure

4.61. The drum transmits the weight directly to the walls while the tromps transmit the weight indirectly. The maximum absolute vertical displacement is 6mm to the negative Z direction, at the top of the key stone of the dome, see Figure 4.61.

The upper 10% of the first principal stresses (S1) are at the drum-dome interfaces, see Figure 4.62, Figure 4.63. The maximum S1=0.69e6MPa is smaller then the tensile strength of stone masonry (ftsm=1.077e6MPa) but greater then the tensile strength of brick masonry (ftbm=0.425e6MPa). The location of the maxiumum S1 is on the drum dome connection and on the drum which is stone masonry, see Figure 4.63. The maximum S1 does not challenge the structure as it is smaller then the stone masonry where it occurs. Also, the tensile strength of brick masonry is a little bit smaller then the maximum of S1 (0.425e6<0.69e6). There is no crack observed at the place of the maximum S1 on the structure.

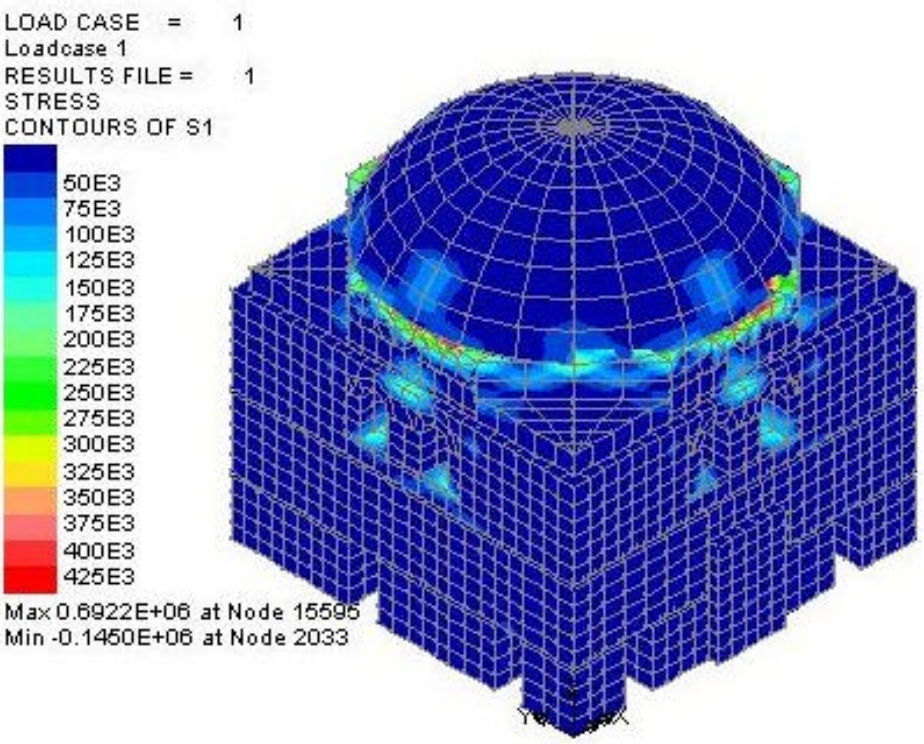

Figure 4.62. S1 1st principal stress contours under self weight.

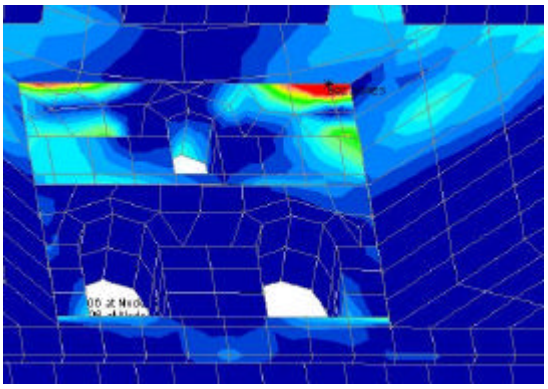

Figure 4.63. S1 1st principal stress contours of drum.

On the bottom corners of the second level windows and around the drum windows are relatively high tensional stresses occurs, see Figure 4.62 and Figure 4.63. These localizations are on the cracks route in east and west walls and it can be concluded that the self weight does not cause the cracks individually but might supports their formation with other loadings. Minimum of third principal stress (S3=-1.07e6MPa) is not higher than the compressive strength (fksm=10.77e6MPa), see Figure 4.64.

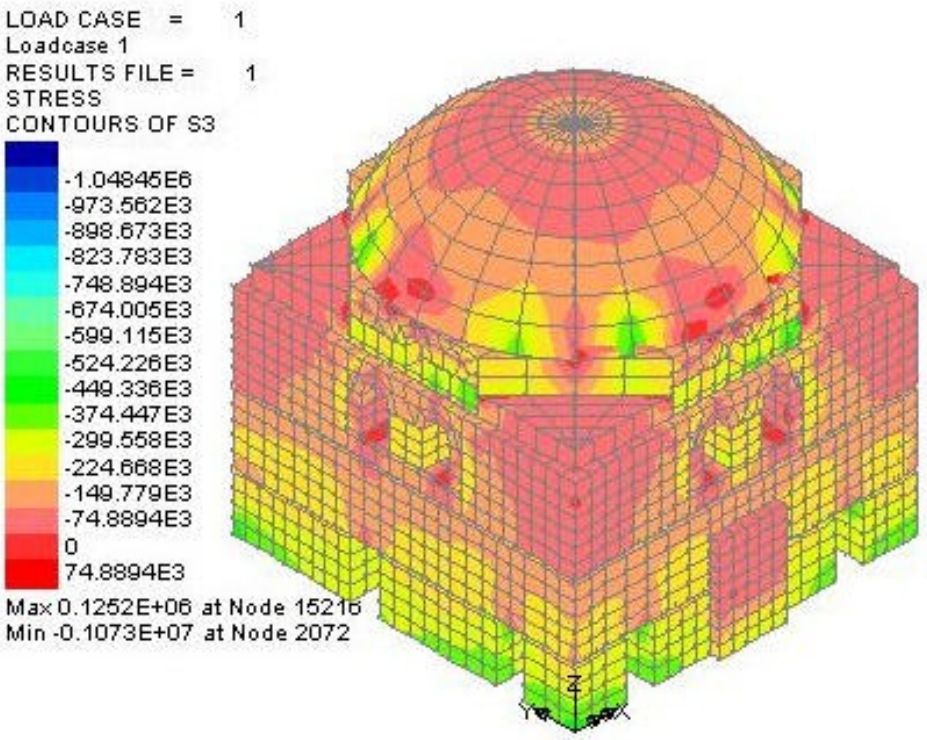

Figure 4.64. S3 3rd principal stress contours.

In general the structure is safe under its self weight. The second level and drum windows have relatively high tensional stress. The drum dome connections also have relatively high tensional stress, see Figure 4.65.

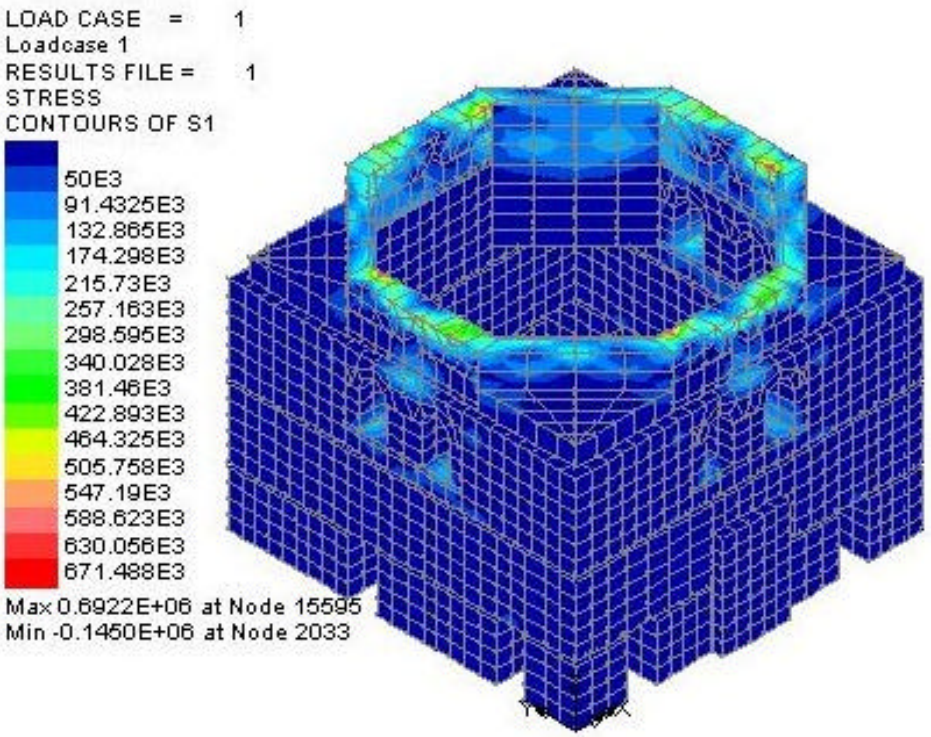

Figure 4.65. S1 1st principal stress of the drum.

4.6.3 Eigen Values and Mode shapes

The dynamic characteristics of the structure have been determined. The mode shapes are presented at Figure 4.66-Figure 4.75 for the first ten modes. The modal frequencies and mass participation factors for the first 10 modes are presented at Table 4.18. Due to partial symmetry of the structure, the frequencies of the 1st and 2nd modes are close to each other, see Table 4.18. The obtained natural frequencies are in the range of 3-10 Hz which is defined as approximate values for masonry (Croci 1998, p.147).

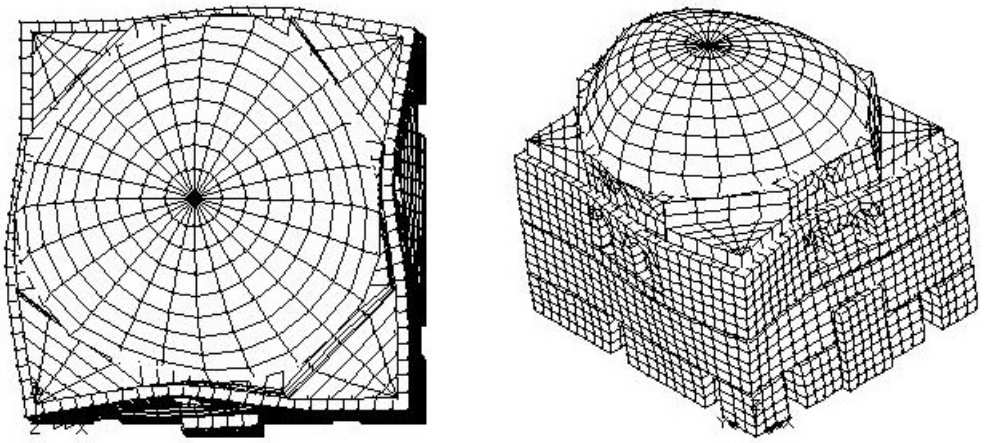

Figure 4.66. 1st mode shapes.

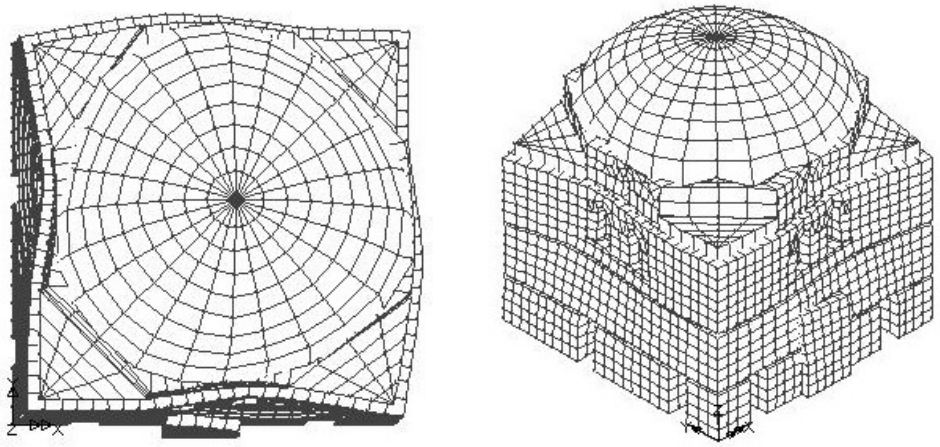

Figure 4.67. 2nd mode shapes.

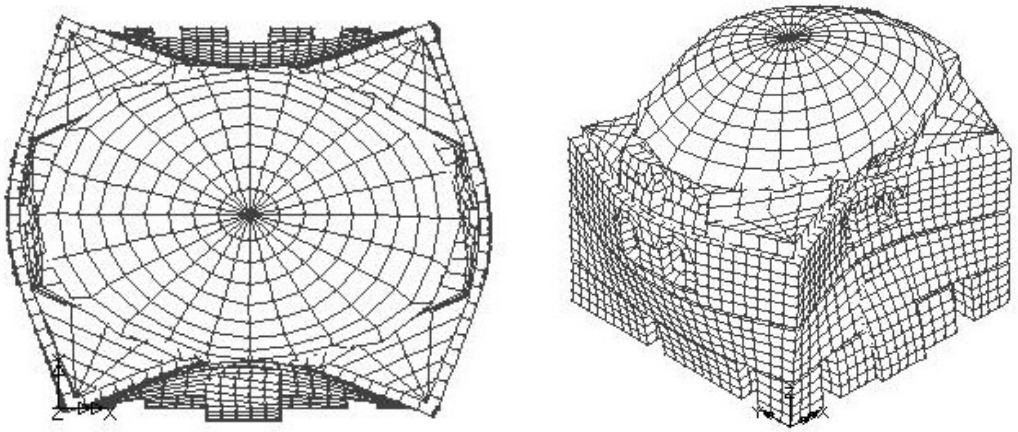

Figure 4.68. 3rd mode shapes.

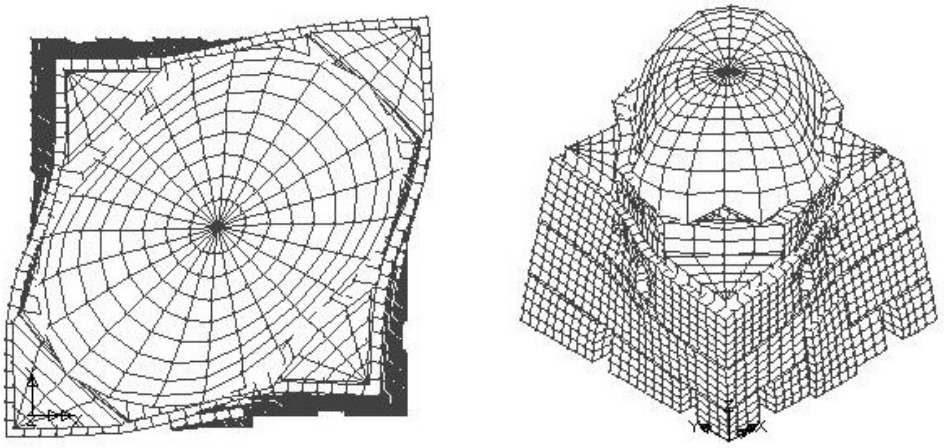

Figure 4.69. 4th mode shapes.

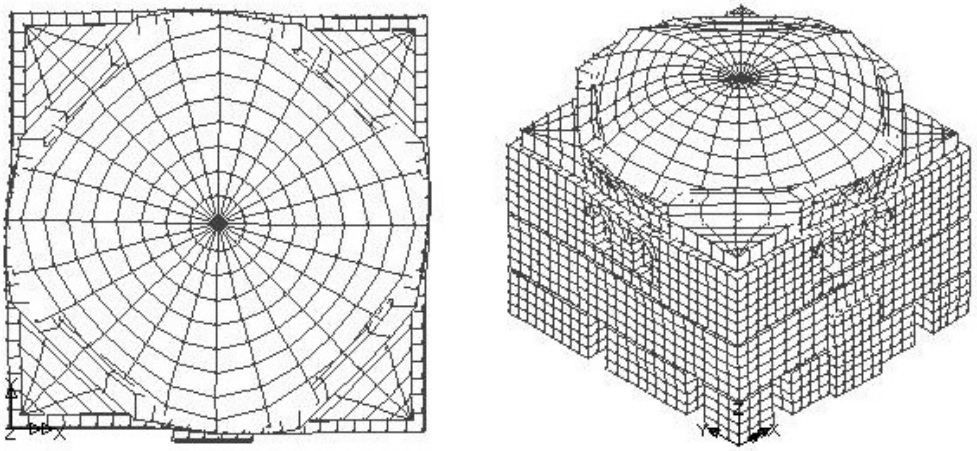

Figure 4.70. 5th mode shapes.

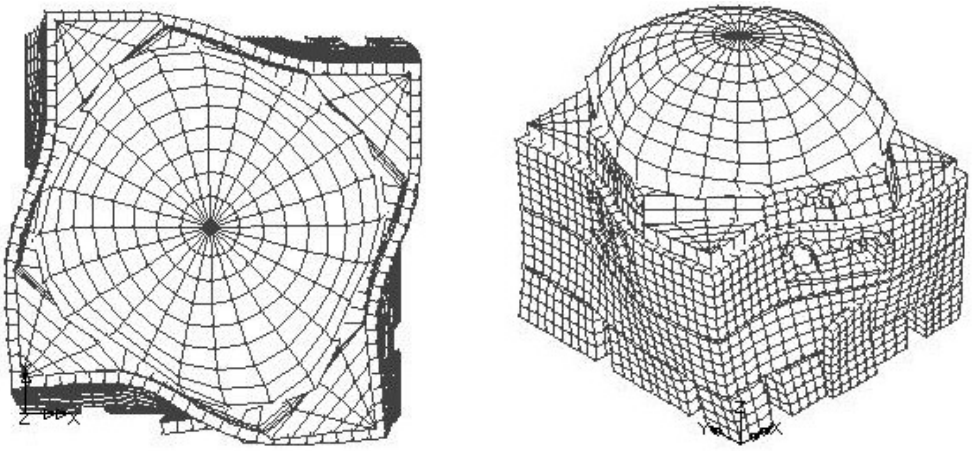

Figure 4.71. 6th mode shapes.

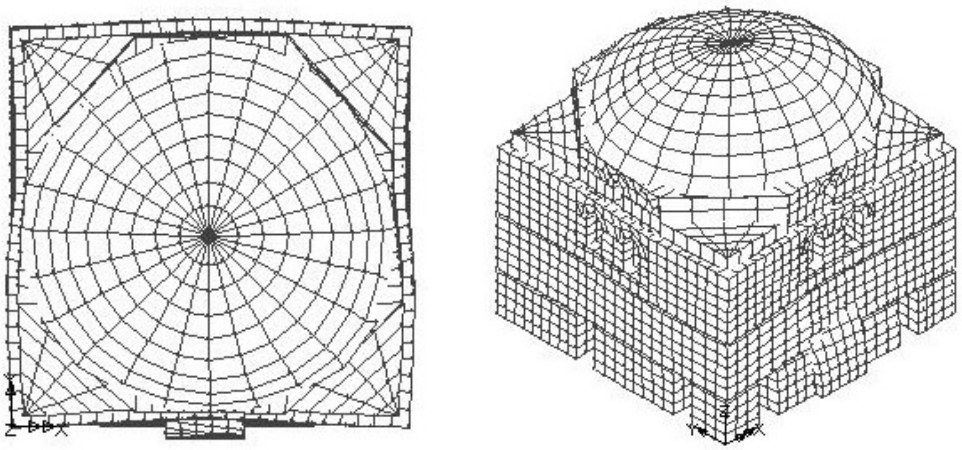

Figure 4.72. 7th mode shapes.

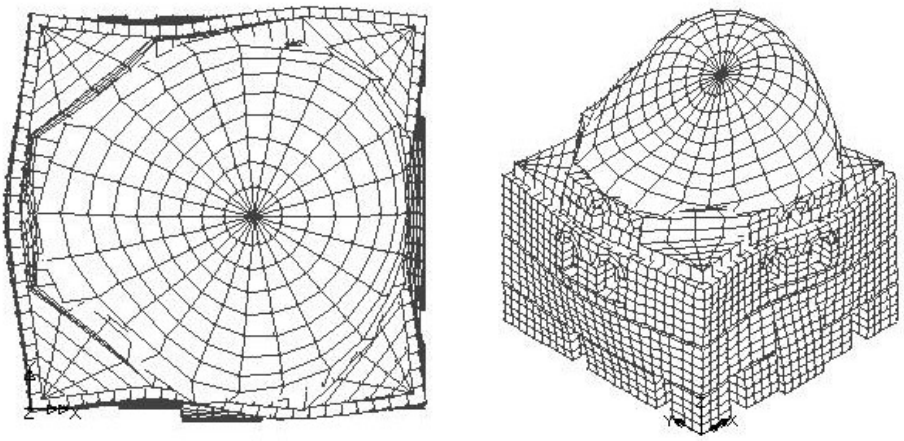

Figure 4.73. 8th mode shapes.

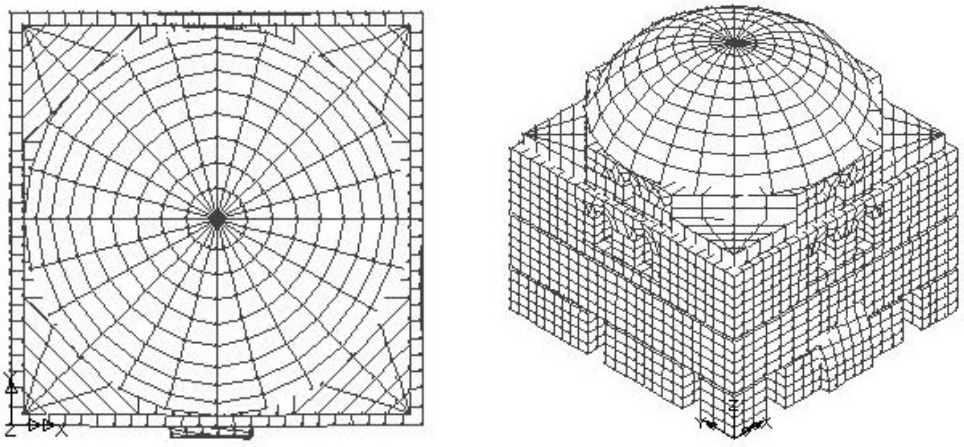

Figure 4.74. 9th mode shapes.

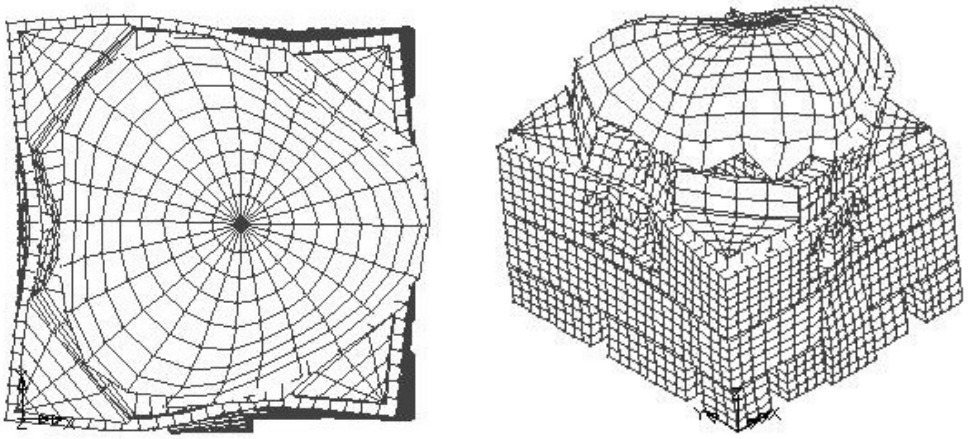

Figure 4.75. 10th mode shapes.

Table. 4.18. Modal frequencies and mass participation factors.

			Mass Participation Factor (%)			
Mode	Eigenvalue	Frequency (Hz)	X	Y	Z	Error Norm
1	894.799	4.76083	37.0818	30.1566	1.23E-03	3.27E-09
2	898.6	4.77093	31.4178	35.2705	1.42E-03	8.52E-10
3	1270.32	5.67252	2.20E-03	1.98E-01	4.83E-04	6.52E-11
4	1885.91	6.91164	7.10E-03	8.28E-04	4.41E-03	2.68E-10
5	2243.99	7.5393	7.91E-03	5.53E-03	16.1162	3.71E-09
6	2433.3	7.85087	1.43E-01	1.44E-04	5.80E-01	7.47E-09
7	2752.06	8.34929	2.26E-01	1.31E+00	2.86E-03	4.27E-09
8	2855.58	8.50486	1.94E+00	2.46E-01	2.39E-04	1.83E-09
9	3242.5	9.06276	3.75E-02	3.07E-01	1.05E-03	2.04E-08
10	3427.06	9.3171	10.4522	9.94E-03	3.13E-06	6.86E-07

4.6.4. Response Spectrum Analyses

The response spectrum analyses have been conducted due to specification of Ministry of Public Works and Settlement (Ministry of Public Works and Settlement 1998). The spectrum curve was defined by Eq. 4.24.

$$A_c = A(T) \times 9.81 \qquad \text{Eq.4.24.}$$

where A_c and A(T) are spectral acceleration and spectral acceleration coefficient corresponding to 5% damped elastic Design Acceleration Spectrum which is normalized by the acceleration of gravity, g, and can be determined by Eq.4.25.

$$A(T) = A_0 \times I \times S(T) \qquad \text{Eq.4.25.}$$

where A_0, I and S(T) are effective ground acceleration coefficient, building importance factor and spectrum coefficient, respectively. The spectrum coefficient, S(T), can be determined by Eq.4.26.

$$S(T) = 1 + 1.5T / T_A \qquad (0 \le T \le T_A) \qquad \text{Eq.4.26a}$$

$$S(T) = 2.5 \qquad (T_A < T \le T_B) \qquad \text{Eq.4.26b}$$

$$S(T) = 2.5(T_B / T)^{0.8} \qquad (T > T_B) \qquad \text{Eq.4.26c}$$

where T, T_A and T_B are natural period of structure and spectrum characteristic periods depending on local site classes, respectively.

The local site class was taken as Z3 and the spectrum characteristic periods were determined to be T_A=0.15 and T_B=0.6 (Ministry of Public Works and Settlement 1998, p. 11).

Effective ground acceleration coefficient was taken as A_0=0.4 as the zone is 1st order seismic zone. The building importance factor was taken as I=1(Ministry of Public Works and Settlement 1998, p. 11). By use of Eq. 4.24, Eq.4.25 and Eq.4.26 the spectrum curve was defined and presented at Figure 4.76.

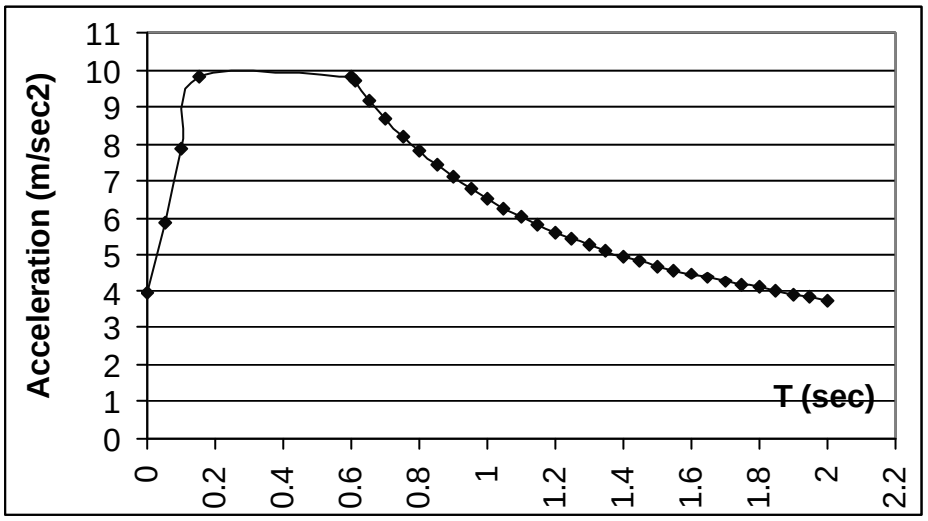

Figure 4.76. The acceleration response spectrum.

The response spectrum analyses are performed for the X and Y directions of the model. The type of spectral response is CQC (Complete Quadratic Combination). All of the ten modes have been taken into account for the analyses.

4.6.4.1. Spectral Excitation in the X Direction

The spectral analysis is performed in the X direction. The upper 1% principal stress, S1, occurs at the west lower lintel place where the wall section decreases considerably, see Figure 4.77, Figure 4.78. The maximum 10% of the S1 occurs at the lintel places at south and north, see Figure 4.77, Figure 4.78. The tensile stresses at the specified lintel places exceeds the tensile strength of stone masonry, ftsm=1.077MPa. The lintel places are presented at Figure 4.78 by the S1. The red regions in the figures are the places where the S1 gets over the tensile strength for stone masonry, ftsm=1.077MPa. The maximum tensile stress is 2.5MPa.

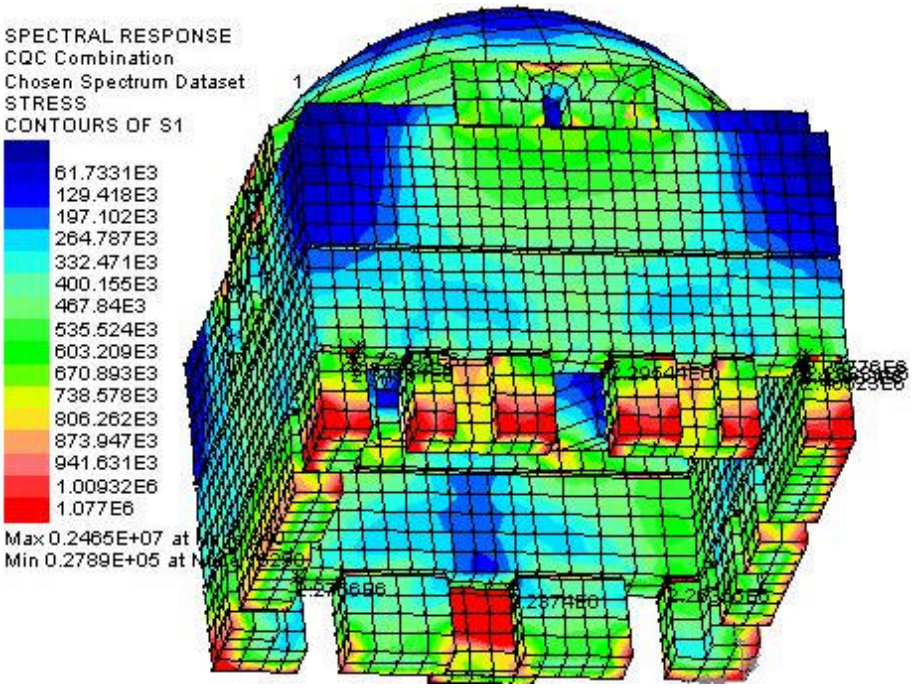

Figure 4.77. The S1 contour plot for spectral excitation in X direction.

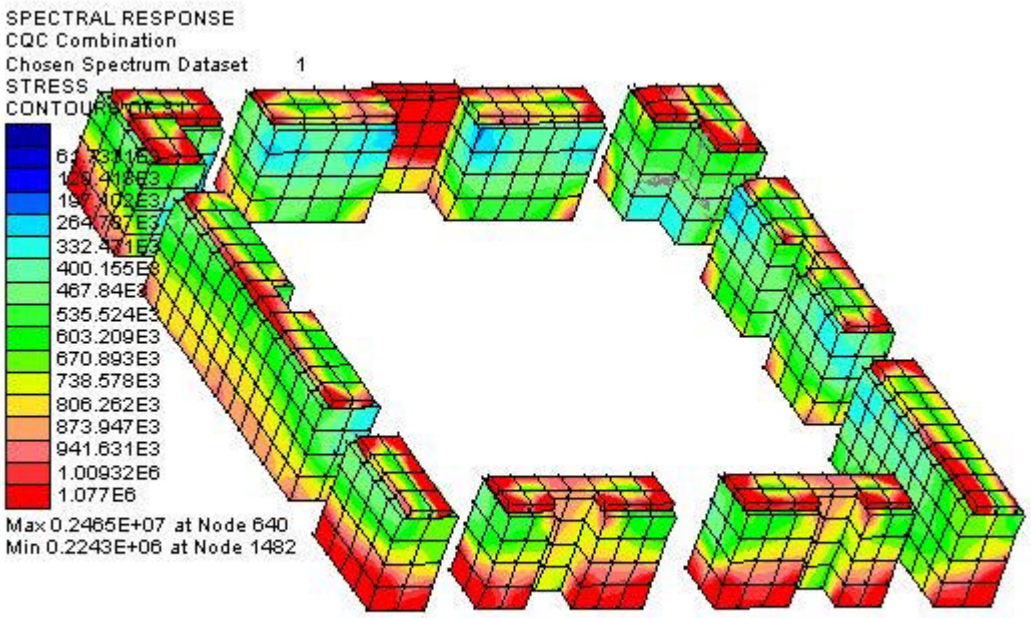

Figure 4.78. The S1 contours of the lintel places.

The tensile stresses are critical at the drum-dome connections where the tensile stress exceeds the strength, see Figure 4.79. The contour key is the same for Figure 4.78 and Figure 4.79. The S1 at the foundations exceeds the strength especially at the north wall, see Figure 4.78. The wall thickness of 110cm distributes the stress and the whole section is prevented to suffer from excessive stress as can be seen at the foundations, see Figure 4.77.

Large tensile stresses occur around the 2nd level windows which are on the crack path, see Figure 4.79. The dome is safe and there is excessive tensile stress at the drum, at the foundation and at the 1st level lintel places, see Figure 4.80.

In the east section, the tensile stress follows the crack pattern observed at the structure while being lower then the tensile strength, see Figure4.81. The same thing is valid for west section, see Figure 4.82. The black line represents the crack at Figure 4.81 and Figure 4.82.

The absolute value of minimum compressive stress (S3) is lower then the compressive strength.

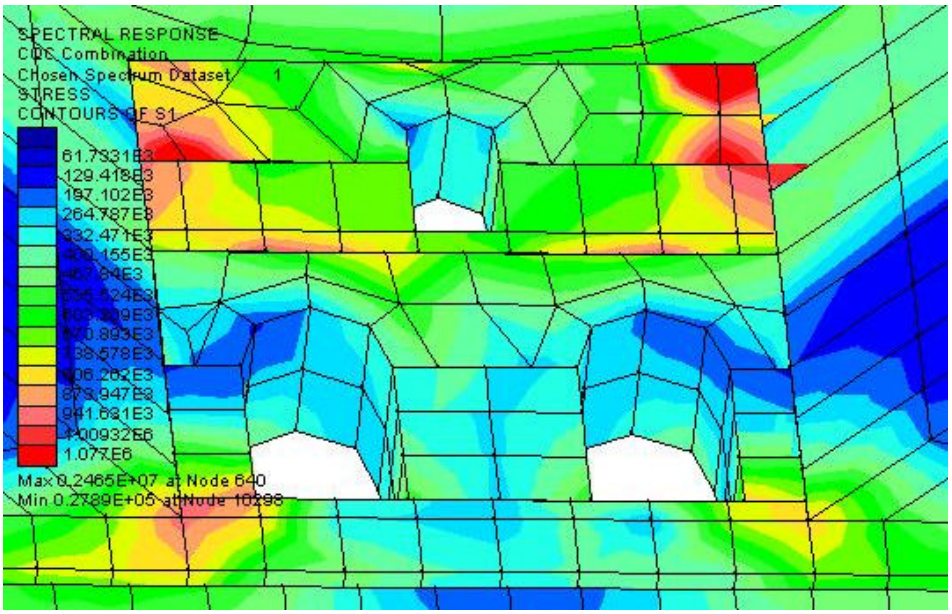

Figure 4.79. The S1 at the drum of east section.

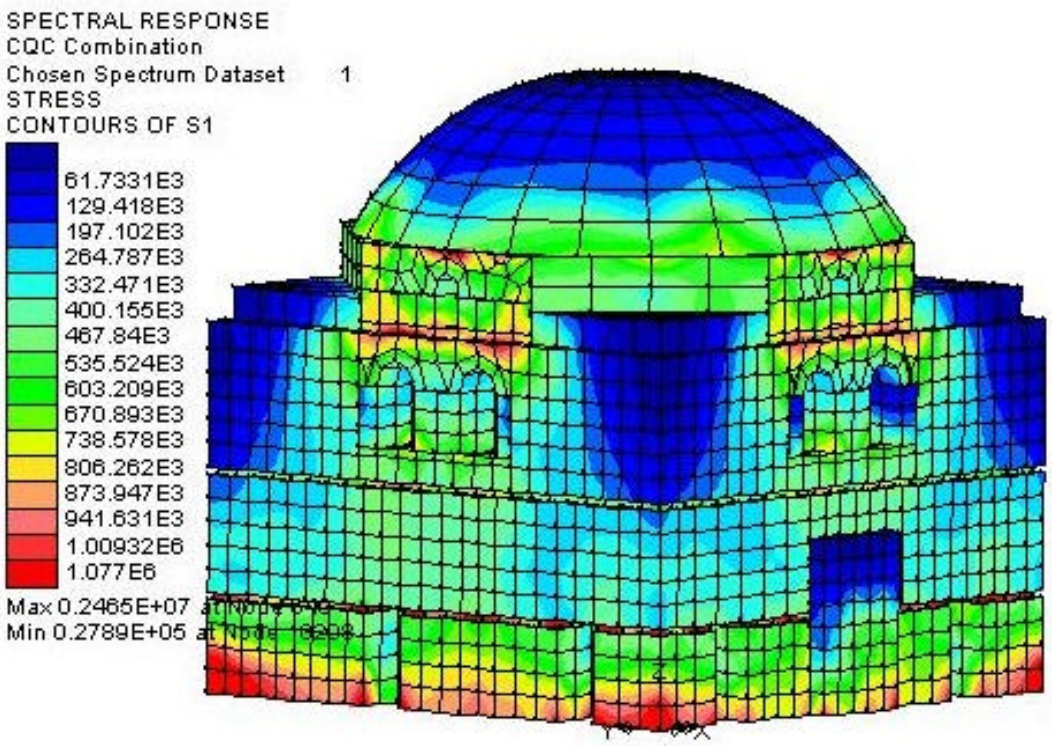

Figure 4.80. S1 of south and west elevations.

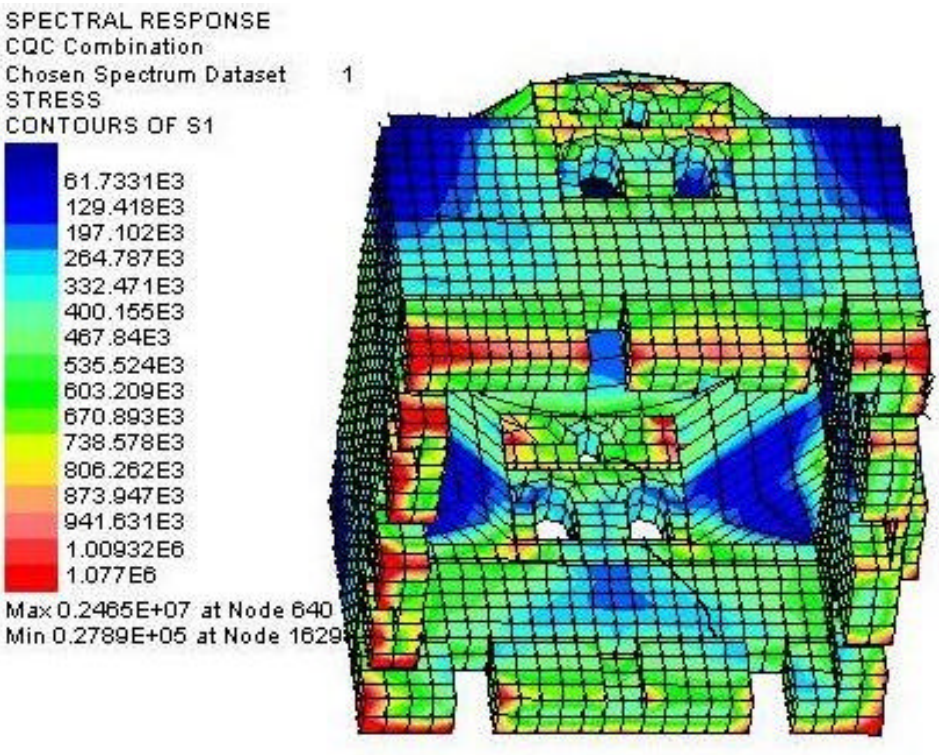

Figure 4.81. S1 contour of east section.

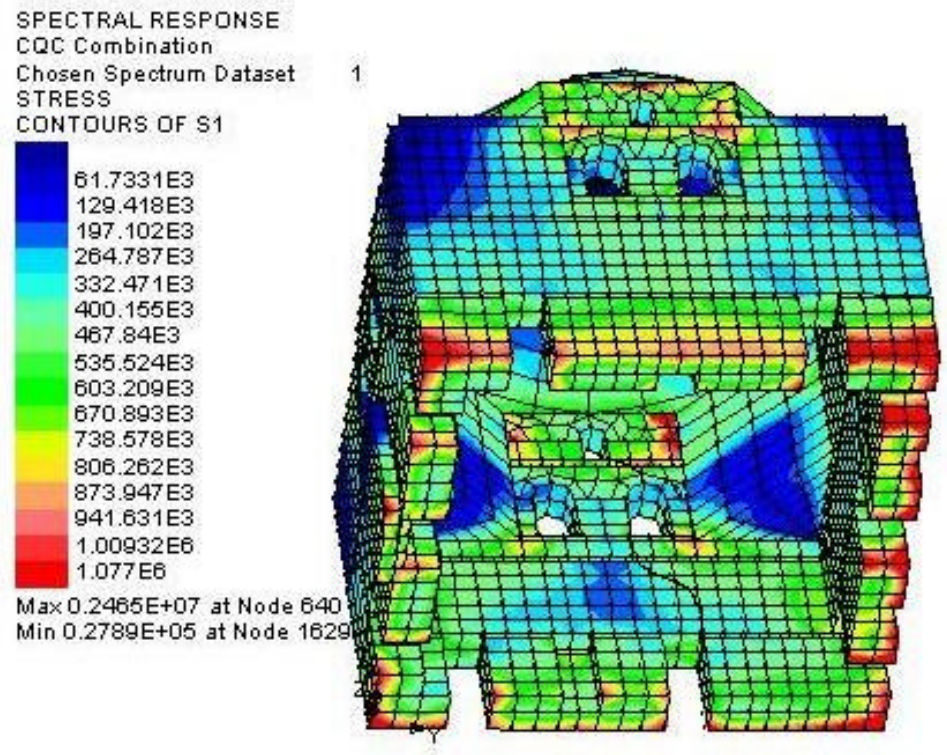

Figure 4.82. S1 contour of west section.

4.6.4.2. Spectral Excitation in the Y Direction

The spectral excitation is performed in the Y direction. The maximum S1 is equal to 2.4MPa which is greater then the tensile strength, at the lower level lintel place at the east section, see Figure 4.83. The place of the maximum S1 is shown by a star with the value S1 see Figure 4.83.

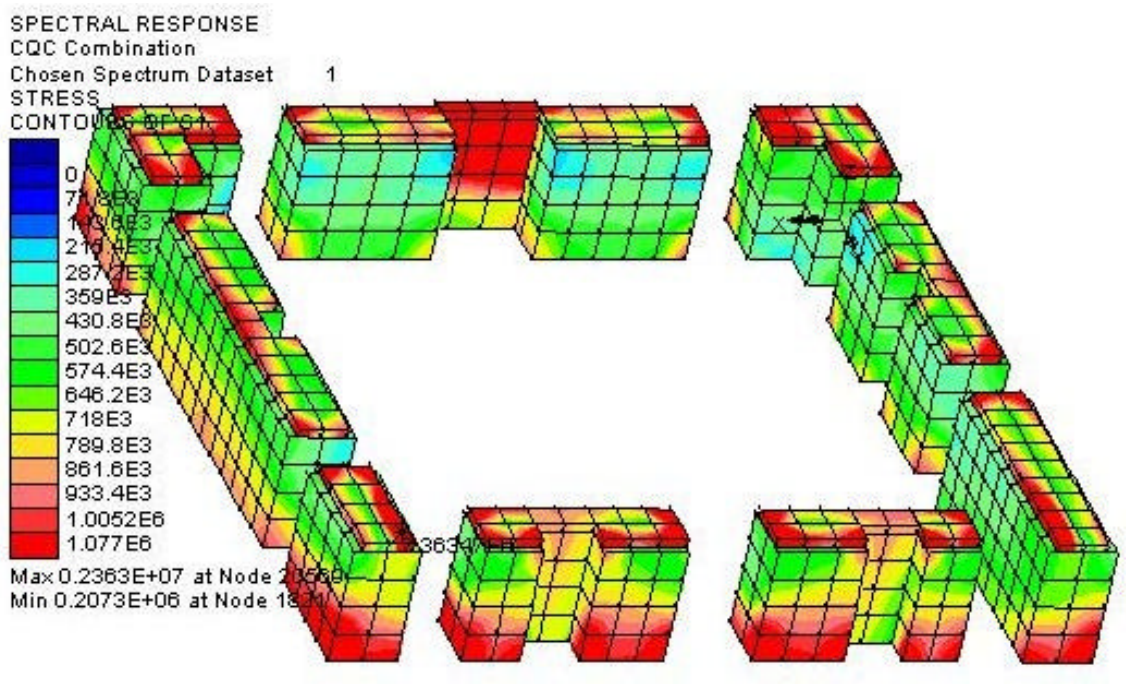

Figure 4.83 S1 contour plot of the lintels.

The upper 10% of the S1 occurs at the north and south lintel places see Figure 4.83. The foundation has tensile stresses larger then the strength especially at the north, see Figure 4.84. The drum also has large tensile stresses. The crack pattern at the east and west section is captured by the tensile stresses which are lower then the strength, see Figure 4.84. The tensile stresses at the foundation are distributed through out the section of the walls, see Figure 4.84. The black line at Figure 4.84 represents the crack at the east section.

In general, the lower level lintel places, the drum, and the foundation, especially at the north, are challenged by the seismic loading.

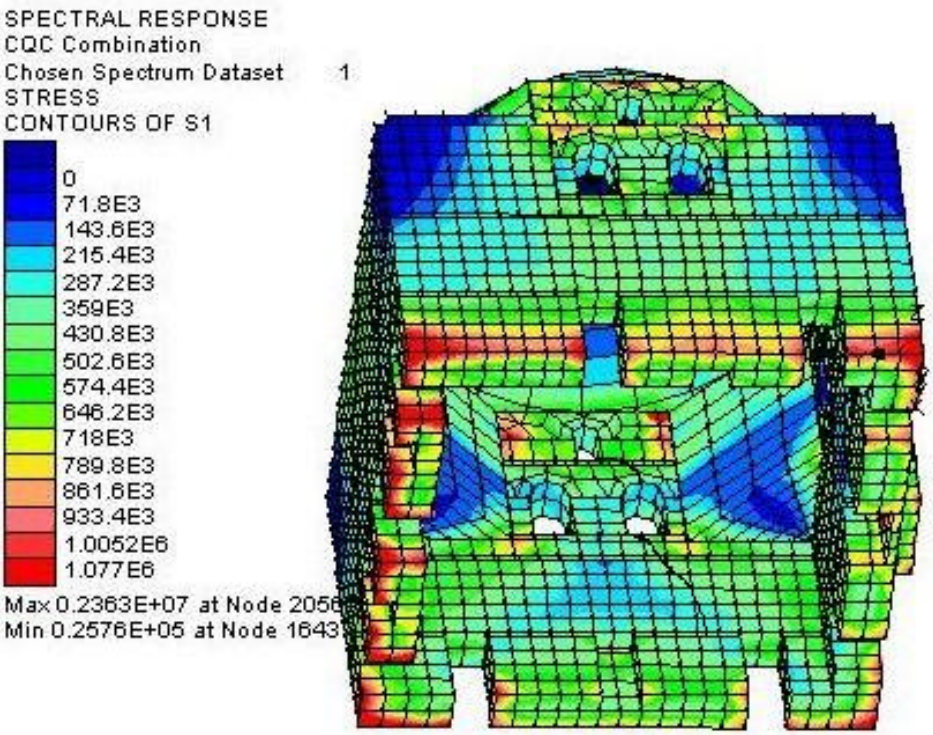

Figure 4.84. S1 contour plot of east section.

4.6.5. Self Weight + Settlement Analyses

As stated in part 4.3.3, the long term observations of settlement point out a settlement towards north direction. By using this information various linear elastic analyses for settlement and self weight combination have been conducted. During these analyses, the settlement quantity has been changed from 1 cm to 2 cm and to 3 cm. The settlement has been acted on the walls by use of variation curves such that settlement starts at a point in the section of the wall with zero and increases towards a direction, generally towards north direction. The variation curves have been changed, the points where the settlement starts have been changed and even the direction of the settlement has been changed. Only the analysis results that can best enlighten the formation of the cracks on the structure will be presented here.

The settlement load is given in Figure 4.85. Settlement starts at the niche at east and near the window at the west from zero and takes the value of 3cm at the north, see Figure 4.85. A local coordinate was defined for settlement analysis which is shown in pink. The settlement value varies with the X coordinate of the node it is applied. The X coordinate is the coordinate of the local axes shown as pink double arrows at Figure 4.85.

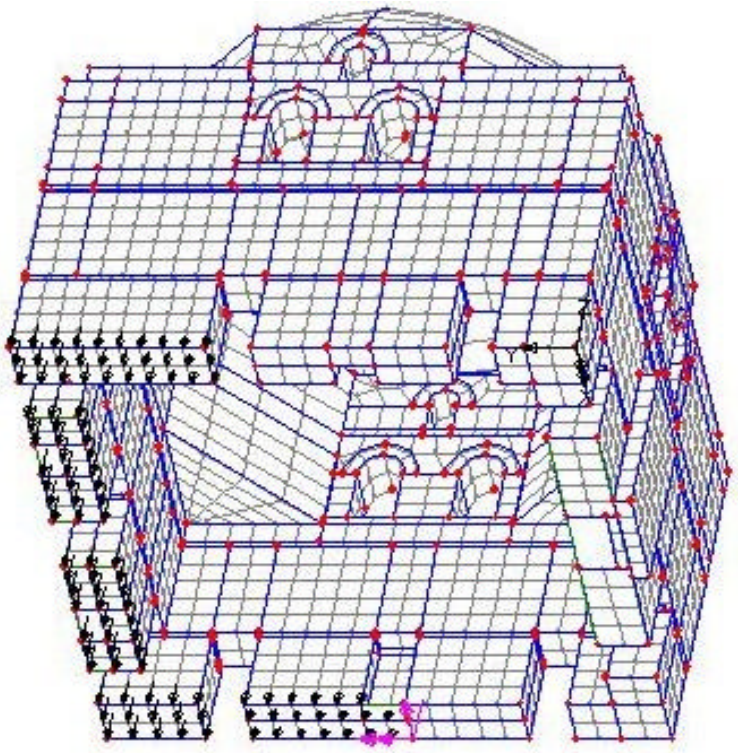

Figure 4.85. The settlement load.

The settlement and the self weight loads have been applied with different load cases and a load combination has been used to combine the results. The contour plot of vertical displacement, DZ, is presented at Figure 4.86. The combination of dead load and settlement of 3cm of the north wall shows a dominancy of the settlement displacement, see Figure 4.86. Also because of 3cm settlement at the north, there is a 3mm rise at the south, see Figure 4.86. The upper 20% of the S1 occurs at the lintel places at the east and west, generally on the cracks route, see Figure 4.87. The maximum S1 is 3.41MPa on the east lintel place close to the existing cracks. The 1st principal stress, S1, follows the crack route on the east section and on the west elevation while partially getting over the tensile strength, see Figure 4.87.

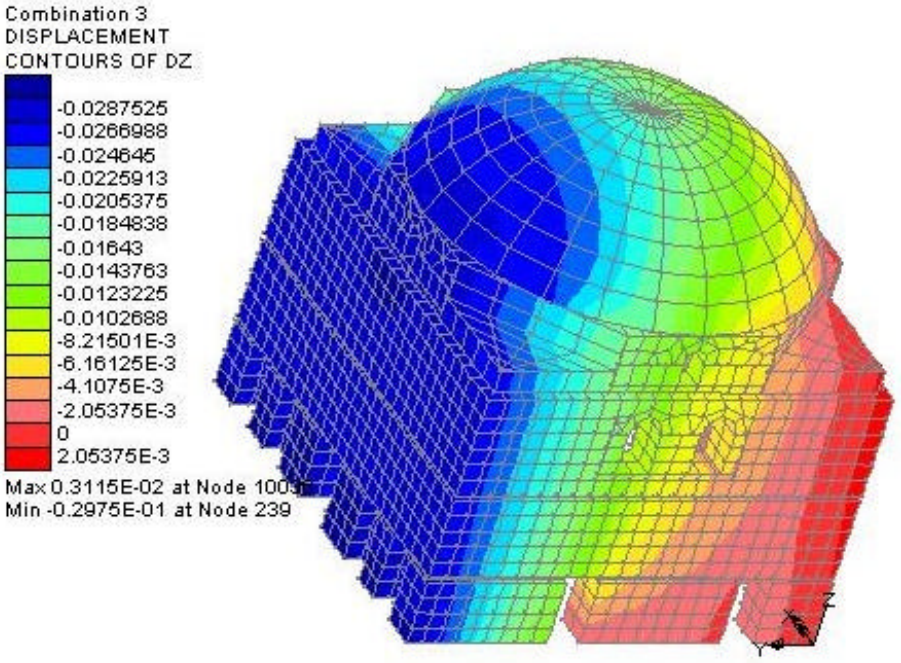

Figure .86. Vertical displacement (DZ) contour.

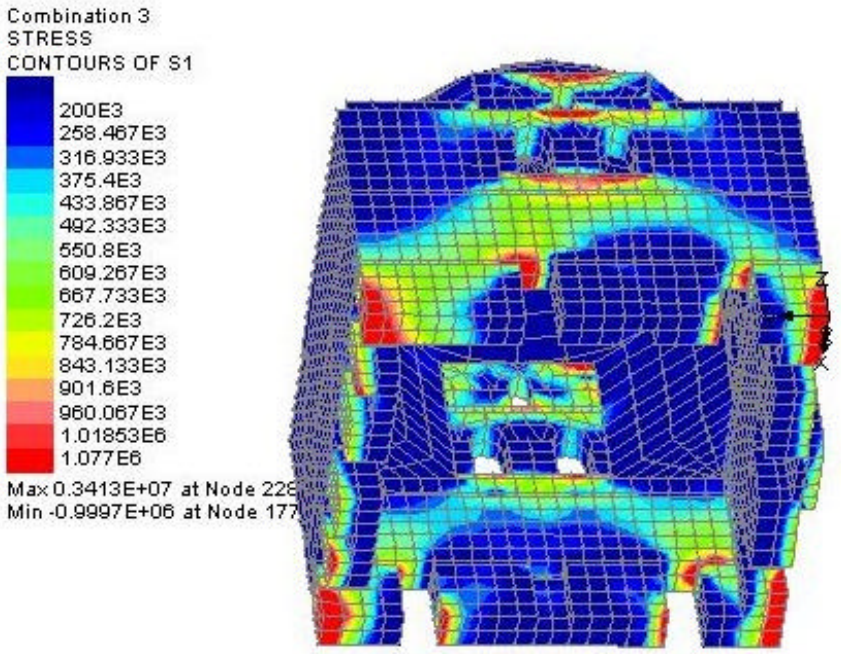

Figure 4.87. 1st principal stress (S1) contour of east section.

There are stress concentrations especially at the north and south foundations which are under the confining pressure of soil. The excessive wall thickness of 110cm prevents the structure from high stresses.

The crack paths on the west section and on the east elevation have been captured by the S1, see Figure 4.88.

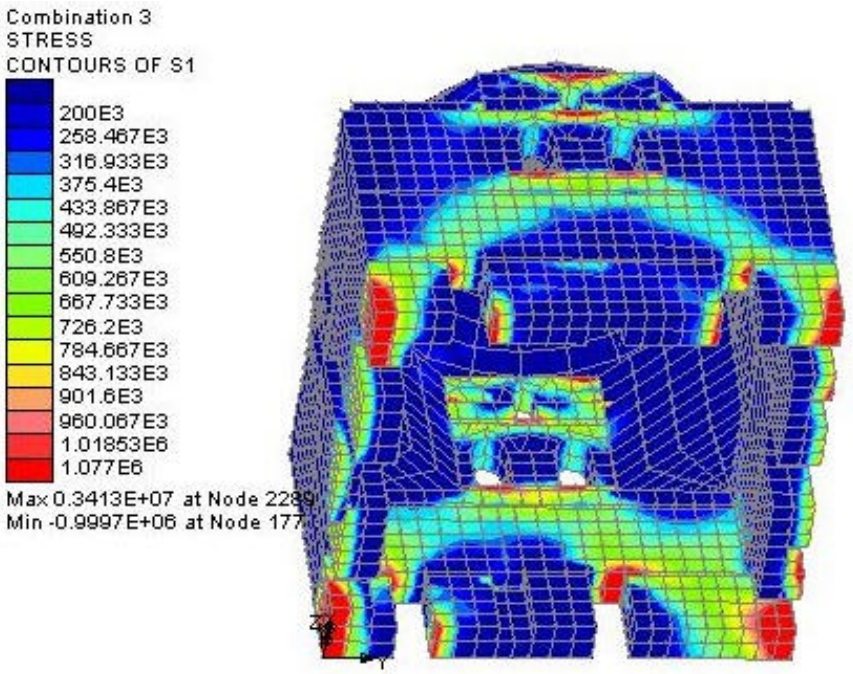

Figure 4.88. 1st principal stress (S1) contour of west section.

The second level windows and the drum of west and east suffer from localized tensile stresses which also capture the existing cracks of the structure, see Figure 4.89 and Figure 4.90. In Figure 4.89 and Figure 4.90, slices taken from the west and east walls of the structure, respectively, are presented with the existing cracks shown as black lines on the structure. The stress localizations at the lintel places can be seen in Figure 4.89 and Figure 4.90. As expected, the crack follows the weakest sections like windows and lintel places which are also subject to the excessive tensile stresses.

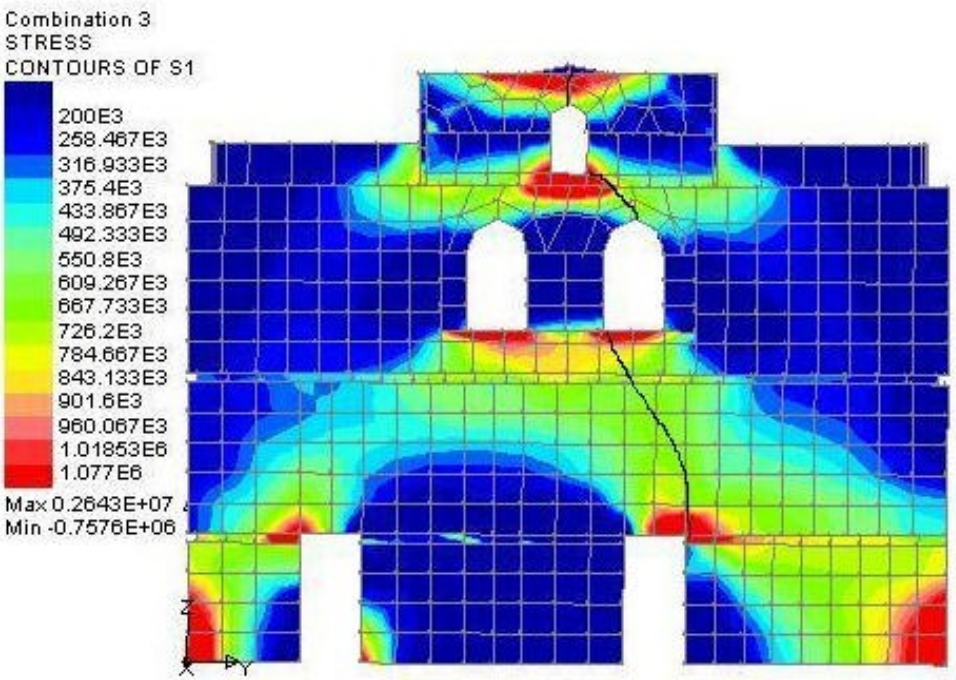

Figure 4.89. S1 contour of slice from west wall.

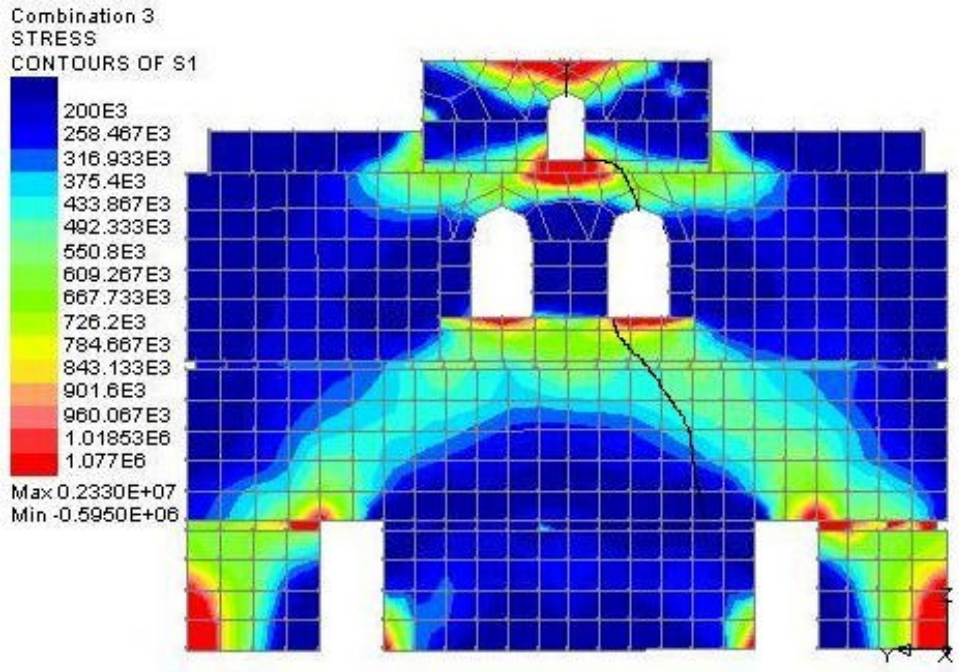

Figure 4.90. S1 contour of slice from east wall.

4.6.6. Nonlinear Settlement Analyses

Various linear elastic settlement analyses have been conducted in the light of the data gathered from long term observations and the observations of cracks on the structure. Some of these linear elastic analyses have been selected for further nonlinear analyses and conducted as nonlinear settlement analyses. In general all of the nonlinear analyses converges to the existing crack behavior to some point. The finite element model is a 3D complex model and trying to reproduce the exact behavior of the real structure with all details is impossible. The aim of the nonlinear analyses are simulation of the general behavior and understanding the safety of the components of the structure. While the reason of the structural cracks has been investigated, the vital parts that are under high stress state have been also investigated during the nonlinear analyses.

The nonlinear analyses of masonry have been investigated and applied by other researchers as presented at Chapter 3. Orthotropic material model has been used to model masonry composite media (Lourenco 1996). Drucker-prager model was used for nonlinear analysis of a historical masonry structure, Kucuk Ayasofya Mosque (St. Sergius and Bacchus Church) (Kocak 1999).

Various material models have been investigated for this study including Mohr-Coulomb, Drucker-Prager, orthotropic Hoffman and cracking concrete models. These models need different material parameters for the analyses. Mohr-Coulomb needs initial cohesion, initial friction angle, final friction angle and dilation angle. Drucker-Prager needs initial cohesion and initial friction angle. Orthotropic Hoffman model needs definition of a complete 3D yield surface with 6 elastic and 11 inelastic parameters. First order estimations with sensibility analyses could be conducted by selecting one of these models. Especially the orthotropic Hoffman model seems to represent the masonry composite media well, as different strengths for tension and compression can be defined for different material axes. On the other hand, conducting a sensibility analyses by such vast number of parameters with a complex 3D model could be computationally impractical. Moreover, a model which needs parameters that can be defined by the data of material tests and which can also represent the expected brittle fracture of masonry is more practical. Because of that Cracking Concrete model of LUSAS FE software has been used for material model of nonlinear analyses.

The cracking concrete model which was developed by Jefferson simulates the tensile cracking while crushing failure because of compression is neglected. The model

assumes that at any one point there are 21 cracking directions for the 3D case which are defined by Bazant and Oh's spherical integration rule and 9 cracking directions for the 2D case (8 in plane 1 out of plane) (FEA Ltd. b 2002, p. 209).

Three crack directions are active at any one time which are defined by the closest directions to the principal strain directions. Total principal strains are used to define the cracking directions rather then stresses because strains grow with the increasing fracture but stresses diminish to zero and do not provide a good measure of previous fracture directions. Each crack behavior is determined by a hyperbolic yield surface which is asymptotic to a Coulomb friction surface (FEA Ltd. b 2002, p. 210).

The crack plane with local and global coordinates is given in Figure 4.91.

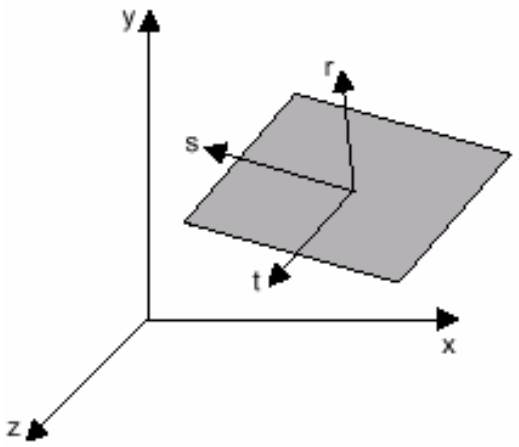

Figure 4.91. Crack plane with local and global coordinates (FEA Ltd. b 2002, p. 209).

In tensile loading an exponential softening curve of stress-strain relationship is defined normal to crack plane, see Figure 4.92.

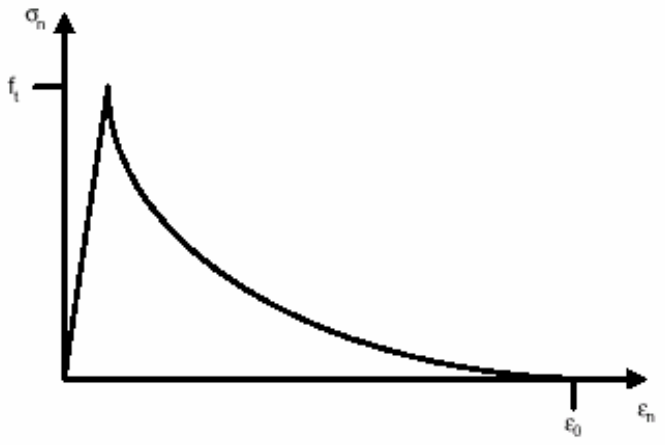

Figure 4.92. Softening curve normal to a crack plane (FEA Ltd. b 2002, p. 211).

The material parameters to be defined for the model are listed below;

E: Modulus of Elasticity.

ν: Poisson's ratio.

f_t: Tensile strength.

G_f: Fracture energy per unit area.

ε_o: Strain at end of softening curve.

μ: Post-fracture friction coefficient (Default=1)

?: Post-fracture dilatancy coefficient (Default=0)

r: Ratio of shear strength to tensile strength (Default=1.5).

a: Reduction factor for the proportion of incremental shear plastic strains included in the effective plastic strain parameter (Default=0.5).

Also restrictions are defined as given below.

r>μ to ensure that the yield surface is convex.

$\varepsilon_o > 1.5 f_t/E$ to ensure that the softening function is a valid shape (FEA Ltd. b 2002, p. 215).

The yield surface in local stress space is given in Figure 4.93.

Figure 4.93. Yield surface in local stress space (FEA Ltd. b 2002, p. 218).

This model is chosen to model masonry because masonry also fails with a brittle fracture. The tensile failure is dominant for masonry so neglecting compressive failure, “crushing”, does not make much deviation from the real phenomenon of masonry.

Only the parameters of E, ν, f_t and $\boldsymbol{e}_o$ are defined and the default values for the remaining parameters are used. The parameters defined are given in Table 4.19.

Table 4.19. Material parameters.

	Stone Masonry	Brick Masonry
E (Pa)	1.10E+09	2.70E+08
Poisson's ratio ν	0.17	0.17
Density (?:kg/m3)	2.20E+03	1700
ft (Pa)	1.07E+06	1.07E+06
Strain at end of soft.curve e	0.003	0.003

Strain at end of softening curve for distributed fracture or fracture energy per unit area for localized fracture can be defined. The aim of the analyses is to understand the overall behavior so a distributed fracture approach is more sensible. The strain at the end of softening curve value is taken as 0.003, equal to the value for concrete. A sensibility analyses has been conducted by 0.002 and 0.004 and almost the same results are obtained with the 0.003 value.

The settlement has been acted starting with zero at the beginning of the niche at the east and at the end of the window at the west and reach to 0.01m at the north with a linear variation with respect to the node’s X axis of local coordinate shown as pink in Figure 4.94.

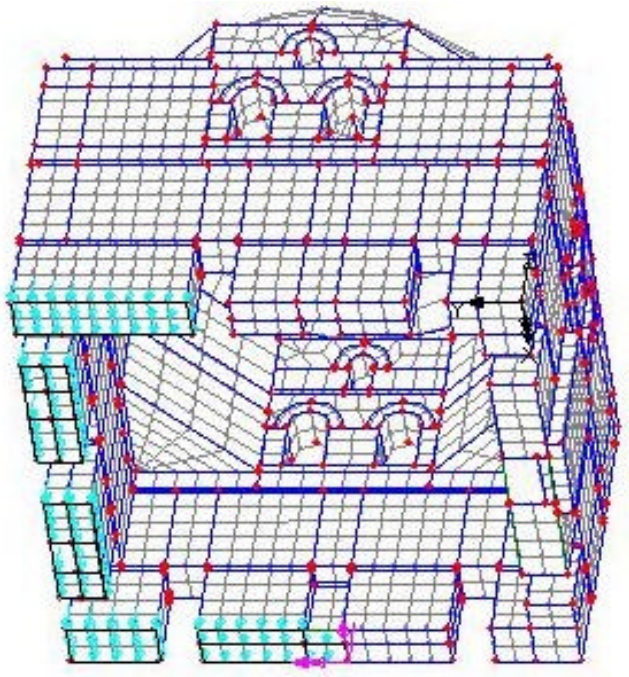

Figure 4.94. The settlement load.

The nonlinear analysis has been performed by acting the self weight plus the settlement load. The nonlinear analysis has been conducted by use of load curves defined for self weight and for the settlement load so, the nonlinear analysis facilities like step reductions due to uncorverged increments could not be used.

The load curves for the loads are defined such that the apse of the load curve is increment number and the ordinate is the load factor. The load curve for the self weight load is taken to be constant through out the analysis, see Figure 4.95. The load curve for the settlement load is taken to be linearly variable with respect to the increment number, see Figure 4.96.

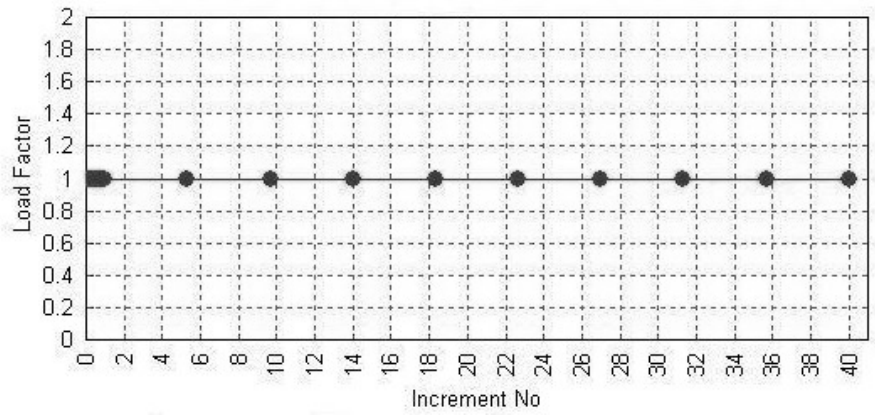

Figure 4.95 The load curve for self weight.

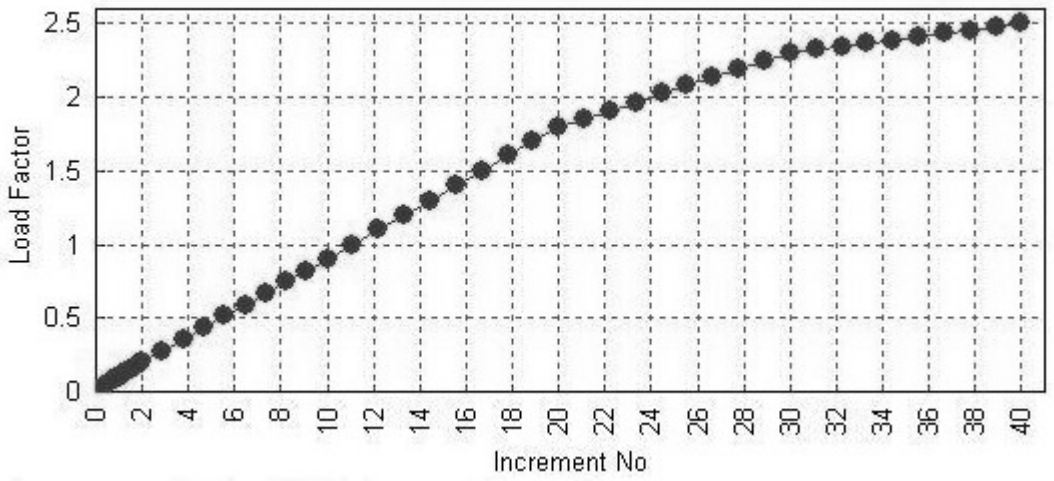

Figure 4.96. The load curve for the settlement load.

At every increment the load factors are multiplied with the assigned loads and acted on the structure. The analysis has been set up for 40 increments and a total of 2.5cm settlement was expected. As the nonlinear analysis control facilities could not be used with the load curves, the analysis fails after the first cracks formation. The automatic analysis could be conducted by use of control facilities but in that case only settlement load could be acted and self weight could not be defined which is thought to be important for the stress state of the structure.

The pre-failure and initiation of the cracks have been captured with taking into account the self weight while without self weight the whole behavior could be simulated under only settlement. For that case, the observation of the behavior under self weight is important and the pre-failure observation with the final stress state is thought to be enough for the assessment of the structure.

The maximum absolute settlement is 1.35cm at the last increment of 15^{th}, at the north foundation. The contour plot of vertical displacement, DZ, of the combination of the settlement and self weight is given in Figure 4.97.

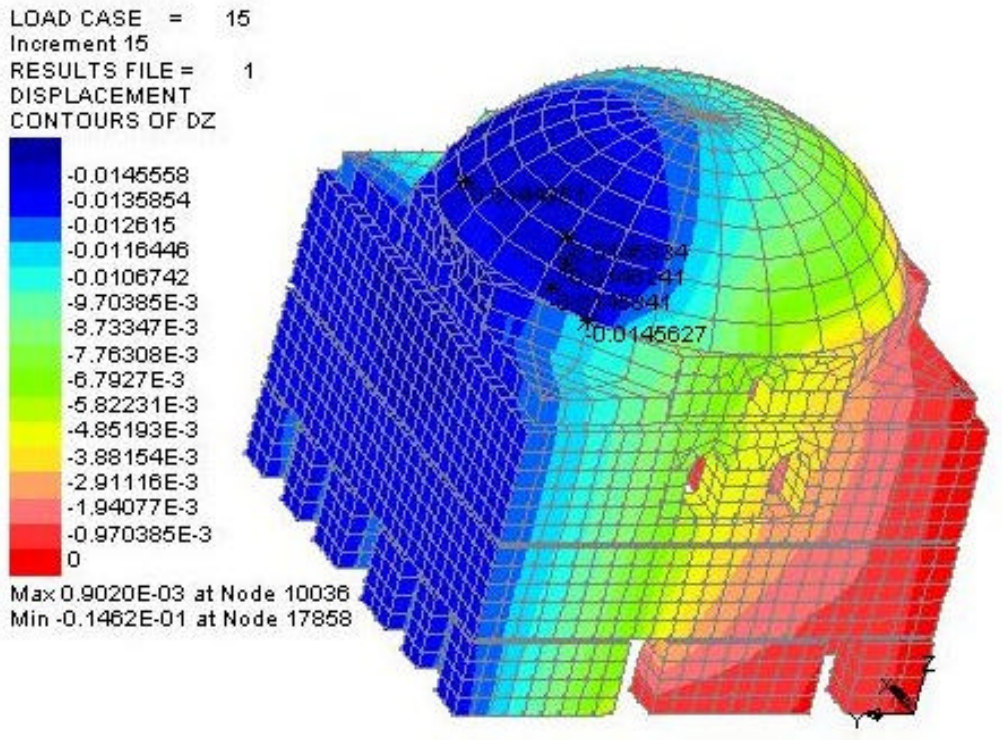

Figure 4.97. The vertical displacement contour.

The maximum absolute value of the displacement is obtained at the north of the dome, 1% of maximum absolute value of DZ are also given in Figure 4.97. Under only self weight the maximum absolute displacement occurred at the key stone of the dome and the deviation to north because of settlement is an expected behavior, see Figure 4.97.

The variation of the 1st principal stress, S1, at the east section and west elevation with respect to the increments can be seen from Figure 4.98 to Figure 4.105. In order to decrease the number of figures, only the odd numbered increments are presented.

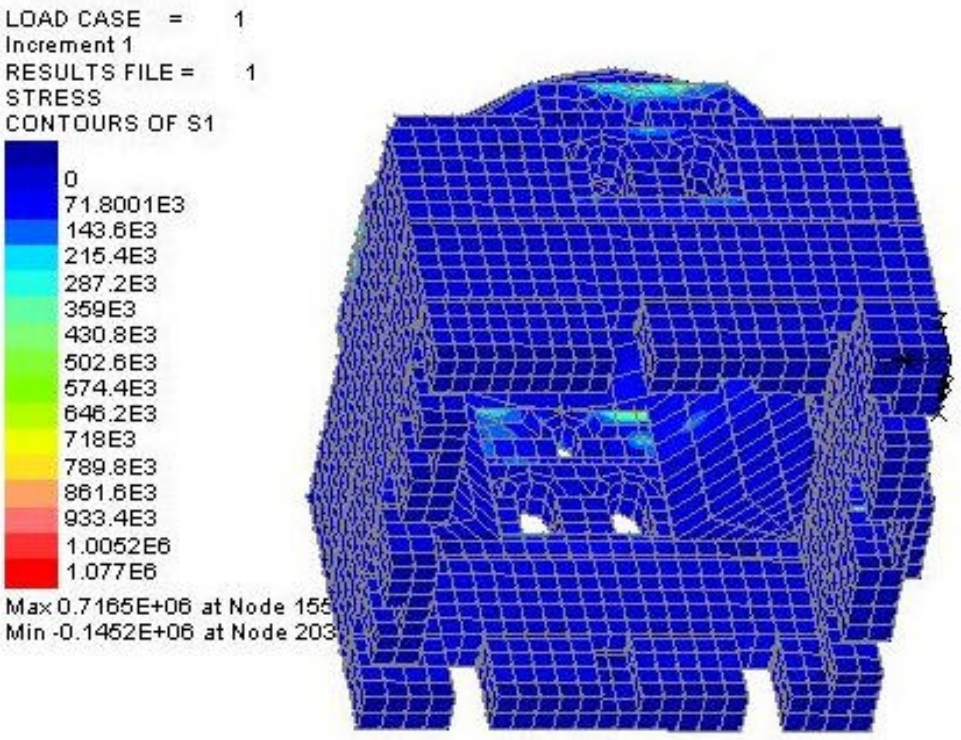

Figure 4.98. The S1 contours of 1st increment for east section.

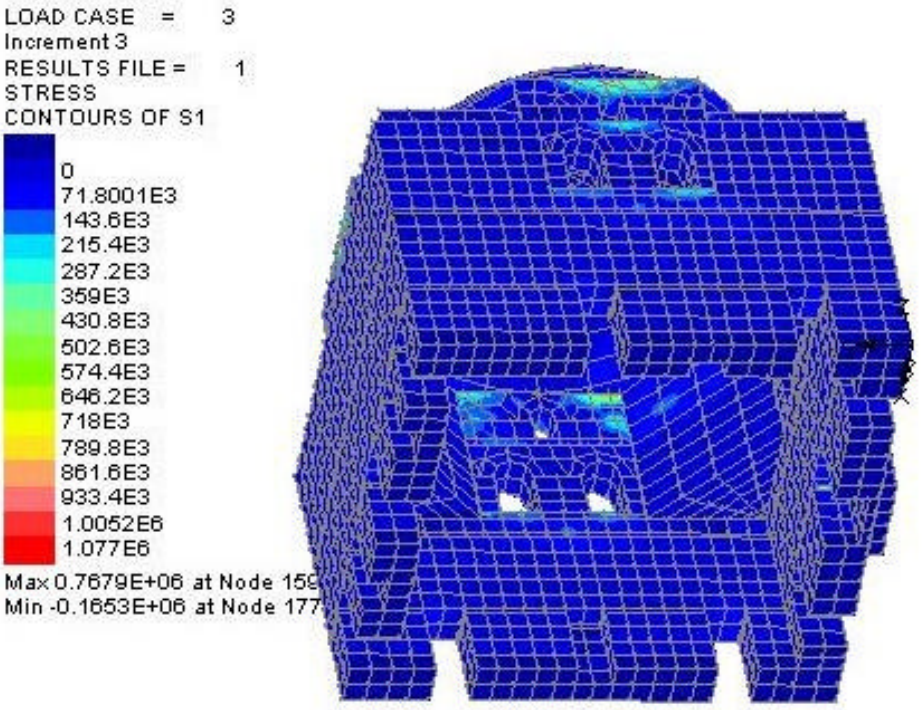

Figure 4.99. The S1 contours of 3rd increment for east section.

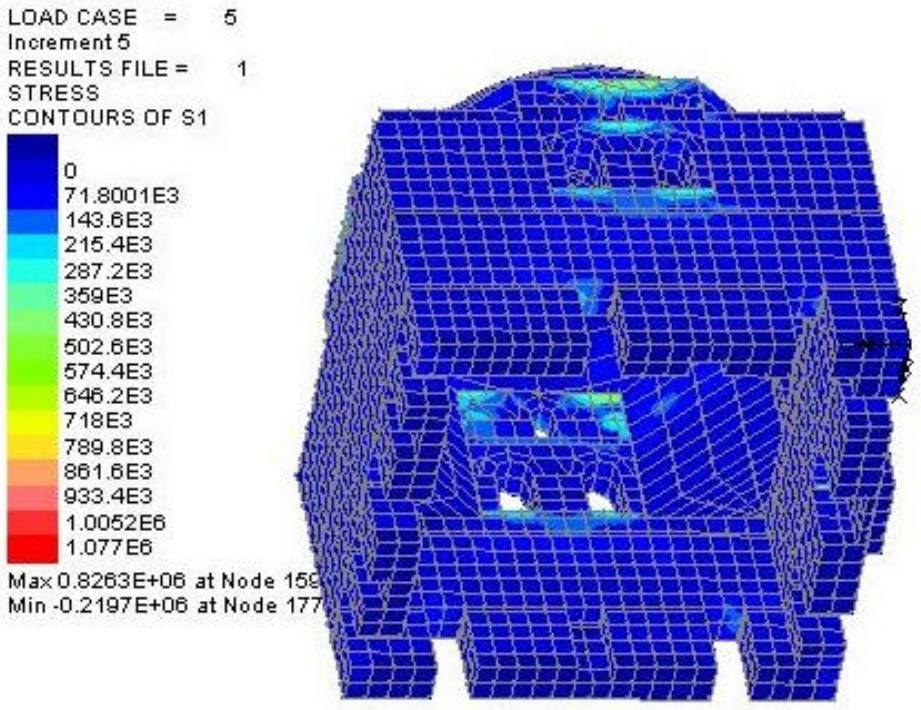

Figure 4.100. The S1 contours of 5th increment for east section.

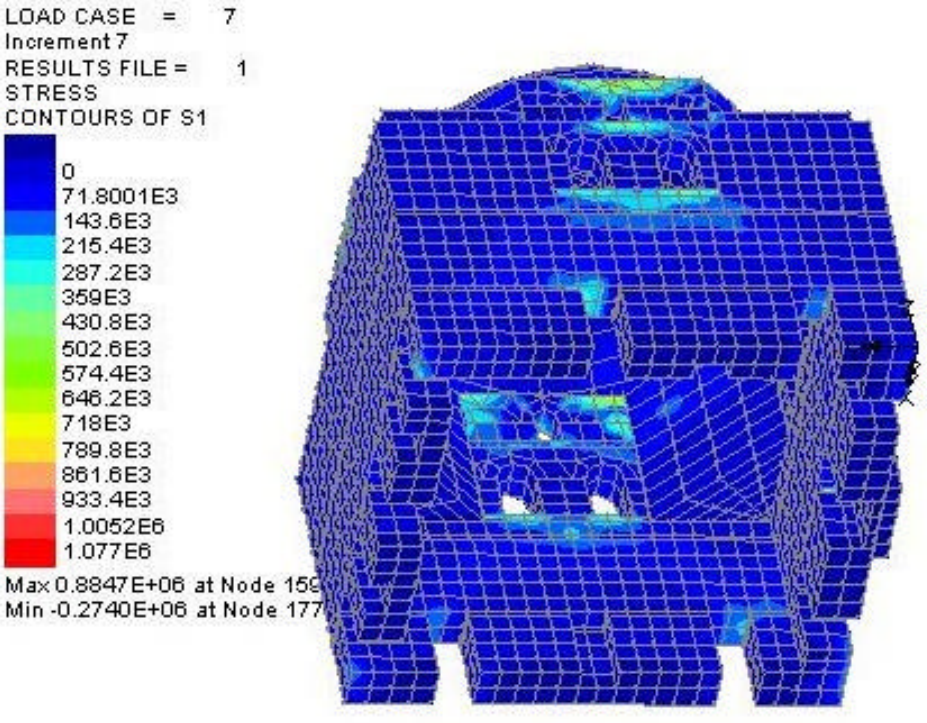

Figure 4.101. The S1 contours of 7th increment for east section.

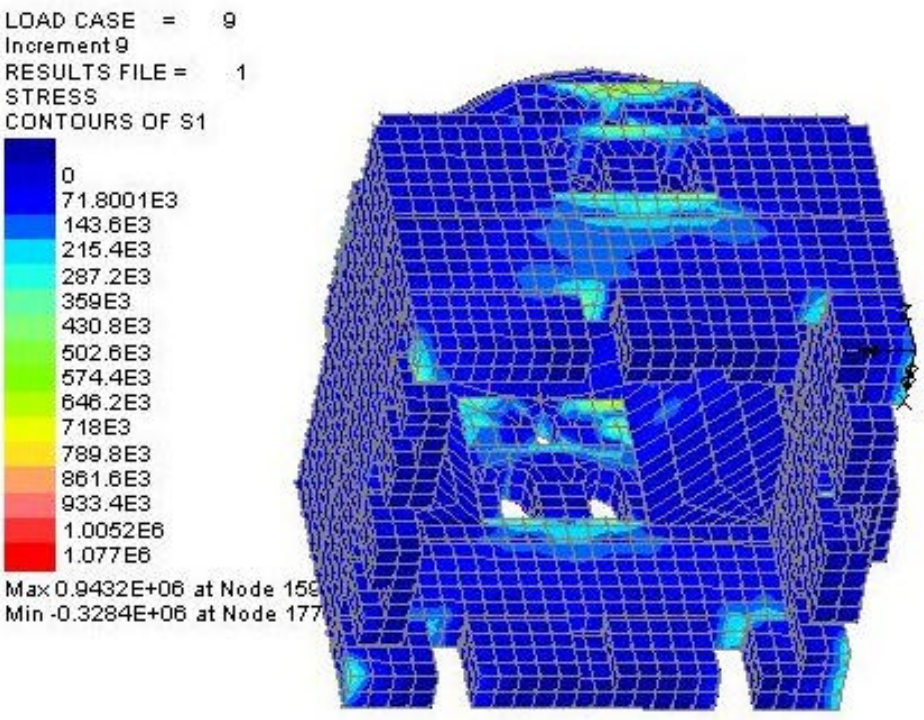

Figure 4.102. The S1 contours of 9th increment for east section.

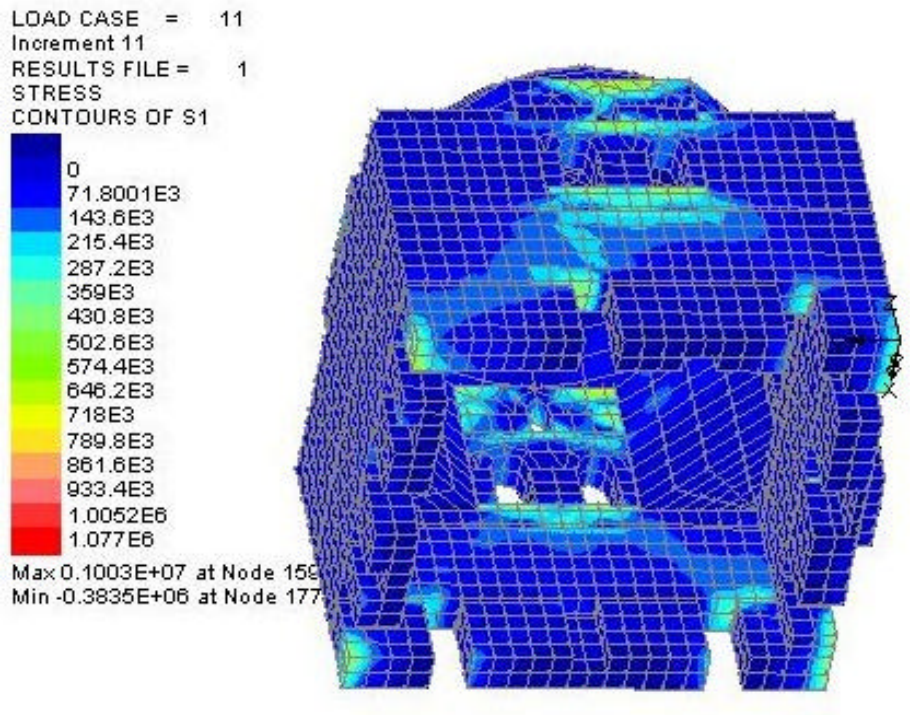

Figure 4.103. The S1 contours of 11th increment for east section.

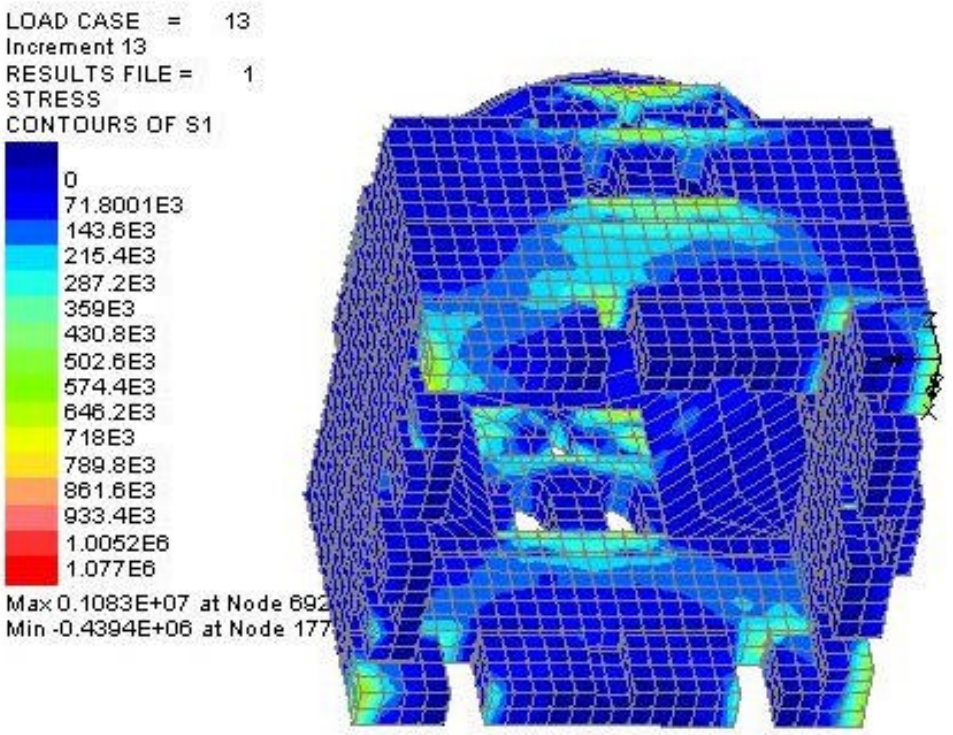

Figure 4.104. The S1 contours of 13th increment for east section.

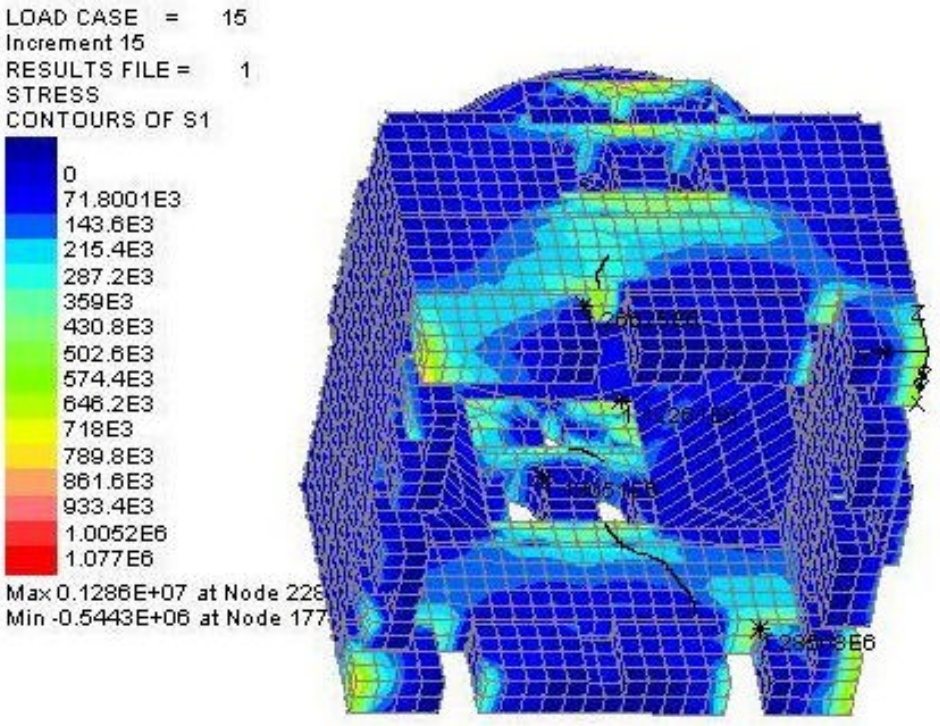

Figure 4.105. The S1 contours of 15th increment for east section with existing cracks.

The stress concentrations start at the drum and 2nd level windows on the east section and west elevation, see Figure 4.99-Figure 4.102. The stress concentrations at

the drum and second level window unite with the concentrations at the 1st level window and the empty lintel places, see Figure 4.102-Figure 4.104. The existing cracks of the structure are shown with the black line in Figure 4.105. The 1st principal stresses capture the existing cracks at the east section and west elevation very well. The stress concentrations at the north and south foundations are due to the nature of the loading such that the settlement load is given as a displacement at the north foundation. But the real phenomenon is that the settlement occurs because of the self weight and the soil response to that weight. The difference in the phenomenon and the loading may cause such stresses not observed on the structure. Also these parts are under the soil and have confining pressure of soil. More over, as the sections of the structure are excessive, i.e. 110cm wall thickness, these concentrations does not challenge the structure and diminish in the section as occurs at the south foundation, see Figure 4.105.

The lintel places at the west and east and the drum of the east section have the upper 10% S1, see Figure 4.105.

The maximum S1 at the 15th increment is 1.286MPa at the east lintel place on the 1st level windows, see Figure 4.105.

The variation of the 1st principal stress, S1, at the west section and east elevation with respect to the increments can be seen from Figure 4.106 to Figure 4.113. In order to decrease the number of figures, only the odd numbered increments are presented.

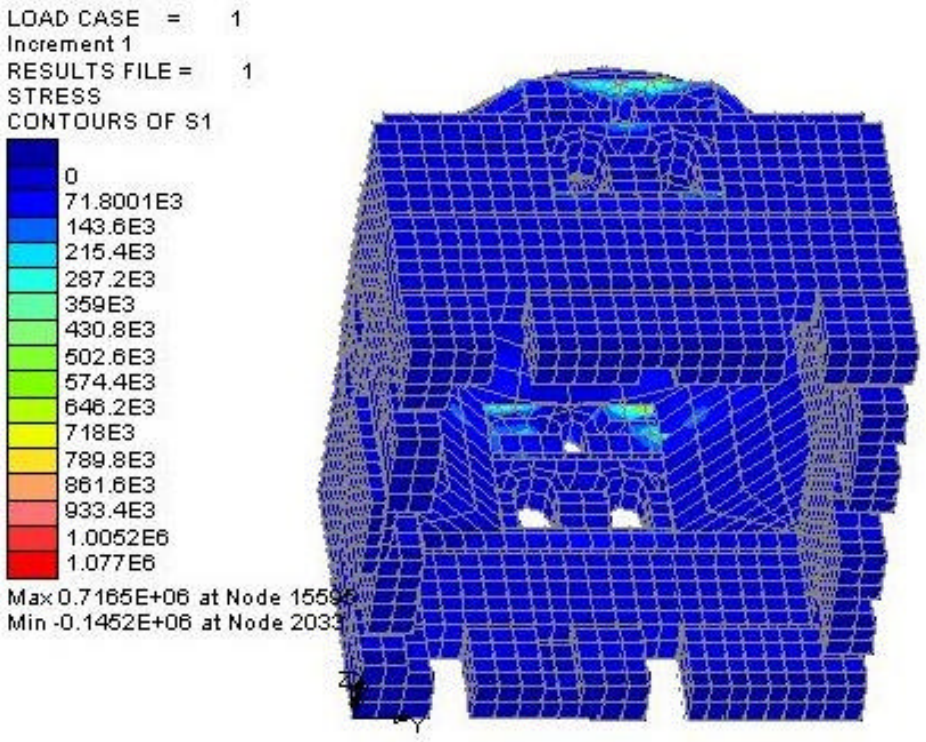

Figure 4.106. The S1 contours of 1st increment for west section.

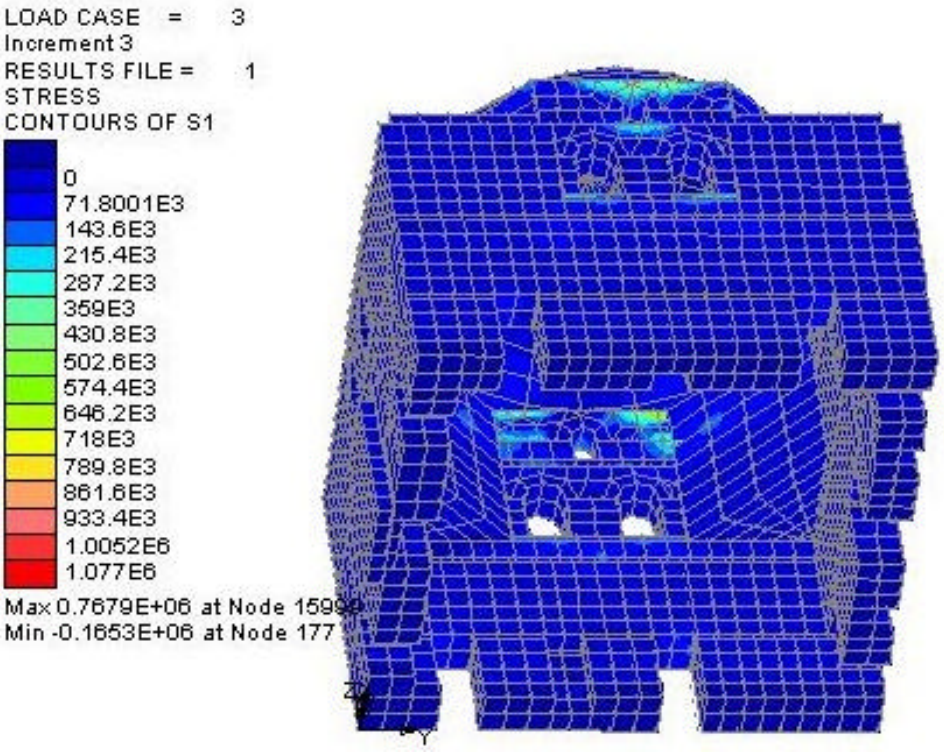

Figure 4.107. The S1 contours of 3rd increment for west section.

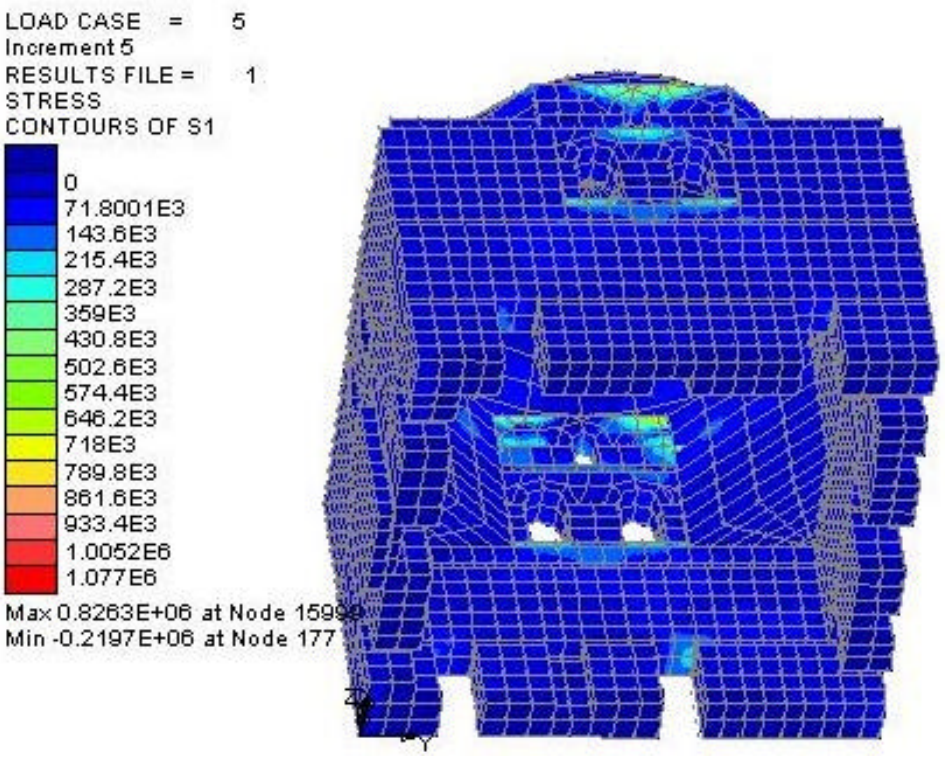

Figure 4.108. The S1 contours of 5th increment for west section.

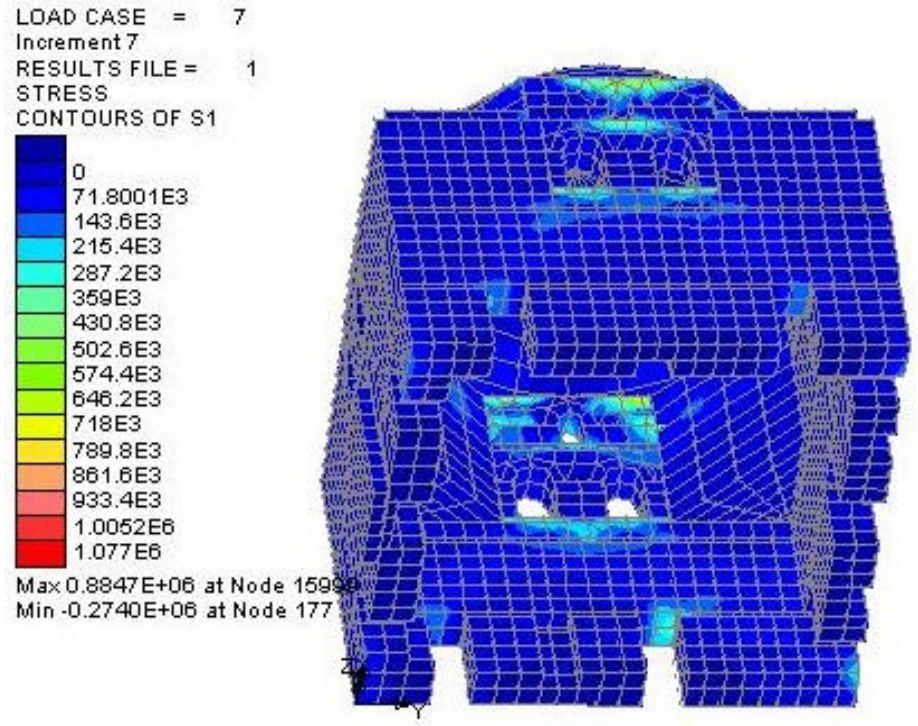

Figure 4.109. The S1 contours of 7th increment for west section.

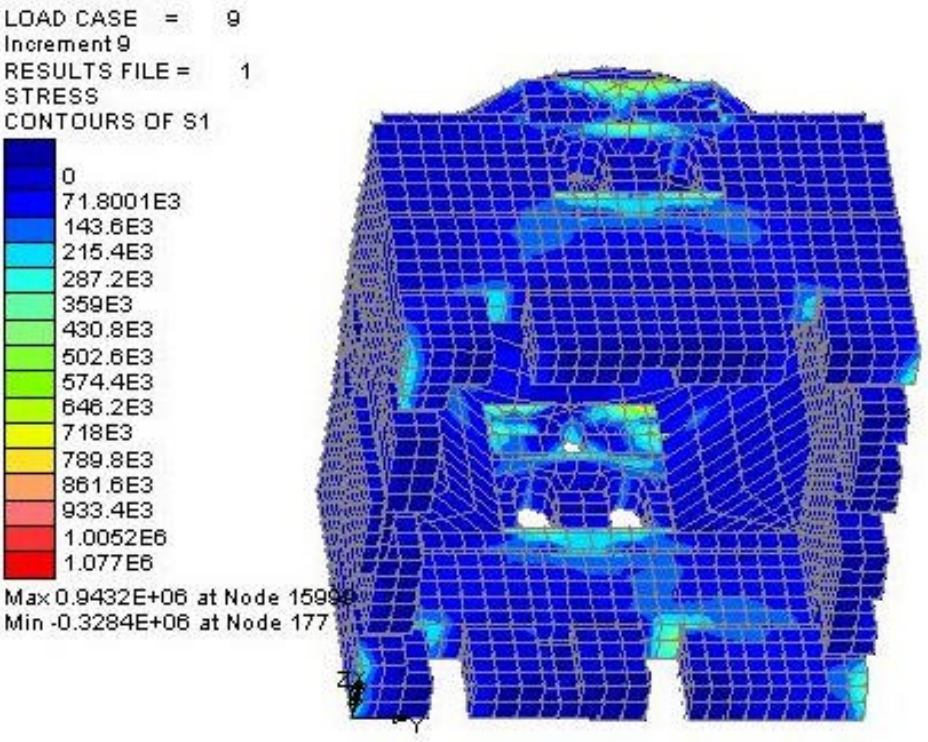

Figure 4.110. The S1 contours of 9th increment for west section.

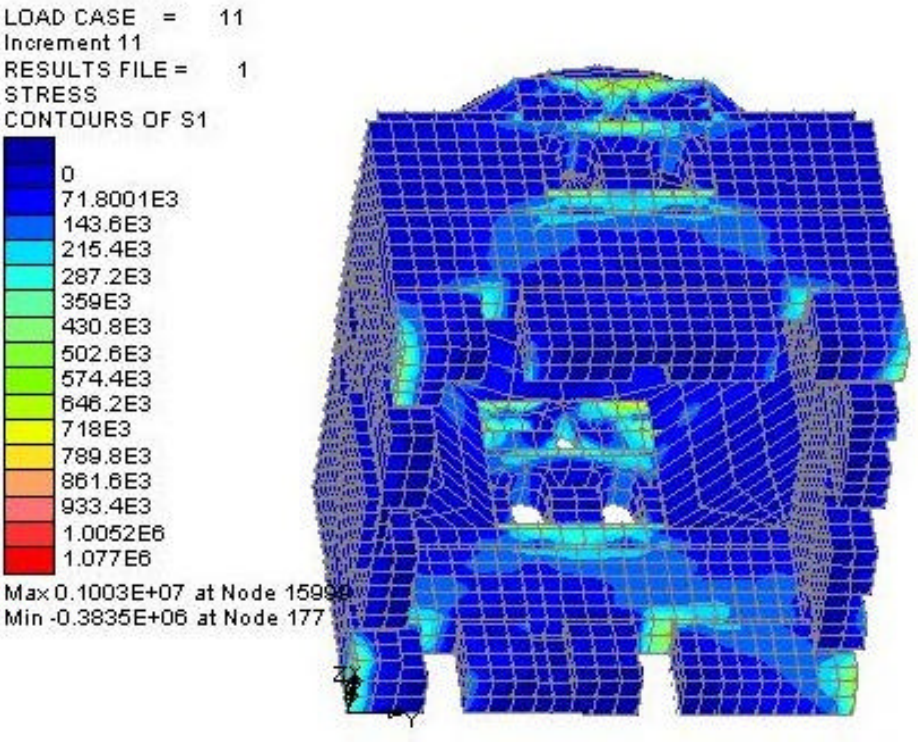

Figure 4.111. The S1 contours of 11th increment for west section.

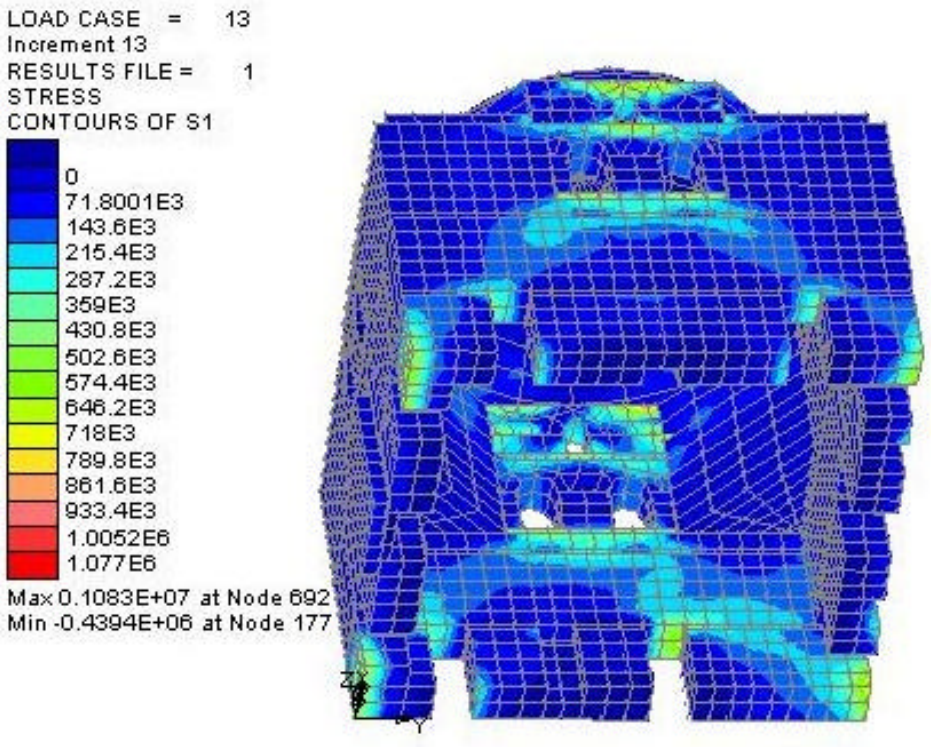

Figure 4.112. The S1 contours of 13th increment for west section.

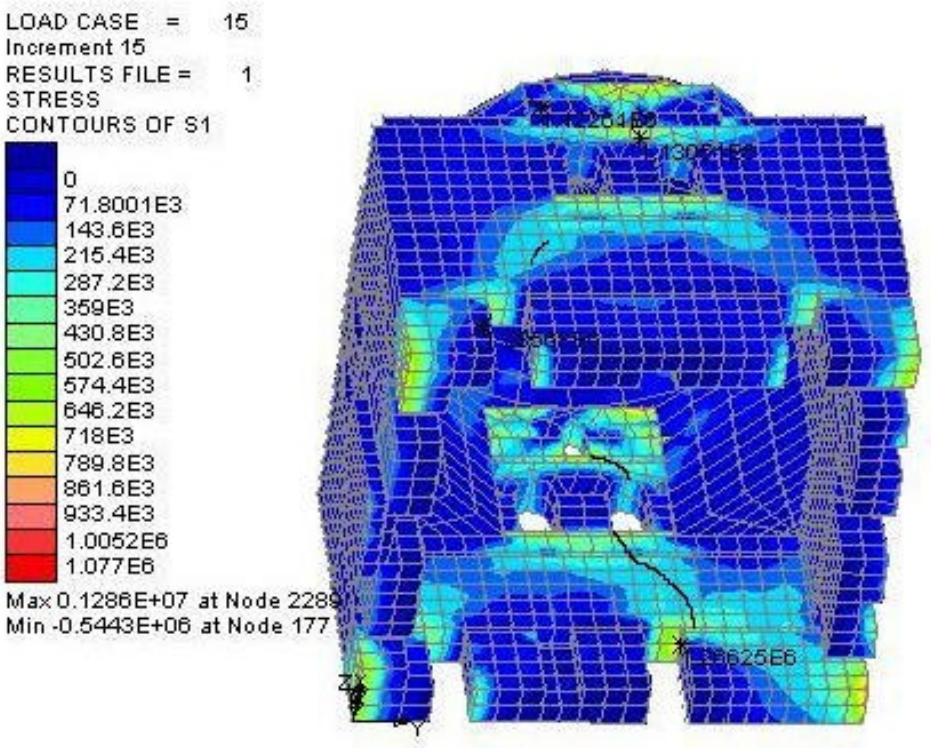

Figure 4.113. The S1 contours of 15th increment for west section.

The stress concentrations start at the west and east drum and 2nd level windows, see Figure 4.106-Figure 4.110. These concentrations unite with the ones at the lintel places, see Figure 4.111-Figure 4.113. The cracks on the west section and east elevation are captured by the S1 very well, see Figure 4.113.

In Figure 4.114, a slice of the west wall is presented. The existing cracks and the upper 10% of S1 are also shown. The S1 stresses captures the cracks very well, see Figure 4.114.

In Figure 4.115, a slice of the east wall is presented. The existing cracks and the upper 10% of S1 are also shown. The S1 stresses captures the cracks very well, see Figure 4.115.

The existing cracks and the stress concentrations follow the weakest sections, i.e. the windows, the lintel places. The cracks obtained from the nonlinear analysis starts at the bottom of the drum windows and tend to diffuse, see Figure 4.116. As stated before, because of the load curve analysis, the diffusion of the cracks could not be obtained. The obtained cracks are on the path of the existing cracks observed at the structure.

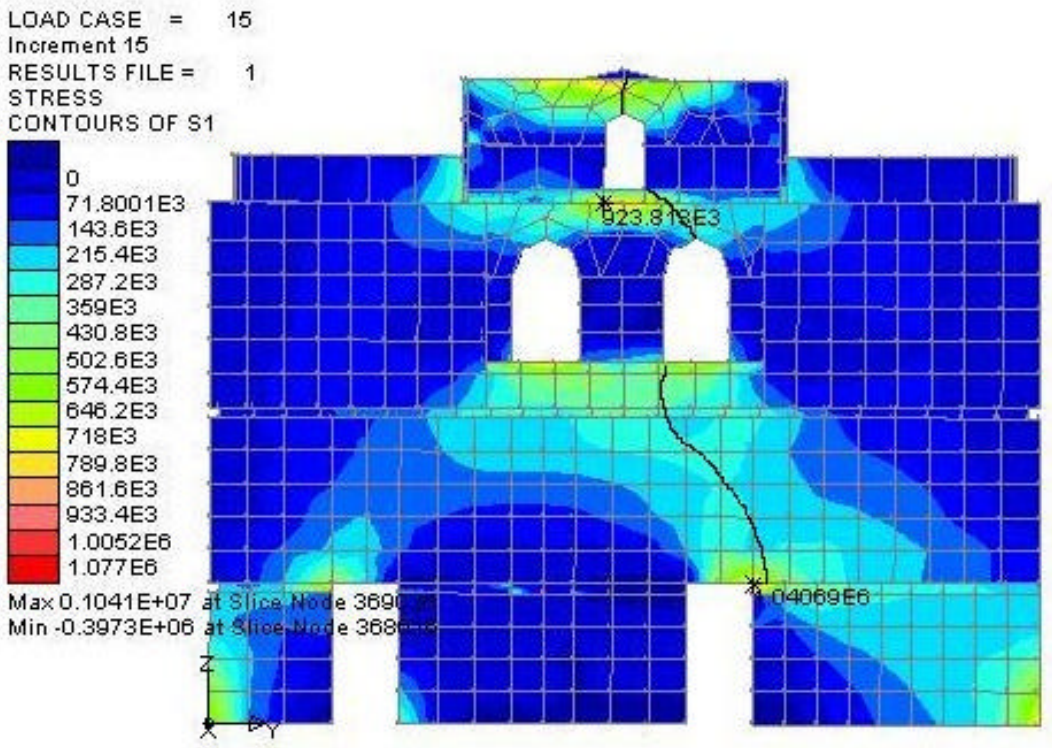

Figure 4.114. S1 contour of west wall slice.

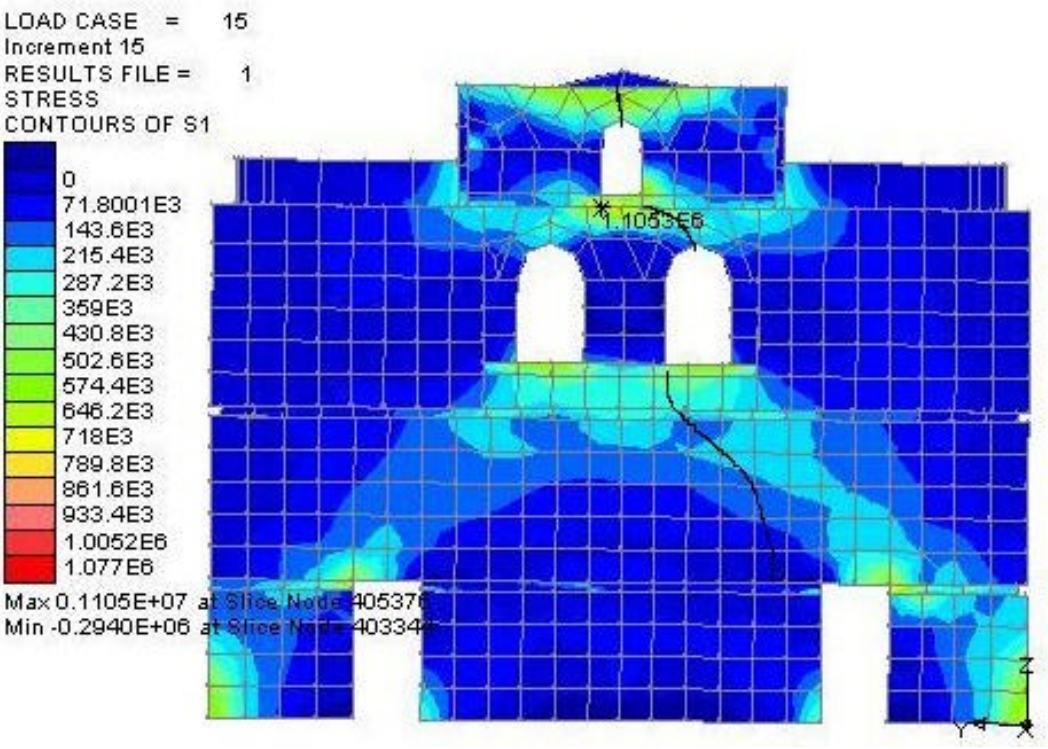

Figure 4.115. S1 contour of east wall slice.

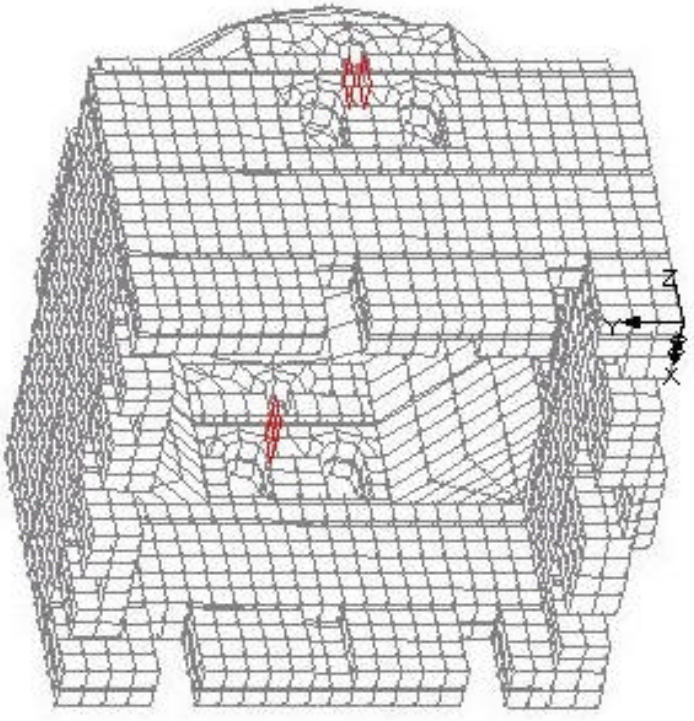

Figure 4.116. Cracks obtained by nonlinear analysis.

The drum and the walls of the west and east are under high stress state with respect to north and south, see Figure 4.117 and Figure 4.118.

The lintel places forms weak zones and makes the structure vulnerable to excessive stresses. The window openings also are on the route of the cracks and excessive stresses. The section of the drum is smaller then the walls and with the heavy dome resting on it and the drum windows, the drums of especially east and west are vital.

The maximum absolute value of compressive stress is 4.6MPa which is lower then the compressive strength fksm=10.77MPa, at the west section lintel place, see Figure 4.119. The lower 10% of 3rd principal stress, S3, is given in Figure 4.119. The stress concentrations occur at the zone of the settlement initiation at the east and west. Compressive stresses are lower then the strength as expected. This validates the assumption of compatibility of the tensile cracking failure of masonry and not including the compressive crushing. The excessive sections of the structure distribute the stresses efficiently.

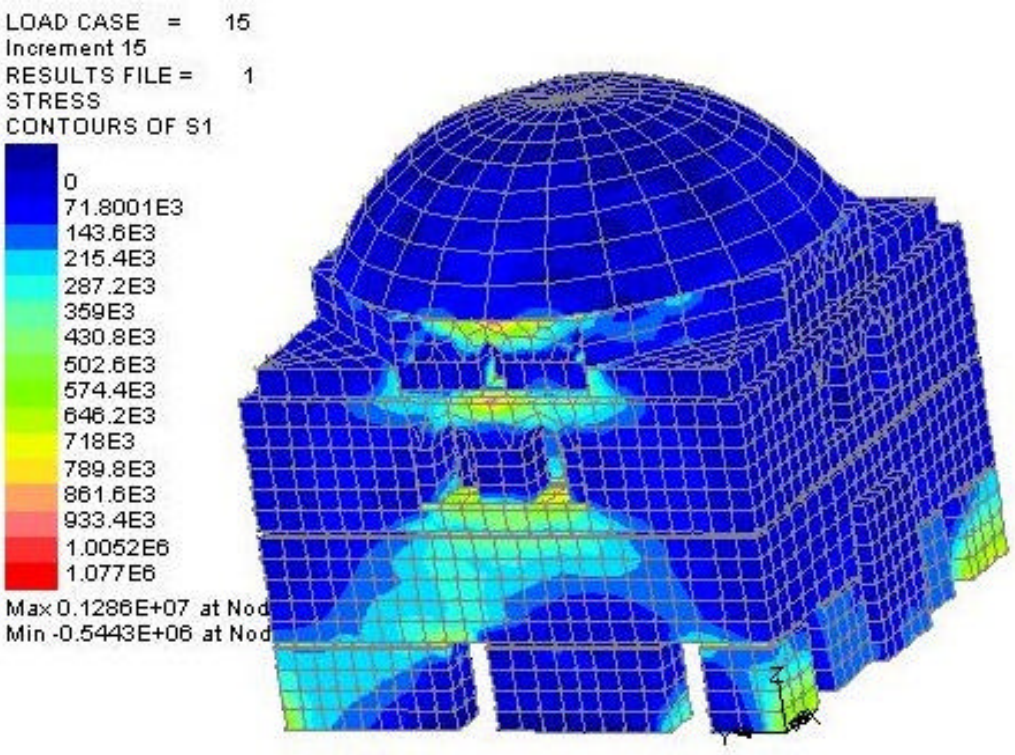

Figure 4.117. S1 contour of west and south elevations.

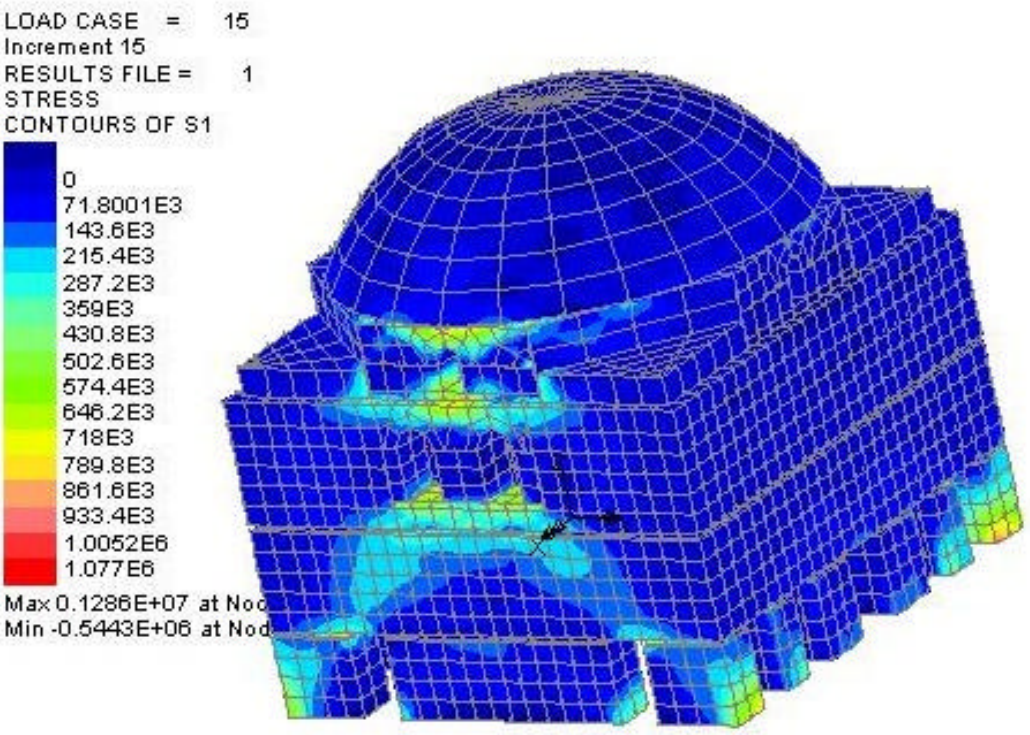

Figure 4.118. S1 contour of east and north elevations.

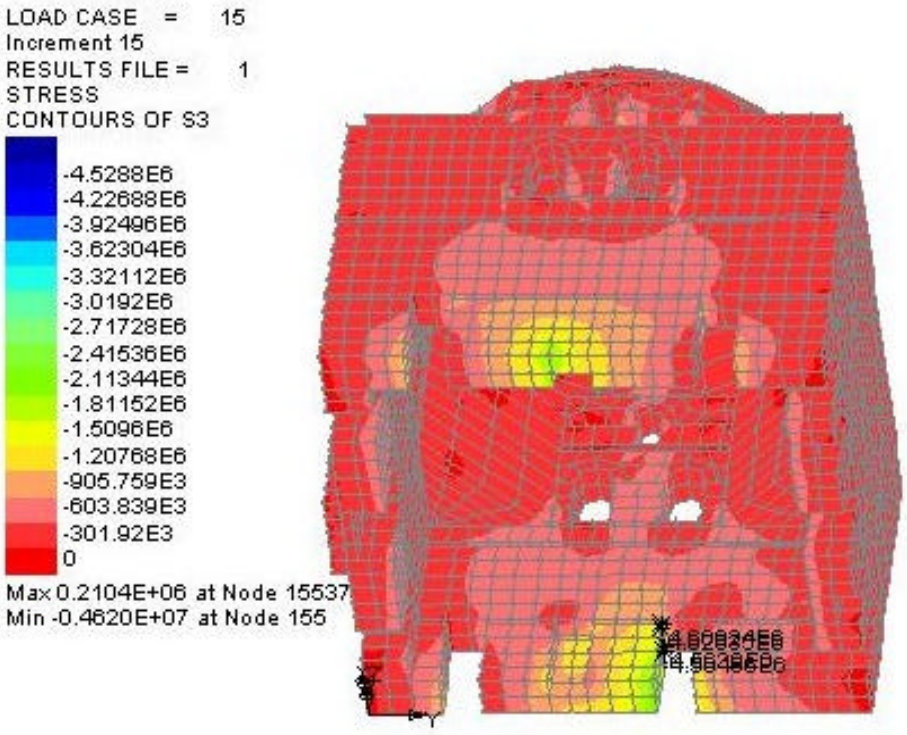

Figure 4.119. S3 contour of west section.

Chapter 5

CONCLUSIONS AND RECOMMENDATIONS

In this thesis, finite element modeling of historical masonry structures has been investigated. Urla Kamanli Mosque is selected as a case study to demonstrate the implementation In order to gather data for finite element modeling, history investigation, measurement survey, material tests, long term observations of moisture, crack opening and settlement have been conducted. The results of this study are given below.

1. The visual investigation of the structure concludes that the materials of the structure are highly deteriorated because of moisture especially at the first 1m above the ground level in the structure. Since the structure has not been used for a long time, it is in the poor condition; even considerable plant formations on the structure observed. There are two main structural cracks on the east and west walls of the structure. The missing wooden lintels of the structure decrease the wall sections considerably.
2. According to the history investigation, the structure was constructed around early 14^{th} century and mid 15^{th} century. The structure belongs to a group of structure named Yahsi Bey Külliyesi, which consists of a Turkish bath, a primary school, a tomb and two fountains. Urla is an earthquake prone region and the structure has survived earthquakes of last 500 years. But the part of the minaret above the balcony had collapsed in the 20^{th} century because of a storm.
3. Measurement survey was performed for determining the dimensions of the structure, the localization of the cracks and material degradations for use in 3D finite element modeling. During the measurement survey, the structure had been investigated thoroughly.
4. Relative moisture long term observations have been conducted monthly for more than a year. In general, the relative moisture at the first 50cm is higher than the moisture at the first 2m above the ground level. The moisture readings in winter are higher than it is in summer as expected. The relative moisture content readings give an idea about the reasons of the material degradation observed especially in the first 1 m level of the structure.

5. Long term crack monitoring has been conducted on the east and west section and elevations. It is observed that the cracks are active; as the cracks opens in winter, they close during summer months. Probably the underground water level changes between the seasons play a significant role on that observation.
6. Settlement long term observations show that the structure tends to settle towards north direction. Settlement long term observations data have been used for determining the loading scenarios for finite element analyses.
7. Nondestructive tests and destructive tests have been applied on stone, brick and mortar of the structure. The stones used at the structure are lime stone according to the XRD results. The nondestructive tests results are generally in close relation to the destructive test results. Material tests data have been used in finite element analyses.
8. The region of the Urla Kamanli Mosque is in 1st degree seismic zone. The expected peak ground acceleration for a return period of 475 years is 0.4g while the expected MSK intensity is 7.5 for a return period of 475 years.
9. The underground water level is low at the region and there is no danger of underground water. On the other hand, there are two wells near the structure which may cause seepage during rains. Seepage may cause differential settlement of the structure.
10. According to the finite element analysis, structure is safe under its self weight. The highest tensional stresses occur at the drum dome connections and at the second level windows and drum windows which are on the cracks route on the east and west walls.
11. The mode shapes and modal frequencies are determined. The 1st and 2nd modal frequencies are very close to each other because of partial symmetry of the structure.
12. Seismic analyses are conducted as response spectrum analyses. In both directions of loading (X and Y), the empty lintel places are under high stress concentrations. The drum-dome connections also suffer from high stresses. The crack pattern is captured by the seismic analyses at lower stress values than the strength.
13. Linear elastic settlement analysis with self weight was conducted. The settlement displacement was given towards north direction with a maximum value of 3cm. The crack pattern on the structure is obtained. There are stress

concentrations on the lintel places, on the drum dome connections and on the 2nd level and drum windows, on the east and west walls.

14. Cracking concrete model featured in LUSAS was used for nonlinear settlement analysis. The crack patterns, obtained using nonlinear settlement analysis are in good agreement with the existing cracks observed in the structure. The results show that the cracking concrete model is suitable for macro modeling of masonry.
15. A combination of self weight, settlement and seismic action may cause the formation of cracks on the structure.

The recommendations of are given below.

1. The structural engineer should take part in history investigation, measurement survey, long term observations and materials tests for gathering data for structural analysis of historical structures.
2. Long term observations of moisture, crack opening, settlement, temperature etc. should be conducted due to the need of the structure that is investigated.
3. The use of relations available in the literature between nondestructive and destructive tests gives results different from the results of destructive tests. The nondestructive tests should be related to the destructive tests for every case separately rather than using the available relations in the literature directly.
4. The materials of the historical masonry structures are generally highly deteriorated and are not available in the sizes the test standards put forward. More flexible standards for testing of these materials should be defined.
5. Development of a constitutive law which has parameters determined by tests on constituents of masonry and morphology of the wall should be a challenge for the researchers.
6. Sampling and testing of materials are generally a problem for the historical structures. A data base for the tests and results of the materials on the historical masonries should be created world wide.

REFERENCES

Alkan M, Urla (Izmir) Ilçesi Yenice Mahallesi Kamanli Mevkii, 18D.IIb ve 18D.IIc Paftalardaki 6 Nolu Parsel Alaninin Jeolojik Etüd Raporu, (1994).

ASTM, Standard Method for Laboratory Determination of Pulse Velocities and Ultrasonic Elastic Constants of Rock (D2845-69), 1969.

ASTM, Standard Test Method for Pulse Velocity Through Concrete, (C597-97), 1997.

Bathe K. J, *Finite Element Procedures,* (Prentice Hall Inc. New Jersey, 1996).

Berto L, Saetta A, Scotta R, Vitaliani R, An Orthotropic Damage Model For Masonry Structures, *International Journal for Numerical Methods in Engineering*, **55**, (2002) p.127-157.

Binda L, Saisi A, Tiraboschi C, Investigation Procedures for the Diagnosis of Historic Masonries, Construction and Building Materials, **14**, (2000), 199-233.

Chandrupatla T. R, Belegundu A. D, *Introduction to Finite Elements in Engineering,* (Prentice Hall, New Jersey 1991).

Croci G, *The Conservation and Structural Restoration of Architectural Heritage* (Computational Mechanics Publications, Boston, 1998).

Çakmak A.S, Davidson R, Mullen C.L, Erdik M, Dynamic Analysis and Earthquake Response of Hagia Sophia, *Protection of Architectural Heritage against Earthquake Seminar*, Istanbul, (1992), p.19.

Demir H and Polat Z, *Report of 30 October 1983 Erzurum Earthquake* (Turkish Chambers of Civil Engineers, Istanbul Division, Istanbul, 1983) (In Turkish).

European Committee for Standardization, *Eurocode 6* (Brussels, 1996).

Fanning P.J, Boothby T.E, Three-dimensional Modelling and Full-Scale Testing of Stone Arch Bridges, *Computers and Structures*, **79**, (2001), 2645.

FEA Ltd. a *Modeller User Manual* (Surrey 2002).

FEA Ltd. b *Theory Manual 2* (Surrey 2002).

Giambanco G., Rizzo S., Spallino R., 2001. Numerical Analysis of Masonry Structures via Interface Models, *Computer Methods in Applied Mechanics and Engineering*, **190**, (2001) p.6493-6511.

Giordano A., Mele E., Luca A, Modelling of Historical Masonry Structures: Comparison of Different Approaches Through a Case Study, *Engineering Structures*, 24, (2002) pp.1057-1069.

Heyman J, Cracking of Domes, *The Stone Skeleton* (Cambridge University Press, New York, 1995).

Heyman J, *The Masonry Arch* (Ellis Horwood Series in Civil Engineering, New York, 1982).

Ispir N, Urla (Izmir) Ilçesi 75 Pafta, 277 Ada, 24 Nolu Parsel Alaninin Zemin Etüd Raporu, (2000).

Koçak A., *Linear and Nonlinear Analysis of Historical Masonry Structures under Static and Dynamic Loads Case Study: Küçük Aya Sofya Mosque* , PhD Thesis, Yildiz Technical University, Istanbul, 1999.(In Turkish).

Lourenco P.B., *Computational Strategies for Masonry Structures* (Delft University Press, Netherlands, 1996).

Lourenço P.B., Assessment of the Stability Conditions of a Cistercian Cloister, *2nd International Congress on Studies in Ancient Structures*, Istanbul, (2001), 669.

Ministry of Public Works and Settlement, Government of Republic of Turkey, *Report of Çaldiran Earthquake* (Baylan Press , Ankara, 1977) (In Turkish).

Ministry of Public Works and Settlement, Government of Republic of Turkey, *Specification for Structures to be Built in Disaster Areas* (Ankara, 1998).

Orhon A.V, *The Aspects of Masonry Construction Adopted in Turkey and a Search for Earthquake Resistant Multistorey Residential Buildings* (MSc Thesis, Dokuz Eylül University Architecture Faculty, 1995), p. 72.

Proceq, *DIGI-Schmidt 2000 Model ND/LD,* Zurich, 2001.

RILEM, Test for Mortars and Renders, *Materials and Construction,* 13, (1980).

Roca P., Analysis of Gothic Structure , *Proceedings of the Second International Conference Studies in Ancient Structures* edited By Görün Arun, Nadide Seçkin, (Yildiz Technical University, Faculty of Architecture, Istanbul,2001), p.291-300.

Sofraine R.A, Popa G, Nappi A, Facchin G, Dynamic Response of Church Steeples, *Proceedings of the Second International Conference Studies in Ancient Structures* edited By Görün Arun, Nadide Seçkin, (Yildiz Technical University, Faculty of Architecture, Istanbul, 2001),

Stylianidis K, Ignatakis C, The Analysis of a Byzantine Monument The Case of St. Panteleimon Church in Thessaloniki, *Structural Conservation of Stone Masonry International Technical Conference*, Athens, (1989), p.131.

Tunçoku S.S, *Characterization of Masonry Mortars Used in Some Anatolian Monuments in Konya, Beysehir and Aksehir*, PhD Thesis, Middle East Technical University, Ankara (2001).

Ulusay R, Gökçeoglu C, Binal A, *Rock Mechanics Laboratory Experiments,* Turkish Chambers of Geology Engineers, Ankara, 2001. (In Turkish).

Ünay A. I, *A Method for the Evaluation of the Ultimate Safety of Historical Masonry Structures* , PhD Thesis, Middle East Technical University, Ankara (1997).

WEB_1: Attainable Life Association. http://www.uyd.org.tr/bem.html, 17/07/2004.

WEB_2: Images of St Peter. http://www.saed.kent.edu/~erobison/stpeters.html , 17/07/2004.

WEB_3: General Directorate of Disaster Affairs. http://www.deprem.gov.tr/linkhart.htm, 22/07/2004.

WEB_4: Izmir Deprem Senaryosu ve Deprem Master Plani, http://www.koeri.boun.edu.tr/depremmuh/izmirrapor2002.htm, 22/07/2004.

WEB_5: Strong Earthquakes Occurred in Izmir and vicinity in 20th century. http://www.koeri.boun.edu.tr/depremmuh/s342.jpg . 22/07/2004.

WEB_6: Case Studies of LUSAS. http://www.lusas.com/case/civil/hagia.html , 22/07/2004.

Wenzel F., Frese B., Vratsanou V., Structural Analysis of the Auguste –Victoria Church of the Ascension in Jerusalem Assessment of its Safety by Employing Response Spectrum Modal Analysis, *Structural Conservation of Stone Masonry International Technical Conference*, Athens, (1989), p. 475.

Zienkiewicz O.C, Taylor R.L, a, *The Finite Element Method Volume 1 Basic Formulation and Linear Problems*, (MacGraw Hill, London, 1987).

Zienkiewicz O.C, Taylor R.L, b, *The Finite Element Method Volume 2 Solid and Fluid Mechanics Dynamics and Nonlinearity*, (MacGraw Hill, London, 1987).